ONGERUBRICEERD

TNO-report
1999-CMC-R054

Shock transmission analyses of a simplified frigate compartment using LS-DYNA

20000127 049

TNO Building and Construction Research

Contact person
ir. W. Trouwborst

Centre for Mechanical Engineering
Schoemakerstraat 97
P.O. Box 49
2600 AA Delft
The Netherlands

Phone +31 15 269 53 60
Fax +31 15 269 53 61

Date
13 December 1999

Author(s)
Ir. W. Trouwborst

Sponsor : Ministry of Defence
Directie Materieel Koninklijke Marine
Afdeling Maritieme Techniek
Postbus 20702
2500 ES Den Haag

Monitoring Agency : TNO Defence Research
Classified by : Ir. T.N. Bosman
Classification date : 6 december 1999

Title : ONGERUBRICEERD
Managementuittreksel : ONGERUBRICEERD
Abstract : ONGERUBRICEERD
Report text : ONGERUBRICEERD
Appendices : ONGERUBRICEERD

The classification desination ONGERUBRICEERD is equivalentto Unclassified

Project number : 006.93213/01.01
Approved : Ir. G.J. Meijer
Visa : Ir. G.T.M. Janssen

Number of pages : 115

All rights reserved.
No part of this publication may be reproduced and/or published by print, photoprint, microfilm or any other means without the previous written consent of TNO.

In case this report was drafted on instructions, the rights and obligations of contracting parties are subject to either the Standard Conditions for Research Instructions given to TNO, or the relevant agreement concluded between the contracting parties. Submitting the report for inspection to parties who have a direct interest is permitted.

DISTRIBUTION STATEMENT A
Approved for Public Release
Distribution Unlimited

1999

ONGERUBRICEERD

AQF00-04-1019

DTIC QUALITY INSPECTED 1

TNO Building and Construction Research provides a comprehensive research and development service specifically geared to the needs of the construction and engineering industry.

Netherlands organization for applied scientific research (TNO)

The Standard Conditions for Research Instructions given to TNO, as filed at the Registry of the District Court and the Chamber of Commerce in The Hague shall apply to all instructions given to TNO.

Managementuittreksel

Titel	:	Shock transmission analyses of a simplified frigate compartment using LS-DYNA
Auteur(s)	:	ir. W. Trouwborst
Datum	:	29 November 1999
Opdrachtnr.	:	A98/KM/118
Rapportnr.	:	1999-CMC-R054

Dit rapport geeft de resultaten van een aantal eindige-elementenberekeningen aan een tweedimensionaal model van een compartiment van een fregat. Deze berekeningen zijn uitgevoerd met LS-DYNA. Doel van deze berekeningen is het verklaren van het schoktransmissie probleem, gedefinieerd als:

- Voor hoger liggende dekken neemt de maximum amplitude van de versnellingen af, en de frequentieinhoud neemt af (minder hoge frequenties).
- Voor hoger liggende dekken wordt de maximum snelheid kleiner, en de stijgtijd (tijd benodigd voor het bereiken van de maximale snelheid) wordt groter.

Tijdens schoktesten worden bovengenoemde verschijnselen voortdurend waargenomen, maar tot nu toe zijn deze niet met succes gereproduceerd tijdens simulaties.

Er zijn berekeningen uitgevoerd aan een aantal verschillende modellen, waarbij de effecten van een niet-symmetrisch schot, niet-symmetrische dekken, Rayleigh demping en plasticiteit op de responsies in het schot onderzocht zijn.

De belangrijkste conclusie is dat zowel een niet-symmetrisch schot als plasticiteit een aanzienlijk effect hebben op de responsies in het schot. Dit effect treedt echter op onafhankelijk van de lokatie in het schot, en wijkt daarmee af van het gemeten schoktransmissie effect. De modellering van de dekken en Rayleigh demping beïnvloeden de responsies in het schot vooral voor grotere tijden, maar hebben geen effect op de maximale snelheden in het schot (deze treden op binnen enkele milliseconden).

Bovenstaande conclusie geldt helaas niet voor een model met de dimensies gebaseerd op de ontwerptekeningen, omdat de mate van niet-symmetrie dan te klein is. Voor dit model wordt de vloeigrens niet overschreden, en ook imperfecties hebben te weinig invloed op de responsies om het schoktransmissie probleem te verklaren.

Uit analyse van een eenvoudig massa-veersysteem met acht graden van vrijheid blijkt dat het wel mogelijk is om de verschijnselen van het schoktransmissie probleem na te rekenen. Dit vereist echter onrealistische waarden voor massa's en veerstijfheden. Aangezien het grootste effect van de schoktransmissie gemeten wordt onderin het schip, wordt aanbevolen om het huidige model uit te breiden met de dubbele bodem, inclusief 'fluid-structure' interactie (cavitatie, 2DCAV of stekelvarken theorie).

Contents

1. Introduction

This report describes the results of a number of analyses that have been carried out using LS-DYNA to find a physical explanation for the so-called shock transmission problem or shock attenuation. The attenuation of the shock, which is always measured during shock trials, has the following characteristics:

- At higher deck levels, the maximum amplitudes of the accelerations decrease, and higher frequencies disappear.
- At higher deck levels, the maximum velocities become smaller, and the rising time (time to maximum velocity) increases.

Thus far, this phenomenon is not found using numerical analyses. Within this report, a two-dimensional model is used representing a longitudinal slice of a frigate. The third dimension in athwarthships direction is infinitely long.

Phenomena investigated are nonsymmetry of the bulkhead and of the decks, element size, plasticity of the material and Rayleigh damping. Analyses have been carried out for three different basic models, namely a generic model, a model with dimensions based on the design drawings and a simple eight degrees of freedom mass-spring model.

2. Problem and model description

Illustration attenuation of shock

The attenuation of the shock can be illustrated using some signals as measured during the shock trials of the M-frigate. Fig. 2.1 shows accelerations as measured at the same bulkhead and at the centerline, but at different deck levels. It is clear that at higher deck levels the maximum amplitudes of the measured accelerations decrease, while the higher frequencies disappear. Integration of these measured accelerations results in fig. 2.2, showing a decrease of the maximum velocity and an increase in the rising time for higher deck levels.

Basic model

The used model is equal to that as used in ref. [4] to [7], but it is reduced to a two-dimensional model. So (see e.g. fig. 3.1 a)):

- F-, G- and H-deck are located at Y=0.0, Y=-3.0 m and Y=-6.0 m respectively. Thicknesses of these decks are 7, 6 and 5 mm respectively.
- All decks range from X=-7.2 m to X=7.2 m, with the X-coordinate in the length direction of the ship.
- The bulkhead ranges from Y=0.0 to Y=-11.2 m. At Y=-11.2 m accelerations are prescribed corresponding with the kick-off velocity pulse as used in ref. [4] to [7], see fig. 2.3 (t=0, v=0, t=2.94 ms, v=1.69 m/s, t=49.6 ms, v=0). The thickness of the bulkhead is 6 mm between F- and G-deck, 7 mm between G- and H-deck and 9 mm for the part below the H-deck.
- In Z-direction, the model has only one element. Because the time step depends on the element size, all analyzed models have only square shell elements. Symmetry conditions are applied at the nodes at Z=0 and at the maximum Z-coordinate (which depends on the used element size).
- The material has a Young's modulus of $2.06 \bullet 10^{11}$ N/m^2, a Poisson's ratio of 0.30 and a density of 7800 kg/m^3.

In search for the reason for the attenuation of the shock wave, this basic model has been varied during the analyses (see e.g. fig. 3.4 a), 3.5 a), 3.6 a)). These variations will be discussed in the chapters with results.

3. Initial results without damping

This chapter presents some initial results as calculated for the basic model. One aspect investigated is the element size. Because one reason for the attenuation of the shock wave might be the occurrence of bending waves in the bulkhead, some non-symmetrical aspects are investigated. At first instance, responses are compared using the calculated velocities at the connections between the three decks and the bulkhead, and at the F-deck at X=7.2 m.

3.1 Effect of element size, symmetrical model

Runs are carried out using the basic model as described in the previous chapter, with element size 0.1 m and 0.01 m. Results are shown in fig. 3.1 and 3.2. Using 0.1 m, the model has 544 elements and 1090 nodes. The time step becomes $1.67 \bullet 10^{-5}$ s. Using 0.01 m, the model has 5440 elements and 10882 nodes, and the time step becomes $1.67 \bullet 10^{-6}$ s. CPU-time for this run is approximately 2 hours.

No effect of element size

As fig. 3.1 and 3.2 show, the responses for both models are exactly equal and symmetrical with respect to the bulkhead. Velocity responses in the bulkhead show a high-frequent signal around the input kick-off velocity, causing an overshoot with a factor 2.

3.2 Nonsymmetrical excitation

Fig. 3.3 gives results for the same model with element size 0.01 m with a nonsymmetrical excitation. The vertical prescribed accelerations at the bulkhead at Y=-11.2 m are unchanged, but also horizontal accelerations are prescribed in the negative X-direction. These horizontal accelerations are equal to the vertical accelerations multiplied with ($\sin \alpha$ / $\cos \alpha$), with α equal to 30 degrees. In this way the shock wave approaches the bulkhead having an angle of 30 degrees with it.

Unchanged vertical responses

As fig.3.3 a) shows, indeed bending waves occur within the bulkhead. Responses at the decks are still symmetrical with respect to the bulkhead, see fig. 3.3 c). Comparison of fig. 3.3 b) with fig. 3.2 b) shows that vertical responses are hardly influenced by the nonsymmetrical excitation.

3.3 Nonsymmetrical bulkhead

Another nonsymmetrical aspect that has been investigated is a stiffener at one side of the bulkhead. This stiffener ranges from Y=-8.0 m up to the F-deck at the negative X-side of the bulkhead. The width is 0.1 m and the thickness is 9 mm. The

element size is still 0.01 m and only the vertical excitation is used. Results are shown in fig. 3.4.

Large effect on responses, no attenuation of shock found

As fig. 3.4 a) shows, again bending waves occur in the bulkhead. Now, responses at the decks are not symmetrical with respect to the bulkhead, see fig. 3.4 c). Fig. 3.4 b) shows that the vertical responses become quite different. Maximum velocities within the bulkhead are approximately 2.0 m/s, while a lot of high frequencies are present within these velocities. Velocities within the bulkhead at the different deck levels are still very close to each other, so attenuation of the shock wave is not found.

3.4 Effect of transverse frames

According to fig. 3.4 b) and c), velocities at the decks are quite large when compared to the input velocity pulse. Therefore an analysis has been carried out with the previously used symmetrical model, while the transverse frames are included. These transverse frames (HP220x12, see ref.[4]) are simply modeled as webs with dimensions 200x12 mm. Distance between the cross-sectional stiffeners is 1.8 m. Results are shown in fig. 3.5.

Effect on deck responses

Comparison of fig. 3.5 with fig. 3.2 shows that indeed the velocity at the F-deck becomes much smaller, so in the remaining analysis the transverse frames will be included in the model.

3.5 Nonsymmetrical model

Next, the models from section 3.3 and 3.4 are combined, so the model has a nonsymmetrical bulkhead (stiffener at one side of bulkhead) and transverse frames at the decks. The element size is still 0.01 m. Results are shown in fig. 3.6.

Combination of section 3.3 and 3.4

Comparing fig. 3. 6 b) with 3.4 b) shows that the responses in the bulkhead are unchanged, while the responses at the decks have smaller amplitudes, as also found in the previous section. To make sure that the results from fig. 3.6 are correct and not caused by instability of the time integration process (although the energy balance is correct), the same model has been analyzed using a reduced time step (factor 0.5). This resulted in the same responses.

Another run has been carried out using the same model, but without the part of the H-deck at the positive X-coordinate. So an additional nonsymmetrical effect is incorporated in the model. Responses for this case are equal to the responses as shown in fig. 3.6.

3.6 Synthesis

Two types of responses

Roughly spoken, two types of responses are found. The first type shows maximum velocity amplitudes of 3.4 m/s (twice the input kick-off velocity) within the bulkhead. This type of solution oscillates around the input kick-off velocity. The second type shows maximum velocity amplitudes of 2.0 m/s within the bulkhead, while for time values larger than the time corresponding with the maximum velocity a lot of high frequencies occur.

Nonsymmetry of bulkhead is important

A typical example of the first type of solution is fig. 3.5 b), and fig. 3.6 b) represents the second type of solution. The second type of solution occurs only in case of a nonsymmetrical bulkhead. Both types of solution do not show the attenuation of the shock wave. Responses within the bulkhead are very close to each other, independent of the deck level.

Regarding the results, a different modeling of the decks (with or without transverse frames, removing one side of the H-deck) do not influence the responses within the bulkhead.

With respect to the second type of solution, with the high frequencies present within the velocity responses, it is expected that only a small amount of damping will have a large influence on the results. This will be investigated in the next chapter.

4. Effects of Rayleigh damping

4.1 Rayleigh damping, small element size

As in ref. [6], damping is introduced using Rayleigh damping:

$$C = a_0 M + a_1 K ; \tag{4-1}$$

with C, M and K the damping-, mass- and stiffness matrix respectively. In ref [6], coefficients a_0 and a_1 were calculated using a damping of 5.5 percent of the critical damping at discrete frequencies of 0.5 and 60 Hz, which resulted in values for a_0 and a_1 of 0.34272 and $2.8937 \bullet 10^{-4}$ respectively. Fig. 4.1 a) shows the resulting damping values as function of the frequency.

Effect of Rayleigh damping on stable time step size

Unfortunately, these damping values have an extremely large effect on the stable time step size of the time integration process. According to ref. [3], page 116, stability requires that:

$$dt_{wd} \leq \sqrt{dt_{nd}^2 + a_1^2} - a_1 ; \tag{4-2}$$

with dt_{wd} and dt_{nd} the time steps for the cases with and without Rayleigh damping respectively, and a_1 the stiffness proportional Rayleigh damping coefficient. With the current values (dt_{nd} $1.67 \bullet 10^{-6}$ s (section 3.1), a_1 $2.8937 \bullet 10^{-4}$), this results in a value for dt_{wd} of $4.82 \bullet 10^{-9}$ s.

However, using the above mentioned values for the Rayleigh damping coefficients and a time step of $2.0 \bullet 10^{-10}$ s still results in an unstable time integration process (extremely large energies of order 10^{20} followed by a core dump). Besides, the CPU-time as estimated by LS-DYNA becomes 33400 hours.

Therefore, coefficient a_1 has been set to $1.0 \bullet 10^{-6}$, see fig. 4.1 b) for the resulting damping coefficients as function of the frequency. According to eq. 4.2 now dt_{wd} becomes $9.46 \bullet 10^{-7}$ s. Indeed, applying a multiplication factor to dt_{nd} of 0.1 (so dt_{wd} is equal to $1.67 \bullet 10^{-7}$ s) results in a stable time integration process. The resulting CPU-time becomes 34 hours.

Results for the nonsymmetrical model from section 3.5 are shown in fig. 4.2. Comparison of fig. 4.2 with fig. 3.6 b) shows that the damping is so small (fig. 4.1 b)) that it hardly influences the responses.

So the only way to analyze the structure with sufficiently large Rayleigh damping coefficients and with reasonable CPU-times is to increase the element size of the

model. Fortunately, according to section 3.1 this is allowed (no significant differences in the responses).

4.2 Rayleigh damping, larger element size

The models from section 3.4 and 3.5 (fig. 3.5 and 3.6) are remeshed using an element size of 0.1 m in stead off 0.01 m. For both models, two analyses are carried out, one without Rayleigh damping and one with Rayleigh damping with values according to fig. 4.1 a). Because of the larger element size dt_{nd} is $1.67 \bullet 10^{-5}$ s. Using the value for a_1 of $2.8937 \bullet 10^{-4}$, eq. 4-2 results in a value for dt_{wd} of $4.81 \bullet 10^{-7}$ s. Indeed, applying a multiplication factor of 0.02 to dt_{nd}, so using a time step of $3.34 \bullet 10^{-7}$ s results in a stable time integration process. The CPU-time of these analyses is slightly above one hour.

Symmetrical model and Rayleigh damping

Results for the symmetrical model are shown in fig. 4.3. Comparison of fig. 4.3 a) with fig. 3.5 b) shows that indeed the element size does not effect the responses. As fig. 4.3 b) shows, Rayleigh damping does influence the maximum velocities, but not the ratio between the maximum velocities. Although not clear from fig. 4.3 (and 3.5 b)), the highest maximum velocity occurs at the F-deck level and the smallest maximum velocity occurs at the H-deck level, so in fact opposite to the attenuation of the shock wave as always measured.

Nonsymmetrical model and Rayleigh damping

Results for the nonsymmetrical model are shown in fig. 4.4. Unfortunately, when comparing fig. 4.4 a) with fig. 3.6 b), it is clear that because of the occurrence of bending the larger element size is not allowed. Responses are quite different for the case with the larger element size, because a lot of high bending frequencies can not be described by the coarser mesh.

4.3 Effect of element size in case of nonsymmetrical bulkhead

Results symmetrical model versus physical insights

For both the symmetrical model and the nonsymmetrical model (stiffener at one side of bulkhead) accelerations within the bulkhead at the H-deck level are shown in fig. 4.5, both for an element size of 0.01 m and 0.1 m. As the velocity of sound is 5139 m/s, it can be calculated that:

- at 1.0 millisecond the shock wave (positive upwards acceleration of 574.83 m/s^2) reaches the H-deck level,
- at 3.3 milliseconds the reflection from the F-deck level, which can be seen as a free boundary except for the F-deck itself (so reflected as tensile shock wave), reaches the H-deck level, resulting in twice the input acceleration,
- at 3.94 milliseconds the deceleration part of the input pulse (-36.219 m/s^2) reaches the H-deck level, so the positive input pulse vanishes resulting in a decrease of the acceleration to a value of approximately 574.83 m/s^2,

- at 5.3 milliseconds the first reflection from the bottom at Y=-11.2 m reaches the H-deck level (2 times 11.2 m and 5.2 m). As the bottom with the prescribed motions can be seen as a fixed boundary, the tensile downwards directed wave is reflected as a tensile upwards directed wave, resulting in an acceleration equal to zero,
- at 6.24 milliseconds (3.3 + 2.94) the tensile reflection from the F-deck level vanishes, resulting in a decrease of the acceleration to approximately -574.83 m/s^2,
- at 7.6 milliseconds a compressive downwards directed wave reflected from the F-deck level reaches the H-deck level, resulting in an acceleration of approximately two times -574.83 m/s^2,
- at 8.24 milliseconds (5.3 + 2.94) the first reflection from the bottom vanishes, resulting in an increase of the acceleration to a value of -574.83 m/s^2,
- at 9.6 milliseconds a compressive upwards directed wave reflected from the bottom reaches the H-deck level, resulting in an acceleration equal to zero,
- at 10.54 milliseconds (7.6 + 2.94) the compressive downwards directed reflection vanishes, resulting in an increase of the acceleration to a value of 574.83 m/s^2.
- at 11.9 milliseconds again a tensile downwards directed wave reaches the H-deck level.

All these values can be recognized within the responses of the symmetrical model, see fig. 4.5 a). The situation at 11.9 milliseconds corresponds with that at 3.3 milliseconds, explaining the periodicity within the accelerations of approximately 8.6 milliseconds, see fig. 4.5 a). This periodicity corresponds with four times the length of the bulkhead, because:

- a compressive upwards directed wave is reflected at the F-deck level as a downwards directed tensile wave,
- which is reflected at the bottom as an upwards directed tensile wave,
- which is again reflected at the F-deck as a downwards directed compressive wave,
- which is again reflected at the bottom as an upwards directed compressive wave.

So the results for the symmetrical model correspond very well with physical insights.

Dispersion of input wave

Fig. 4.5 b) shows the same results for the nonsymmetrical model. It is clear that the bending as introduced by the nonsymmetrical bulkhead causes dispersion of the input shock wave, which depends strongly on the element size. This dispersion causes the occurrence of the more realistic second solution type from section 3.6 (case with element size 0.01 m from fig. 4.5 b) is the case from fig. 3.6).

4.4 Synthesis

It has been tried to investigate the effect of Rayleigh damping on the responses. Because the stiffness proportional part of the Rayleigh damping has a large effect

on the stable time step, it is not possible to use the smallest values for the Rayleigh damping coefficients as used in ref. [6] (5.5 percent at frequencies of 0.5 and 60 Hz) in combination with the element size of 0.01 m.

To increase the time step, both the symmetrical and the nonsymmetrical model are analyzed using an element size of 0.1 m. Unfortunately, for the nonsymmetrical model this is not allowed, because the larger element size results in an incorrect description of the bending waves within the bulkhead. If Rayleigh damping is included, the effect on the responses is obvious, but:

- the largest effect occurs at larger time values,
- responses within the bulkhead at the different deck levels have smaller maximum amplitudes, but the attenuation of the shock is not found.

Rayleigh damping not responsible for attenuation of shock

So, although based on an element size of 0.1 m, Rayleigh damping is not able to cause the reduced severity of responses at higher deck levels within the bulkhead, mainly because some time is needed to get a reasonable effect of the Rayleigh damping on the responses.

An extensive discussion of the responses within the bulkhead at the H-deck level shows that calculated responses are correct. From this discussion it is of course clear that responses (travelling times of incoming and reflected waves) depends on the height of the bulkhead (reflection at F-deck level or at B-deck level?). However, the attenuation of the shock wave is always found within measurements, independent whether the bulkhead ranges from tank top to F-deck level or to B-deck level (fig. 2.1), so this can not be a reason for the fact that thus far the attenuation of the shock wave is not found within the calculated responses.

Thus far, in all cases responses at the decks start at later time values, which implies that for smaller time values the largest part of the energy remains within the bulkhead, which can be a reason for the more or less equal responses within the bulkhead at the different deck levels. Therefore, in the next chapter analyses are carried out with the aim to increase the influence of the decks.

5. Effects of decks on bulkhead responses

5.1 Decks with larger masses and stiffness

To increase the effects of the decks on the responses within the bulkhead, the density of the elements at the H-deck level from X=-1.0 to -7.2 has been multiplied with a factor 20. This corresponds with a distributed mass at the deck of 741 kg/m^2. Results are shown in fig. 5.1. Comparing fig. 5.1 with fig 4.4 a) shows that the responses within the bulkhead are unchanged.

Another run has been carried out with the Young's modulus for all decks multiplied with a factor 10. Again, this does not influence the responses within the bulkhead.

No effect of decks on bulkhead responses

So although the changes within the decks are quite large, this does not effect the responses within the bulkhead at the different deck levels. Therefore, within the next section analysis results as based on a model without decks are discussed.

5.2 Results for models without decks

Still based on an element size of 0.1 m, two models without decks are analyzed. Fig. 5.2 a) gives the responses for a symmetrical bulkhead, and fig. 5.2 b) gives the responses for a bulkhead with a nonsymmetrical stiffener at the negative X-side. These figures can be compared with fig. 4.3 a) and 4.4 a) respectively. The only difference is that all the decks are removed from the model.

Removing decks does not effect initial response in bulkhead

Comparison of fig. 5.2 with fig. 4.3 a) and 4.4 a) shows that indeed the responses are very close to each other. While for the nonsymmetrical case the responses are equal for the whole time period, in the symmetrical case responses for larger time values are different. For larger time values, in the symmetrical case energy moves from the bulkhead into the decks.

5.3 Energy distribution

To verify the effects of the decks, energy distributions as function of time are investigated:

- fig. 5.3 shows the energy distribution for the symmetrical model including decks,
- fig. 5.4 shows the energy distribution for the nonsymmetrical model (stiffener at one side of bulkhead) including decks,
- fig. 5.5 shows the energy distribution for the symmetrical model without decks (only bulkhead),

- fig. 5.6 shows the energy distribution for the nonsymmetrical model without decks (only bulkhead with stiffener at negative X-side).

Energies of decks negligible

From fig. 5.3 it can be concluded that:
- For the first 25 milliseconds the most important component is the kinetic energy.
- After 50 milliseconds the total energy remains constant (no loading, no external work).
- After 50 milliseconds, an exchange between kinetic and internal energy (used for deformations) occurs.
- For the first 25 milliseconds, which determines the initial responses within the bulkhead, the total energy is nearly equal to the kinetic energy within the bulkhead, compare fig. 5.3 a) and b).
- Indeed, the energies within the decks are very small, see fig. 5.3 c) to e).

As fig. 5.4 shows, the same conclusions hold for the nonsymmetrical model. For the first 25 milliseconds the total energy is determined by the kinetic energy within the bulkhead and the nonsymmetrical stiffener at the bulkhead, while the energies within the decks are relatively small. Note that, because mass and volume are changed due to the stiffener at the bulkhead, the total energies are different.

Comparing fig. 5.5 with fig 5.3 a), and fig. 5.6 with 5.4 a), b) and f) clearly shows that the decks have a negligible effect on the energies, certainly for the first 25 milliseconds determining the initial responses within the bulkhead.

Because for the nonsymmetrical model which includes bending waves within the bulkhead the element size of 0.1 m is too large, in fig. 5.7 and 5.8 the energies are shown for both the symmetrical model and the nonsymmetrical model with an element size of 0.01 m.

Fig. 5.7 a) to e) are exactly equal to fig. 5.3 a) to e), except for a factor 10 within the energies. This is caused by the fact that the dimension in Z-direction is also reduced with a factor 10 (0.1 m versus 0.01 m) resulting in the same factor for mass and volume and so for energies. This correspondence in energies of course is related to the correspondence in responses (same responses for symmetrical model, independent of element size).

In case of a nonsymmetrical model, responses are dependent on the element size. Therefore energies from fig. 5.8 (element size 0.01 m) show a different behaviour than energies from fig. 5.4 (element size 0.1 m). Because of the larger deformations (bending), the internal energy becomes the largest component, see fig. 5.8 a). This internal energy mainly originates from the bulkhead and the stiffener at the bulkhead, see fig. 5.8 b) and f). It still holds that energies within the decks are very small, see fig. 5.8 c) to e).

5.4 Synthesis

Within this chapter it has been shown that indeed the energies within the decks are negligible when compared to the energies within the bulkhead and the nonsymmetrical stiffener at the bulkhead. As a result, responses within the bulkhead at the different deck levels are not influenced by the decks. Even in case of large modifications of the decks (density of H-deck at negative X-coordinates times 20, Young's modulus of all decks times 10), the responses do not change. This conclusion is once more confirmed by the results for models without decks, so models describing only the bulkhead with or without a stiffener at the negative X-side.

The fact that nearly all energy remains within the bulkhead, explains the more or less same responses within the bulkhead, independent of the deck level, and so the reduced severity of the responses at higher deck levels is not found.

6. Effect of plasticity

6.1 Stresses from previous analyses

Nonsymmetry causes yielding, small element size required

One aspect not investigated thus far is the effect of plasticity. For some of the most important analyses from the previous chapters, the maximum Von Mises stress as found for all elements during the whole time interval of 0.15 seconds is listed in table 6.1. The only case with Von Mises stresses much larger than the yield stress of 350 N/mm^2 is the nonsymmetrical case with element size 0.01 m (showing again that the element size of 0.1 m is not allowed (bending)). For this case, at a certain time value the maximum number of elements with a Von Mises stress larger than the yield stress equals 88. Within the next section this analysis will be repeated including the effect of plasticity.

Table 6.1 Summary of maximum Von Mises stresses

Case	Fig. No.	Elem. Size [m]	Max. Von Mises stress [N/mm^2]	Location
Symmetrical	4.3 a)	0.1	188.5	F-deck, X=1.8 m
Nonsymmetrical	4.4 a)	0.1	258.1	Bulkhead, Y=-10.8 m
Nonsymmetrical, ρ of H-deck*20	5.1	0.1	258.5	Bulkhead, Y=-10.8 m
Symmetrical, no decks	5.2 a)	0.1	62.9	Bulkhead, Y=-11.2 m
Nonsymmetrical, no decks	5.2 b)	0.1	354.1	Bulkhead, Y=-10.8 m
Symmetrical	3.5	0.01	223.1	F-deck, X=1.8 m
Symmetrical, loading 30 degrees	3.3	0.01	167.4	F-deck, X=0.0 m
Nonsymmetrical	3.6	0.01	1189.0	Bulkhead, Y=-8.0 m

6.2 Small element size, nonsymmetrical model including plasticity

Results for the nonsymmetrical model (nonsymmetrical stiffener at negative X-side of bulkhead) including the effect of plasticity are shown in fig. 6.1 and 6.2. An ideal elastic-plastic material behaviour is assumed, with a yield stress of 350 N/mm^2. Comparing fig. 6.1 with 3.6 b) shows that plasticity has a damping effect on the high-frequencies. The maximum velocities within the bulkhead are slightly smaller, while the velocity at the F-deck becomes considerably smaller. Responses within the bulkhead at the different deck levels are close to each other, so the attenuation of the shock wave is not found.

Because during tests accelerometers are of course always located outside the centerline of the bulkhead, responses of nodes of the nonsymmetrical stiffener at the different deck levels are also investigated. These nodes are located at X=-0.1 m.

The responses are very close to those as shown in fig. 6.1, so the eccentric location of the accelerometers does not cause the attenuation of the shock.

Plasticity has damping effect

Comparing fig. 6.2 with fig. 5.8 shows that:

- The plasticity causes an increase of the contribution of the internal energy to the total energy (fig. 5.8 a), 6.2 a)).
- At larger time values, the internal energy is the dominant term (fig. 6.2 a)).
- The larger internal energy originates from the bulkhead, which was the region with the largest elastic stresses (fig. 5.8 b), 6.2 b)).
- The energies in the decks become smaller, see fig. 5.8 c) to e) and 6.2 c) to e). This corresponds with the smaller maximum velocity at the F-deck, compare fig. 3.6 b) and 6.1 (smaller velocities lead to smaller kinetic energies, but also to smaller deformations and so internal energies).

6.3 Synthesis

Using an elastic material model, the largest Von Mises stresses were found in the bulkhead for the nonsymmetrical case. Again, according to the Von Mises stresses it is not allowed to use a (larger) element size of 0.1 m, because of bending. The Von Mises stresses (1189 N/mm^2) are much larger than the yield stress (350 N/mm^2).

Therefore the nonsymmetrical model has been analyzed again using an element size of 0.01 m and an ideal elastic-plastic material model. Responses at the deck become smaller. Responses within the bulkhead are only slightly influenced. The effect of the occurrence of plasticity is comparable with that of damping, and therefore (see chapter 4) it has the largest effect on the responses for larger time values. For this reason, the attenuation of the shock wave is not found within the thus calculated responses.

7. More nonsymmetrical effects within model

As the effect of the nonsymmetry of the model (vertical stiffener at one side of the bulkhead) on the responses within the bulkhead is large (compare fig. 3.5 and 3.6), within this chapter some analyses results are presented for models with changed nonsymmetrical effects.

7.1 Modifications of nonsymmetrical stiffener at bulkhead

Increased thickness of nonsymmetrical stiffener has large effect

Fig. 7.1a) shows results for the nonsymmetrical model, with the thickness of the vertical stiffener at the negative X-side of the bulkhead increased from 9 to 18 mm. This is the only difference in the model for the results from fig. 3.6 and 7.1 a). As fig. 7.1 a) shows, the maximum velocities become smaller, while for larger time values the responses contain less high frequencies. Responses at the F-deck become quite different. Fig. 7.1 b) gives results for the same model using an elastic-plastic material model. While for the original case (with thickness 9 mm, see fig. 6.1 and 3.6 b)), plasticity resulted in:

- more or less unchanged maximum velocities in the bulkhead,
- large damping of the higher frequencies for larger time values,
- a reduced maximum velocity for the deck responses,

for the current case (with thickness 18 mm, compare fig. 7.1 a) and b)), plasticity results in reduced maximum velocities in the bulkhead. So the effects of plasticity do depend on the amount of nonsymmetry within the model.

No effect of discontinuities in bulkhead

To get discontinuities within the bulkhead, an analysis has been carried out using a thickness of 9 mm, 18 mm and 27 mm for the vertical stiffener at the negative X-side of the bulkhead below the H-deck, between G- and H-deck and between F- and G-deck respectively. Results for an elastic material model are shown in fig. 7.2. These responses are comparable with those of the previous case, compare fig. 7.2 with 7.1 a). Fig. 7.3 a) shows the same results in case of an elastic-plastic material model. Again, responses are comparable (fig. 7.3 a) and 7.1 b)). As in section 6.2, the effect of the location of accelerometers during tests (eccentric with respect to bulkhead) is small, compare fig. 7.3 a) and b).

The fact that for the analyses above plasticity has a larger effect than for the original model can be explained considering the Von Mises stresses for the elastic case. For the original case (fig. 3.6 b)) the maximum Von Mises stress is 1189 N/mm^2, and for the modified case (fig. 7.2) the maximum Von Mises stress is 1498 N/mm^2.

Another discontinuity has been analyzed. The part of the vertical stiffener at the negative X-side of the bulkhead between G- and H-deck has been moved to the positive X-side. Thickness of the stiffener is still 9 mm, as in the original case. Results for an elastic material model are shown in fig. 7.4, and fig. 7.5 gives the

responses in case of an elastic-plastic material model. From fig. 7.4, 7.5 and 3.6 it can be concluded that:

- The current modification results in less high frequencies, compare fig. 7.4 a) with fig. 3.6 b). The responses are close to each other.
- The eccentricity of accelerometers cause more high frequencies within the responses, compare fig. 7.4 a) and b).
- Plasticity has an effect comparable to the original model (fig. 3.6 b) and 6.1), namely less high frequencies and hardly a reduction of the maximum velocities, compare fig. 7.4 and 7.5. The maximum Von Mises stress for the elastic case was 1057 N/mm^2, so comparable with the original case (1189 N/mm^2).

Correspondence calculations and measurements of shock trials

Quite remarkable is the following observation:

- In case of an elastic-plastic material model (fig. 7.5), the velocities within the bulkhead correspond quite well with the input kick-off velocity pulse, with the velocity equal to zero at 50 milliseconds.
- In case of an elastic material model (fig. 7.4), the decay time decreases, resulting in a zero velocity at approximately 25 milliseconds. Within the total time of the input pulse of 50 milliseconds a second positive velocity pulse occurs.
- The same phenomena (shorter decay time, second positive pulse within total time of kick-off pulse) can be found in measurement signals of shock tests:
  - Fig. 5.5 from ref. [8] shows some velocities as measured during the full scale shock trials of the FFG-59. Signals V2000V and V2002V clearly show the decreased decay time and the second positive pulse within the total time of the theoretical kick-off pulse.
  - Fig. 5.8 from ref. [8] shows some velocities as measured during the full scale shock trials of the DDG-53. Especially signals A3003V, A3206V and A4000V show the phenomena.
  - For the M-frigate shock trials, the duration of the kick-off pulse is approximately 20 milliseconds (as can be derived from some measurements). As fig. 2.1 e) and f) of this report show, the same phenomena can be found within some accelerations. Other examples are fig. 3.27 (H-deck, starboard side), 3.28 (K-deck), and 3.30 (J-deck) of ref. [9]. Because these phenomena are present within the measurements, in many cases they do also occur within the results of the optimal state estimation method, see e.g. fig. 5.1 b) and 8.8 b) of ref. [9].
- So the correspondence between the calculated responses and the responses as measured during full scale shock trials confirms once more the importance of nonsymmetry of the bulkheads (although attenuation of the shock wave is still not found within the calculated responses).

A final modification that has been analyzed is again based on the model from fig. 3.6 a). Now at Y-coordinates -1.5 m, -4.5 m and -7.5 m one horizontal row of elements of the vertical stiffener at the negative X-side of the bulkhead is removed. Results are shown in fig. 7.6. Compared with fig. 3.6 b) the maximum velocities within the bulkhead become slightly larger, and the velocity signals contain less

high frequencies. The velocity at the F-deck decreases considerably. The maximum Von Mises stress for this case becomes (1233 N/mm^2), so larger than for the case without these discontinuities (1189 N/mm^2), and it occurs within the bulkhead at Y=-7.5 m, so at one of the discontinuities.

7.2 Nonsymmetry of decks

It has been tried once more to get a model with a large amount of energies within the decks at relatively small time values. Starting point is again the model from fig. 3.6 b). At the negative X-side of the three decks, a longitudinal girder with height 0.1 m and thickness 7 mm has been added. Results for this model are shown in fig. 7.7. As fig. 7.7 a) shows, the velocities within the bulkhead at the different deck levels have slightly smaller maximum velocities, but the largest influence is still found at larger time values. As fig. 7.7 b) shows, at the negative X-side the deck responses start much earlier (larger stiffness), but still at time values larger than the time value corresponding with the maximum velocities within the bulkhead. As expected, the energies within the decks and the added longitudinal girder increase, but at time values being too large to have an effect on the maximum velocities within the bulkhead.

No effect of decks on bulkhead responses

The same model has been analyzed once more using a multiplication factor for the density of the H-deck of 20. Responses do hardly change when compared to fig. 7.7. So, as in chapter 5, it seems to be impossible to find a model such that at small time values the effect of the decks on the responses within the bulkhead becomes large (which requires large responses and so energies of the decks at time values corresponding with the maximum velocities within the bulkhead). Note that the current model with element size of 0.01 m corresponds with a spacing for the 100x7 girders at the decks of 0.01 m!

7.3 Other nonsymmetrical models for bulkhead

Three analyses have been carried out to investigate the effect of horizontal stiffeners and struts at the bulkhead. Starting point is the symmetrical model from fig. 3.5 with element size 0.01 m. The first model contains horizontal stiffeners at the bulkhead at Y=-1.5 m, -4.5 m and -8.0 m. These stiffeners range to X=-0.1 m and have a thickness of 9 mm (so 100x9). Responses for this model are exactly equal to those as shown in fig. 3.5 b), so symmetry of the model is not disturbed. Within the second model a plate is added below these horizontal stiffeners within the plane Z=0, with dimensions 0.1x0.1 m and thickness 9 mm. Results for this model are shown in fig. 7.8. The third model is equal to the second model but the thickness of the plate is increased from 9 to 18 mm. Responses for this model are very close to those as shown in fig. 7.8.

Effect of struts on responses

So while the vertical nonsymmetrical stiffener at the bulkhead cause a change within the responses from fig. 3.5 b) to fig. 3.6 b), the horizontal struts cause a change within the responses from fig. 3.5 b) to fig. 7.8 a). So both nonsymmetrical structures have a large effect on the responses.

For the models with struts the maximum Von Mises stress is 264 N/mm^2, so these models are not analyzed using an elastic-plastic material model. This stress is found within the bulkhead at Y=-1.6 m, so at the connection with one of the struts.

7.4 Synthesis

Several nonsymmetrical models have been analyzed within this chapter. It is found that model changes within the nonsymmetrical stiffener as an increased thickness can have large effects on the responses within the bulkhead. Once more it is showed that the decks do not influence the responses within the bulkhead, because the decks will effect the responses within the bulkhead for larger time values only (even in case of longitudinal girders at the decks with girder spacing 0.01 m). Using a symmetrical model and adding struts to one side of the bulkhead do also have its effects on the responses.

8. Further reduced element size

Thus far, two different element sizes are used, namely 0.1 and 0.01 m. For the nonsymmetrical model, an element size of 0.01 m resulted in the responses from fig. 3.6 b), and an element size of 0.1 m resulted in the responses as shown in fig. 4.4 a). Based on these results, it was concluded that an element size of 0.01 m was required for nonsymmetrical models. To make sure that the results have converged with respect to the element size, an analysis has been carried out using an element size of 0.0025 m. Responses within the bulkhead are comparable with fig. 3.6 b), but the amplitudes show a further decrease (maximum velocities 1.3 to 1.5 m/s).

So the element size of 0.01 m seems to be too large. However, thus far it was not realized that a reduction of the element size in fact results in a change of the spacing of the nonsymmetrical stiffener at the bulkhead in Z-direction:

- Element size 0.1 m, model has a length in Z-direction of 0.1 m, so stiffener spacing is 0.1 m (symmetry conditions at Z=0 and Z=0.1 m).
- Element size 0.01 m, model has a length in Z-direction of 0.01 m, so stiffener spacing is 0.01 m (symmetry conditions at Z=0 and Z=0.01 m).
- Element size 0.0025 m, model has a length in Z-direction of 0.0025 m, so stiffener spacing is 0.0025 m (symmetry conditions at Z=0 and Z=0.0025 m).

Element size of 0.01 m sufficiently accurate

Therefore, an analysis has been carried out using an element size of 0.0025 m, but with the model length in Z-direction equal to 0.01 m. Now responses are exactly equal to fig. 3.6 b). Energies are exactly equal to fig. 5.8. So results for an element size of 0.01 m are sufficiently accurate. Another analysis has been carried out using an element size of 0.01 m, but with the model length in Z-direction equal to 0.1 m. Now responses within the bulkhead are exactly equal to fig. 4.4 a), but responses at the decks are different. Except for the energies within the decks, energies are equal to fig. 5.4. Energies within the decks are slightly larger. So results for an element size of 0.1 m are sufficiently accurate regarding the responses within the bulkhead, but with respect to the responses within the decks an element size of 0.01 m is required.

Nonsymmetrical bulkhead very important

The results above imply that the change in the responses from fig. 4.4 a) to fig. 3.6 b) is not caused by the element size, but by the fact that the spacing for the nonsymmetrical stiffener at the bulkhead in Z-direction is reduced from 0.1 m to 0.01 m, showing again the large importance of the amount of nonsymmetry within the bulkhead.

9. Additional analyses using different models

During this project, design drawings of some bulkheads were delivered by the Royal Netherlands Navy. Therefore some additional analyses are carried out using dimensions of the bulkhead as built. These analyses are described in this chapter. Besides, the effect of the maximum allowed imperfections is investigated.

9.1 Vertical stiffener as built using T-profiles

According to the design drawings, the bulkhead is stiffened with T6-profiles below the J-deck, with T4.5-profiles between H-deck and J-deck and with T3-profiles between F-, G- and H-deck. Dimensions of these profiles are summarized in table 9.1. To maintain the element size of 0.01 m, the dimensions used within the model are shown in the last columns of table 9.1. Three analyses are carried out with element size of 0.01 m for a model describing the vertical T-stiffener only, so without the bulkhead plate itself. A T6-profile ranges from Y = -11.2 m (K-deck level) to Y = -8.6 m (J-deck level), a T4.5 profile ranges from Y = -8.6 m to Y = -6.0 m (H-deck level) and a T3 profile ranges from Y = -6.0 m to Y = 0.0 m (F-deck level). No boundary conditions are applied and the excitation is equal to that used in the previous chapters.

The first analysis was carried out for the model as described above without imperfections. The second analysis was carried out for the same model using an imperfection (sine function) with amplitudes in X-direction of -8.66 mm at Y=-9.9 m, +8.66 mm at Y=-7.3 m, -10.0 mm at Y=-4.5 m and Y=+10.0 mm at Y=-1.5 m. These amplitudes are the maximum allowed amplitudes based on the relationship L/300 = a, with L the distance between the decks and a the imperfection amplitude. The third model contains the same imperfection with an opposite sign.

No effect of imperfections

Some responses for the perfect model are shown in fig. 9.1. Responses for both imperfect models are exactly equal. Table 9.2 summarizes some results of these analyses. Fig. 9.1 clearly shows that the first type of solution is found, see section 3.6 and fig. 3.5 b). As responses are equal, while quantities as listed in table 9.2 are very close, it is obvious that the maximum allowed imperfections do not influence the solutions. In all cases the maximum Von Mises stresses are close to each other and smaller than the yield stress. The location of the maximum Von Mises stress as shown in table 9.2 corresponds with the discontinuity between the T4.5 profile and

Table 9.1 Summary of dimensions of T-profiles (in mm)

	Web	Flange	Model web	Model flange
T6-profile	149 x 6.85	76 x 14.22	150 x 6.85	80 x 14.22
T4.5 profile	111 x 5.08	44 x 9.52	110 x 5.08	40 x 9.52
T3 profile	74 x 4.44	25 x 6.35	70 x 4.44	20 x 6.35

Table 9.2 Summary of results for perfect and imperfect vertical stiffener built up from T-profiles

	Perfect	Imperfect	Imperfect
Max. Von Mises stress [N/mm^2]	294.63	285.77	300.35
Corresponding time [ms]	16.0	16.0	16.0
Location	Y=-6.0, X=-0.07	Y=-6.0, X=-0.07	Y=-6.0, X=-0.07
Max. magnitude displ. at 49.5 ms	$4.27 \cdot 10^{-2}$	$4.30 \cdot 10^{-2}$	$4.24 \cdot 10^{-2}$
Max. X-component at 49.5 ms	$1.60 \cdot 10^{-3}$	$2.18 \cdot 10^{-3}$	$9.52 \cdot 10^{-4}$
Max. Y-component at 49.5 ms	$4.27 \cdot 10^{-2}$	$4.30 \cdot 10^{-2}$	$4.24 \cdot 10^{-2}$
Max. Z-component at 49.5 ms	$2.34 \cdot 10^{-6}$	$3.72 \cdot 10^{-6}$	$1.41 \cdot 10^{-6}$

the T3 profile. In all cases the maximum X-component of the displacement field at t=49.5 ms, which is a measure for the amount of bending, is relatively small. There can be two reasons for the negligible effect of the imperfections:

- buckling and postbuckling require compressive stresses, while probably not the whole stiffener is in compression (because of reflections),
- in general, mass effects has a stabilizing effect on dynamic buckling. A sufficient time length is needed to cause dynamic buckling, so to accelerate the masses in the transverse (buckling) direction, while during shock the time interval is very short.

9.2 Vertical stiffener as built including bulkhead plate

The model of the previous section is extended with the bulkhead plate. Thicknesses are 7 mm below the J-deck (-11.2 < Y < -8.6), 6 mm between H- and J-deck (-8.6 < Y < -6.0), and 4 mm between F-, G- and H-deck (-6.0 < Y < 0.0). The stiffener spacing according to the design drawings is 0.6 m, and symmetry conditions are applied for the nodes at boundaries Z=-0.3 m and Z=0.3 m. The element size is still 0.01 m, resulting in 83690 nodes and 82480 elements.

No effect of imperfections

Results for the perfect case are shown in fig. 9.2. Again the first type of solution is found, see section 3.6 and fig. 3.5 b). For this model, only one of the imperfections as described in the previous section has been analyzed. Again, the responses are equal to those of the perfect case as shown in fig. 9.2 a). A summary of results is given in table 9.3. As in the previous section, the effect of the imperfection is small, and again, the maximum Von Mises stresses are smaller than the yield stress.

Other solution type than for previously analyzed nonsymmetrical bulkheads

It is remarkable that still the first type of solution is found, while in the previous chapters a nonsymmetrical vertical stiffener at the bulkhead resulted in the second type of solution (section 3.6, fig. 3.6 b)). As discussed previously, this second type of solution is more realistic when compared to measurements. The reason for the occurrence of the first type of solution within the current analyses will be further investigated in the next section.

Table 9.3 Summary of results for perfect and imperfect vertical stiffener built up from T-profiles including bulkhead plate

	Perfect	Imperfect
Max. Von Mises stress [N/mm^2]	290.94	265.62
Corresponding time [ms]	14.2	10.9
Location	X=0.0, Y=0.0, Z=0.0	X=0.0, Y=0.0, Z=0.0
Max. magnitude displ. at 49.5 ms	$4.31 \cdot 10^{-2}$	$4.29 \cdot 10^{-2}$
Max. X-component at 49.5 ms	$1.49 \cdot 10^{-3}$	$2.04 \cdot 10^{-3}$
Max. Y-component at 49.5 ms	$4.31 \cdot 10^{-2}$	$4.29 \cdot 10^{-2}$
Max. Z-component at 49.5 ms	$3.99 \cdot 10^{-6}$	$3.54 \cdot 10^{-6}$

9.3 Model and loading modifications

Some additional analyses have been carried out to find a reason for the fact that:
- within the previous chapters, a symmetrical model resulted in the first type of solution as shown in fig. 3.5 b),
- within the previous chapters, a nonsymmetrical model resulted in the second type of solution as shown in fig. 3.6 b), which is more realistic when compared to measurements,
- within this chapter, a nonsymmetrical model using realistic dimensions results in the first type of solution.

Results for the model from the previous section, while the excitation is applied to the bulkhead at Y = -11.2 m only and not to the T6-profile, are shown in fig. 9.3. As for example in section 3.5, within a second analysis the part of the vertical stiffener between Y = -10.2 m and Y = -11.2 m has been removed, resulting in a large discontinuity at Y = -10.2 m. Responses are given in fig. 9.4. Within a third analysis, a time shift within the excitation for the nodes at Y = -11.2 m has been defined, corresponding with a location of the explosive at X = 20 m, Y = -51.2 m and Z = 30 m. Results of this analysis are shown in fig. 9.5. In all cases the responses are basically equal to those of the previous sections, even for the second case with the large discontinuity at Y = -10.2 m. So using realistic dimensions based on design drawings, it is not possible to get responses following the second type of solution.

In fact, the explanation was already formulated in chapter 8. Reversing the argumentation of the last paragraph of chapter 8, it is clear that:
- a stiffener spacing of 0.01 m leads to responses according to the (more realistic) second type of solution.
- a stiffener spacing of 0.1 m leads to responses according to the first type of solution.

*Nonsymmetry of bulkhead **not** important in case of realistic dimensions*

As the current model has a realistic stiffener spacing of 0.6 m, it is obvious that nonsymmetry of the bulkhead can **not** be responsible for the attenuation of the shock wave. A typical characteristic for the second type of solution is that the nonsymmetrical stiffener contains a relatively large amount of energy. According to chapter 8, a stiffener spacing of 0.01 m gives results according to fig. 3.6 b) and fig.

5.8, so fig. 5.8 gives the energy distribution for the second type of solution. Also according to chapter 8, a stiffener spacing of 0.1 m gives results according to fig. 4.4 a) and fig. 5.4, so fig. 5.4 gives the energy distribution for the first type of solution. So:

- for the second type of solution, 58 percent of the total energy is located within the nonsymmetrical stiffener (fig. 5.8),
- for the first type of solution, 44 percent of the total energy is located within the nonsymmetrical stiffener (fig. 5.4),
- for the current model with realistic dimensions, which results in the first type of solution, only 19 percent of the total energy is located within the nonsymmetrical stiffener, see fig. 9.6.

So when using realistic dimensions as based on design drawings, the effect of the nonsymmetrical stiffener becomes too small.

9.4 Modified time-history for loading

Measured signal as excitation

Using the model from section 9.2 (T-stiffeners including slice of bulkhead with stiffener spacing of 0.6 m), an analysis has been carried out using the measured acceleration at the K-deck as excitation at the nodes with coordinates Y = -11.2 m. Results are shown in fig. 9.7. Although the time step during the calculation was sufficiently smaller than the time step of the measurement signal, the time step for which output was given was set at a larger value to reduce the amount of output. Therefore some of the peak values are missed, compare fig. 9.7 a) with the velocity at the K-deck level from fig. 2.2. As fig. 9.7 b) shows, again the maximum velocities at the deck levels are larger than those of the excitation, and as fig. 9.7 c) shows, phenomena within the responses at the deck levels are comparable with those as found within the solution of the first type.

Short duration pulse

Because it takes only 2.16 milliseconds for the wave to reach the F-deck (11.2 m), followed by reflections, an analysis has been carried out using only the plate of the bulkhead (so without stiffener), and using only a positive input pulse of 574.83 m/s^2 with a duration of 0.2 milliseconds. Results are shown in fig. 9.8. Table 9.4 summarizes the travelling of the waves at the H-deck level. The situation at 9.6 milliseconds corresponds with the situation at 1.0 milliseconds, and so the history as shown in the table will be repeated. The values within the table correspond quite well with fig. 9.8, so the solution is correct. As a result, the velocities at the deck levels

Table 9.4 Summary of incoming and reflected waves at the H-deck level

Time [ms]	Reflection from:	Direction	Type	Sign of acceleration
1.0	Incoming	Upwards	Compressive	Positive
3.3	F-deck	Downwards	Tensile	Positive
5.3	Bottom	Upwards	Tensile	Negative
7.6	F-deck	Downwards	Compressive	Negative
9.6	Bottom	Upwards	Compressive	Positive

become twice as large as the input velocity, either directly when the response started (F-deck), or at later time values, see fig. 9.8 c). So basically indeed the solution of the first type is found (oscillation around input velocity).

Applying the same excitation to the original model (slice of bulkhead including T-profiles) results in fig. 9.9. Comparison of fig. 9.9 with 9.8 clearly shows the disturbances within the responses as caused by partial reflections at impedance changes (from T6 to T4.5 to T3-profiles).

9.5 Synthesis

Within previous chapters, it was concluded that nonsymmetry of the bulkhead might be a reason for the attenuation of the shock wave. Applying a nonsymmetrical stiffener at the bulkhead resulted in a second type of solution, which is much more realistic than a first type of solution when compared to measurements, although the attenuation of the shock wave still was not found (nonsymmetry influences all the responses within the bulkhead, independent of the deck level). However, based on the results of this chapter, it is obvious that in case of real dimensions the amount of nonsymmetry of the bulkhead is too small to explain the attenuation of the shock wave (with real dimensions, again the first type of solution is found).

Results show that the maximum allowed imperfections are too small to have its effects on the responses within the bulkhead.

Reflections at Y=-11.2 m not correct

Based on section 9. 4, it is clear that from a numerical point of view the first type of solution is correct (overshoot of responses with a factor 2 when compared to the input velocity is simply caused by the reflections at the F-deck level). One might argue that in reality at the base of the model no reflections will occur (bottom structure neglected in current model, shock wave (partly) returned to the surrounding water). This might be investigated using a non-radiating boundary condition here, but firstly this reflection has a decreasing effect on the velocity responses, and secondly this reflection reaches the H-deck at 5.3 milliseconds. At this time value, the maximum velocities as caused by the reflection at the F-deck are already past, and therefore this will not cause a better correlation with the measurements (shock attenuation).

Uncertainty about loading, excitation

Finally, it might be discussed whether it is allowed to use a measured signal at a bulkhead (or a derived kick-off velocity pulse) as an excitation within this kind of analysis, because only the first 2 to 4 milliseconds of these signals contain the original input shock wave. Within the analyses, it is not taken into account that for later time values the resulting measured signal is built up from a number of waves travelling both upwards and downwards. So although at the base of the model at Y=-11.2 m the measured signal is correctly followed (fig. 9.7 a)), slightly above the base of the model the calculated response by definition will not correspond with

measurements (in the analysis, the complete measured velocity travels upwards, in reality parts will travel upwards and parts will travel downwards). This might even be the case for the first milliseconds, because the double bottom structure probably will already cause a lot of reflections.

10. Shock and vibration symposium

At the 70th shock and vibration symposium one session dealt with the analysis of the full scale shock trial of the DDG-53. An extremely large model has been developed by Gibbs and Cox Inc. This model contains a detailed, refined model for the CIC-deck. The model has been verified independently by the Electric Boat Corporation. This model has been analyzed by both Weidlinger Associates and the Naval Postgraduate School, using FUSE/SRUE and LS-DYNA/USA respectively. These companies did not have the measurement data available. A comparison between measurements and analysis results has been carried out by NSWC/CD.

Weidlinger Associates uses Rayleigh damping (5 percent at 4 Hz, 1 percent at 40 Hz, 5 percent at 250 Hz). It was concluded that damping did not have effects on the responses at keel and bulkhead, while the late time responses at the CIC-deck become better when applying damping.

The Naval Postgraduate School also uses Rayleigh damping (4 percent at 5 and 250 Hz).

A comparison between analyses results and measurements was presented by Mr. Handleton from NSWC/CD. This comparison was based on the Russell factor. Measurements included in this comparison did also contain a number of measurements at a bulkhead at higher deck levels. Unfortunately, only a few viewgraphs were shown comparing calculated responses with measured responses. Russell factors for all measurements included within the comparison were given as a function of frame number, such that it was difficult to distinguish between measurements at high and low deck levels.

Afterwards these results were shortly discussed with Mr. Handleton and Mr. Winnette. Indeed, no separate comparison was made dependent on the deck level of the measurement. According to Mr. Winnette, within a bulkhead the measured accelerations do show a degradation, but the maximum velocities are very close.

Finally, based on the Russell factor the results from SRUE/FUSE seems to be slightly better than the results calculated with LS-DYNA/USA.

11. Measurements and simplified analyses

11.1 Analysis of measurements

The measurements from shot 2 of the M-frigate trials which were located at the centerline of bulkhead 97 has been integrated twice to obtain displacements, see fig. 11.1 a). Subtraction of these displacements and division by the distance (difference in Y-coordinate as shown in fig. 11.1 a)) results in the strains within the bulkhead, see fig. 11.1 b). Multiplication with the Young's modulus results in the stresses, see fig. 11.1 c).

Reasonable accuracy when using measurements to derive overall stresses

According to fig. 11.1 c), the maximum compressive stress is 60 N/mm^2. According to chapter 9, in case of dimensions based on the design drawings, the maximum stress is approximately 300 N/mm^2. However, see the tables in chapter 9, these maximum stresses occur either within the stiffener at impedance discontinuities or at the F-deck level, where the input shock wave coincides with the reflection. Therefore fig. 11.2 shows stresses as derived for the perfect case from section 9.2. The first two lines represent stresses calculated in the same way as for the measurements (namely displacement at G-deck level minus displacement at H-deck level, divided by the distance of 3 m and multiplied with the Young's modulus). The last line represents the vertical stress component as calculated by LS-DYNA. Apart from the time scale, which contains the same phenomena as fig. 9.2, the levels of the stresses correspond quite well with each other and with those as derived from the measurements. So using measured accelerations to derive overall stresses seems to be reasonably accurate.

11.2 Analyses of 8-dof mass-spring system

As there are eight vertical measurements available at bulkhead 97 (fig. 2.1, 2.2), in this section analyses results will be given for a simple system with eight masses, and seven springs and discrete dampers. This eight degrees of freedom system has been analyzed with LS-DYNA. The aim is to find the same phenomena as present within the measurements (attenuation of shock wave). The eight degrees of freedom are supposed to correspond with the measurement locations (so K-deck, J-deck, H-deck, G-deck, F-deck, E-deck, B-deck and top of mast respectively). In all cases the excitation is located at the first mass (K-deck), with the same pulse shape as used in the previous chapters (fig. 2.3).

Using $F = E \cdot A \cdot \Delta l / l$, with A built up from the area of the T6 profile and the dimensions of the bulkhead plate (stiffener spacing 0.6 m, thickness 7 mm), with length l equal to 1 m, a typical spring stiffness k of $1.32 \cdot 10^9$ N/m is obtained ($F = k \cdot \Delta l$, k =

E•A/l). Using the total mass of the M-frigate of 3400 tonnes, division by 11 (number of bulkheads), division by 14 (width of frigate) and multiplying with 0.6 results in 13.2 tonnes per bulkhead per stiffener spacing. Equal distribution results in a typical mass of 1.656 tonnes. This is case 1 from table 11.1.

Remarkable correspondence with full FEM-results

Basically the responses for case number 1 (fig. 11.3) show the same phenomena as e.g. within fig. 9.2 a), but with a different time scale. This is caused by the different value for the velocity of sound ($\sqrt{E/\rho}$ = 5188 m/s) and the more or less corresponding value for $\sqrt{k/m}$ (= 893 1/s). Therefore case number 2 of table 11.1 has been analyzed ($\sqrt{k/m}$ = 5188 1/s). Comparison of fig. 11.4 with e.g. fig. 9.2 a) shows that now the responses correspond remarkably well. This case will be the starting point for a number of runs in which variables are varied. These variations are listed in table 11.1.

Damping effects mainly late time response

The first variation carried out considers the effect of damping. Viscous dampers are used, with different values for the damping coefficients, see cases 3 to 5 from table 11.1. The notation used for case 5 means that the first damper (between K-deck and J-deck) has a damping coefficient of $1 \cdot 10^8$ Ns/m, while the remaining six dampers has a coefficient of $1 \cdot 10^7$ Ns/m. As fig. 11.5 a) shows, a moderate damping coefficient mainly effects the late time responses. If damping coefficient becomes larger, the responses tend to follow the input pulse (fig.11.5 b)).

Changed mass and spring stiffness effects time scale

The effect of moderate changes within the masses is shown in cases 6 to 8 of table 11.1, see fig. 11.6. For case 8, a linear distribution of the masses is used from 13.84 tonnes at the K-deck up to 1.73 tonnes at the top of the mast. This results in the same total mass. Comparison of fig. 11.6 with fig. 11.4 shows that mainly the time scale changes, because of other frequencies ($\sqrt{k/m}$). The same conclusion holds if only the spring stiffnesses are varied, see case 9 to 11 of table 11.1 and fig. 11.7 a) to c). The change in the time scale within the responses can be explained using the frequency contents of the system ($\sqrt{k/m}$), but also by discussing the velocity of sound. As known from section 9.4 (table 9.4, fig. 9.8) and section 4.3 (fig. 4.5), the overshoot within the velocity responses with a factor 2 when compared to the input

Table 11.1 Summary of analyzed cases using 8-dof mass-spring system

No.	Mass [tonnes]	Spring stiffness [N/m]	Damp. [Ns/m]	Freq. [Hz]	Figure
1	1.656	$1.32 \cdot 10^9$	-	142.1	11.3
2	7.800	$2.10 \cdot 10^{11}$	-	825.8	11.4
3	7.800	$2.10 \cdot 10^{11}$	10^7	825.8	11.5 a)
4	7.800	$2.10 \cdot 10^{11}$	10^8	825.8	11.5 b)
5	7.800	$2.10 \cdot 10^{11}$	10^8 (1) 10^7 (6)	825.8	11.5 c)
6	0.780	$2.10 \cdot 10^{11}$	-	2611.4	11.6 a)
7	78.0 (1) 7.8 (7)	$2.10 \cdot 10^{11}$	-	261.1; 825.8	11.6 b)
8	Lin:13.84-1.73	$2.10 \cdot 10^{11}$	-	620.-1753.3	11.6 c)
9	7.800	$2.10 \cdot 10^{10}$	-	261.1	11.7 a)
10	7.800	$2.1 \cdot 10^{10}$ (1) $2.1 \cdot 10^{11}$ (6)	-	261.1-825.8	11.7 b)
11	7.800	Lin: $2.1 \cdot 10^{11}$ - $3.0 \cdot 10^{10}$	-	825.8-312.1	11.7 c)

pulse is caused by the reflections, and therefore a decreased spring stiffness (fig. 11.7 a)) leads to a smaller velocity of sound and so to another ratio between incoming and reflected waves. Fig. 11.8 shows the accelerations for cases 2, 6 and 9 from table 11.1. At the top of the mast the acceleration roughly doubles (coinciding incoming and reflected wave). At later time values, the acceleration at F-deck and J-deck doubles (reflected wave travelling downwards). The same phenomena can be recognized within fig. 11.8 b) and c), but at different time values (different masses, spring stiffnesses). As a different time scale is one of the phenomena within the shock attenuation, within the next section these analyses are repeated using much larger variations for the different variables.

11.3 Analyses of 8-dof mass-spring system, extreme variations

Table 11.2 summarizes the cases as analyzed. Each variable has been varied using extreme values. An extreme variation of the damping coefficient results in more or less unchanged responses (case 12 and 13, fig. 11.9).

Increased time to maximum velocity at higher deck levels found when high frequencies introduced at low deck levels

An extreme variation of the mass with heavy masses at the K-deck level and small masses at the top of the mast results in very high-frequent responses at the higher levels, see fig. 11.10 b) (case 14). Combining this case with moderately damping results in fig. 11.10 c), showing more or less unchanged responses when compared with fig.11.4 (case 15). Opposite, an extreme variation of the mass with small masses at the K-deck level and heavy masses at the top of the mast results in very high-frequent responses at the lower deck levels, see fig. 11.11 a) and b) (case 16). For this case, clearly the increasing time needed to reach the maximum velocity at higher deck levels is found (as present within the shock attenuation). Combining this case with moderately damping results in fig. 11.11 c) (case 17). So high frequencies at low deck levels seems to cause the increased time to maximum velocity at higher deck levels as measured during shock trials.

When analyzing an extreme variation of the spring stiffnesses with low stiffnesses

Table 11.2 Summary of analyzed cases using 8-dof mass-spring system with extreme variations (L means linear variation)

No.	Mass [tonnes]	Spring stiff. [N/m]	Damp. [Ns/m]	Freq.[Hz]	Figure
12	7.800	$2.10 \cdot 10^{11}$	L 10^{9}-10^{3}	825.8	11.9 a)
13	7.800	$2.10 \cdot 10^{11}$	L 10^{3}-10^{9}	825.8	11.9 b)
14	L $7.8 \cdot 10^{3}$-$7.8 \cdot 10^{-4}$	$2.10 \cdot 10^{11}$	-	26.1-82581.	11.10 a), b)
15	L $7.8 \cdot 10^{3}$-$7.8 \cdot 10^{-4}$	$2.10 \cdot 10^{11}$	10^{7}	26.1-82581.	11.10 c)
16	L $7.8 \cdot 10^{-4}$-$7.8 \cdot 10^{3}$	$2.10 \cdot 10^{11}$	-	82581.-26.1	11.11 a), b)
17	L $7.8 \cdot 10^{-4}$-$7.8 \cdot 10^{3}$	$2.10 \cdot 10^{11}$	10^{7}	82581.-26.1	11.11 c)
18	7.800	L $2.1 \cdot 10^{8}$-$2.1 \cdot 10^{14}$	-	26.1-26114.	11.12 a), b)
19	7.800	L $2.1 \cdot 10^{8}$-$2.1 \cdot 10^{14}$	10^{7}	26.1-26114.	11.12 c), d)
20	7.800	L $2.1 \cdot 10^{14}$-$2.1 \cdot 10^{8}$	-	26114.-26.1	11.13 a), b)
21	7.800	L $2.1 \cdot 10^{14}$-$2.1 \cdot 10^{8}$	10^{7}	26114.-26.1	11.13 c)

at low deck levels and high stiffnesses at high deck levels results in very high-frequent responses at high deck levels, see fig. 11.12 a) and b) (case 18). The low frequencies at low deck levels cause a delayed response (fig. 11.12 a). If damping is introduced, responses become as shown in fig. 11.12 c) and d). Fig. 11.13 shows the responses for the opposite case, with high stiffnesses at low deck levels and low stiffnesses at high deck levels.

Some aspects of shock attenuation found, but with unrealistic model changes

Finally table 11.3 summarizes the results. Case 16 shows the best correspondence with the different phenomena as present within the shock attenuation, but unfortunately the corresponding model changes (small masses at low deck levels, large masses at high deck levels) do not correspond with a real ship structure. None of the cases show a decreased maximum velocity for higher deck levels. However, neglecting the velocity at the K-deck level in fig. 2.2, the remaining measured velocities show a slightly increasing maximum value (probably caused by the reflection at the top).

Table 11.3 Summary of analyzed cases using 8-dof mass-spring system with extreme variations; Frequency contents versus results

Figure number:	Case 14 11.10	Case 16 11.11	Case 18 11.12	Case 20 11.13
Masses at K-deck	Large	Small		
Masses at top of mast	Small	Large		
Stiffness at K-deck			Small	Large
Stiffness at top of mast			Large	Small
Correspondence measures above with ship	++	--	--	++
Frequencies of responses at J-deck	Low	High	Low	High
Frequencies of responses at top of mast	High	Low	High	Low
Correspondence shock attenuation:				
High-frequent at low deck levels	--	++	--	++
Low-frequent at high deck levels	--	++	--	++
Increased time to maximum velocity	--	++	++	+/-
Decreased value for maximum velocity	--	--	--	--

11.4 Synthesis

Using the measurements to derive stresses within the bulkhead, leads to a reasonable correspondence with the calculated stresses.

Using an eight degrees of freedom mass-spring system, it is possible to find responses corresponding very well with those of the full finite element model. To get the same time scale, the value for $\sqrt{k/m}$ has to correspond with the value for $\sqrt{E/\rho}$. Changing the model variables (mass, spring stiffness, damping coefficients) in such a way that the changes are realistic with respect to a real ship structure, the changes within the calculated responses are small. Changing the model variables with large

values, some phenomena as present within the measured attenuation of the shock wave can be calculated, but the resulting model values are unrealistic when compared to a real ship structure.

However, in this way it is possible to find high-frequent responses at low deck levels, low-frequent responses at high deck levels and an increased time to maximum velocity at high deck levels. It is not possible to find a decreased maximum velocity for higher deck levels, but when neglecting the measurement at the K-deck level, in fact the measurements show a slightly increasing maximum velocity for higher deck levels, probably because of the reflections at the top. Regarding the uncertainty in the excitation as discussed in section 9.5, while it is known that the loading of the ship has high-frequent components because of cavitation and so on, the value of these results is questionable (high frequencies introduced by changing $\sqrt{k/m}$ within the model, in stead off within the excitation).

12. Conclusions and recommendations

A number of analyses has been carried out using LS-DYNA to find a physical explanation for the attenuation of the shock wave. The shock attenuation, which is always measured during shock trials, has the following characteristics:

- At higher deck levels, the maximum amplitudes of the accelerations decrease, and higher frequencies disappear.
- At higher deck levels, the maximum velocities become smaller, and the rising time (time to maximum velocity) increases.

Thus far, this phenomenon is not found using numerical analyses. Within this report, a two-dimensional model is used representing a longitudinal slice of a frigate. The third dimension in athwarthships direction is infinitely long.

Analyses have been carried out using three different basic models, namely for a generic model, for a model with dimensions based on the design drawings and for a model containing only eight masses, springs and stiffnesses to represent the different deck levels at bulkhead 97 of the M-frigate.

Based on the results for the generic model as presented in this report (chapter 3 to 8), it can be concluded that:

- Nonsymmetry of the bulkhead such as a vertical stiffener at one side has a very large effect on the responses within the bulkhead. The bending as caused by these nonsymmetrical effects cause a dispersion of the input shock wave.

Generic model: Large amount of nonsymmetry causes realistic responses

- The responses in case of a nonsymmetrical bulkhead become much more realistic when compared to measurements from shock trials. However, the nonsymmetry has its effects on the responses at all locations within the bulkhead, independent of the deck level, and therefore the current analyses do not show the attenuation of the shock wave.
- The maximum velocities within the bulkhead at the different deck levels are reached within a few milliseconds. Because other effects as damping and transport of energy to the decks do need more time to dissipate energy or to reduce the amount of energy within the bulkhead by transporting it to the decks, these phenomena are not responsible for the attenuation of the shock.
- In fact, analyses results show that the decks can be excluded from the model without any effects on the responses within the bulkhead.
- The nonsymmetry of the bulkhead results in stresses within the bulkhead of three times the yield stress. Including plasticity influences the responses within the bulkheads (inclusive the maximum velocities), but again the effects are comparable at each deck level within the bulkhead. So the attenuation of the shock wave is not found.
- So only two phenomena influence the maximum velocities within the bulkhead, namely nonsymmetry of the bulkhead and plasticity within the bulkhead. Damping and the type of model for the decks (large mass, large stiffness) do not influence the responses within the bulkhead.

- Thus far, these conclusions correspond with ref. [4] to [7], describing a number of DIANA analyses carried out for the same compartment using a three-dimensional model. Roughly summarized, in ref. [4] to [7] it was concluded that the mass distribution at the decks, flexible mounted masses at the decks, and damping do have large effects on the deck responses, but that responses within the bulkhead are independent of these model changes. Within these reports, the bulkhead was modeled symmetrically.

Model with dimensions based on design drawings

In addition, based on the results for the model with dimensions based on the design drawings as presented in this report (chapter 9), it can be concluded that:

- The amount of nonsymmetry within the bulkhead as built is too small to find the above mentioned effects within the responses.
- Imperfections, even with the maximum allowed amplitude, are too small to influence the calculated responses.
- Stresses are smaller than the yield stress, so using the current model plasticity can not cause the attenuation of the shock wave.

Based on an analysis of the measurement signals from shot number two of the M-frigate shock trials, it can be concluded that the stresses as derived from these measurements correspond reasonably well with those as calculated (chapter 11).

Eight degrees of freedom mass-spring model

Finally, based on the results for the eight degrees of freedom mass-spring system (chapter 11), it can be concluded that:

- A remarkable correspondence with the responses of the full finite element model can be obtained if values for $\sqrt{k/m}$ are equal to the values for $\sqrt{E/\rho}$.
- A moderate variation of the variable values does hardly effect the responses.
- Changing the variables with several orders, it is possible to find:
  - high-frequent responses at low deck levels,
  - low-frequent responses at higher deck levels,
  - an increased time to maximum velocity for higher deck levels.
- So all phenomena of the attenuation of the shock wave are found, except for the decreasing maximum velocity for higher deck levels. However, neglecting the measurement at the K-deck level, the remaining measurements in fact show a slightly increasing maximum velocity for higher deck levels, probably caused by the reflection at the top.
- Unfortunately, the required values for the masses and spring stiffnesses to find these phenomena are unrealistic when compared to a real ship structure.

Summarizing the results of the two full finite element models, the only effect that might effect the responses in case of realistic dimensions is plasticity, but with the current model the stresses are smaller than the yield stress.

Recommendations

However, following section 9.5 and 11.4, it can be stated that:

- The unrealistic values for masses and spring stiffnesses are necessary within the eight degrees of freedom model to find high-frequent responses at low deck lev-

els. However, in reality the loading itself is high-frequent because of cavitation and so on, and probably high frequencies (reflections, compare fig 9.8 and 9.9) will be introduced by the double bottom structure, which is neglected in the current models.

- It is questionable whether a measured signal or the derived kick-off velocity can be used as excitation within this kind of analysis. Within 2 to 4 milliseconds, these signals contain both the incoming and reflected waves. If indeed the double bottom structure cause reflections, these signals might even contain reflections from the initial beginning. Using these signals as excitation at a truncated structure, results in two difficulties:
  - At the truncation, reflections occur which are not present in reality. This might be avoided by using a non-radiating boundary, but it has been discussed that this will not reduce the amount of overshoot of the calculated responses.
  - The signal forms an input shock wave travelling upwards. In reality, the measured signal is built up from the input wave travelling upwards and reflections travelling downwards. This is not taken into account.

All together, the truncation of the model and the loading seem to cause some inconveniences. Therefore it is recommended to extend the current model with the bottom structure, followed by an analysis including the fluid structure interaction (2DCAV or the porcupine theory as developed in the past). Another possibility can be the replacement of the thus far used prescribed accelerations by a prescribed force. Finally, it can be worthwhile to analyze the measurements of the DDG-53 shock trial regarding the shock attenuation phenomena.

13. References

[1] LS-DYNA User's Manual, Version 940
Livermore Software Technology Corporation, June 1, 1997

[2] J.O. Hallquist
LS-DYNA Theoretical Manual
Livermore Software Technology Corporation, May 1998

[3] MADYMO Theory Manual, Version 5.2
TNO Road-Vehicles Research Institute, July 1996

[4] W. Trouwborst
Transmissie van schok, responsieberekening van een compartiment van een fregat
TNO-report 94-CMC-R1365, November 1994

[5] W. Trouwborst
Shock transmission, response calculation of a compartment of a frigate including plasticity
TNO-report 95-CMC-R1143, January 1996

[6] W. Trouwborst
Shock transmission, response calculation of a compartment of a frigate with discrete masses and Rayleigh damping
TNO-report 97-CMC-R0290, July 1997

[7] W. Trouwborst
Shock transmission, shock response spectra of a compartment of a frigate with discrete masses and Rayleigh damping
TNO-report 97-CMC-R1270, November 1997

[8] W. Trouwborst
Benchmark GUI / OSE version 1.1 using full scale shock trial of FFG-59
TNO-report (DRAFT), March 1998

[9] W. Trouwborst
Application of the optimal state estimation method to the full scale M-frigate shock trials
TNO-report (DRAFT), February 1999

14. Figures

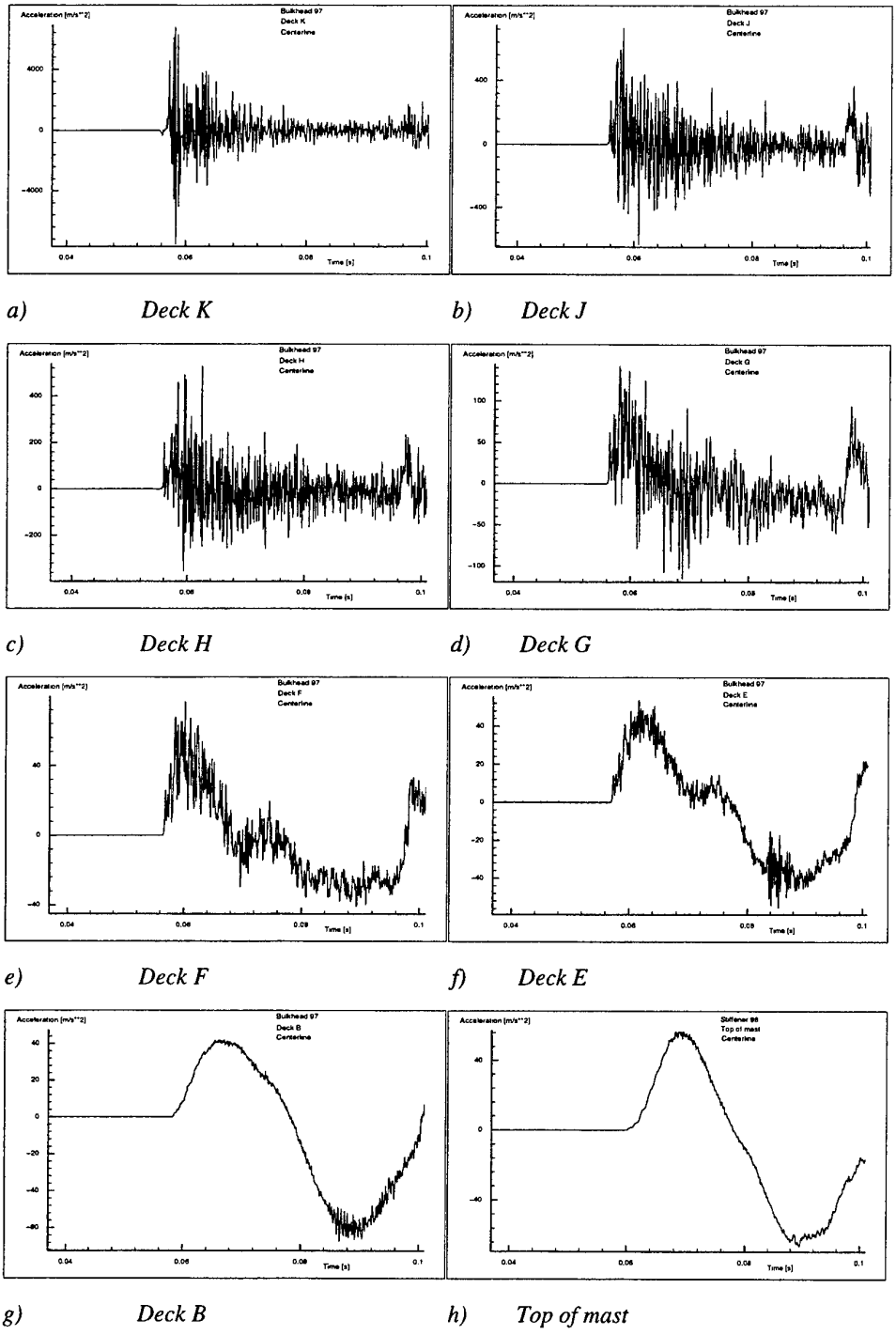

a) *Deck K* *b)* *Deck J*

c) *Deck H* *d)* *Deck G*

e) *Deck F* *f)* *Deck E*

g) *Deck B* *h)* *Top of mast*

Figure 2.1 *Measured accelerations at bulkhead 97 and centerline, different deck levels, shock trials M-frigate, shot number 2*

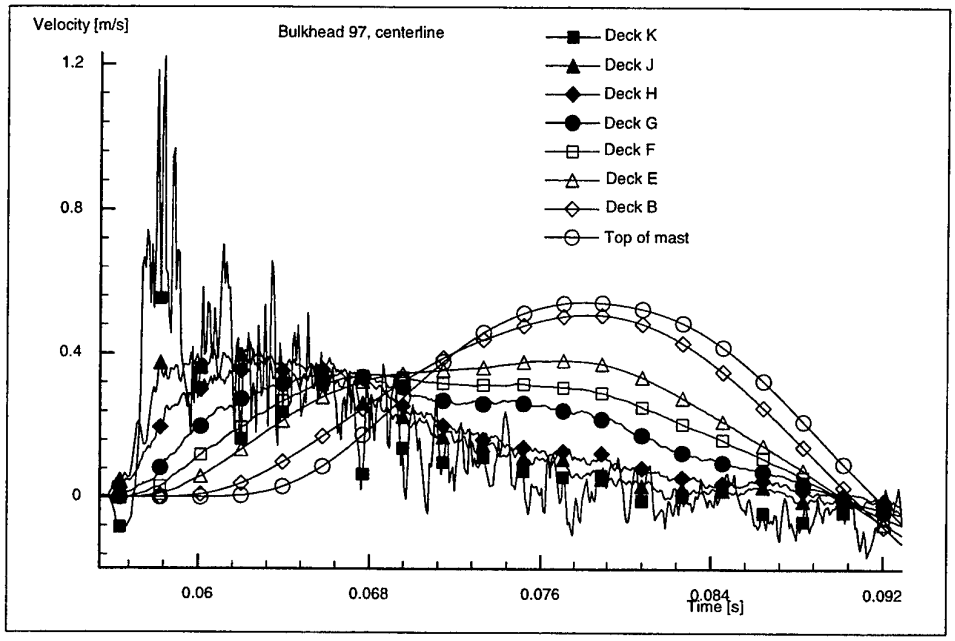

Figure 2.2 Velocities as integrated from measured accelerations at bulkhead 97 and centerline, different deck levels, shock trials M-frigate, shot number 2

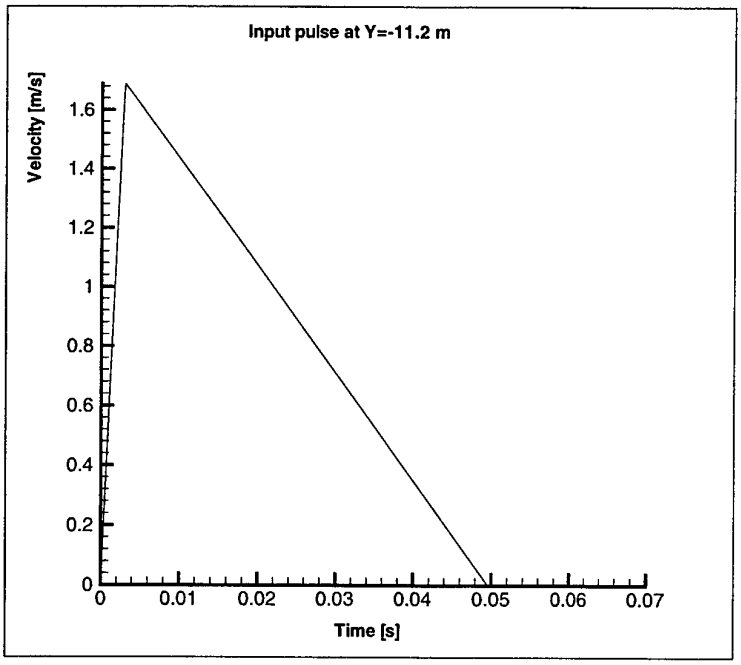

Figure 2.3 Input velocity pulse at Y=-11.2 m

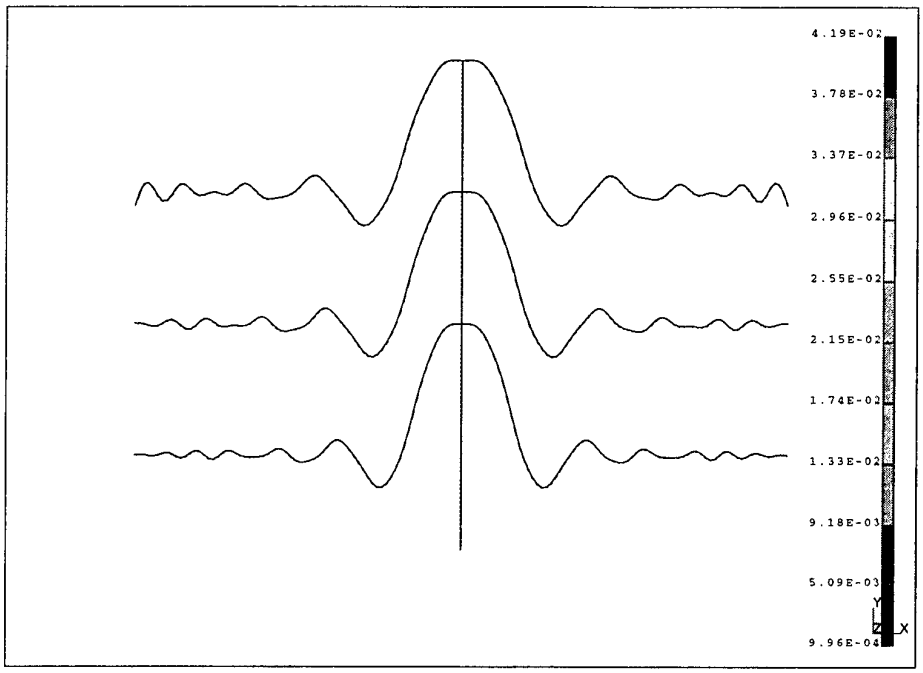

Figure 3.1 a) Deformed geometry at time 49.696 ms, element size 0.1 m

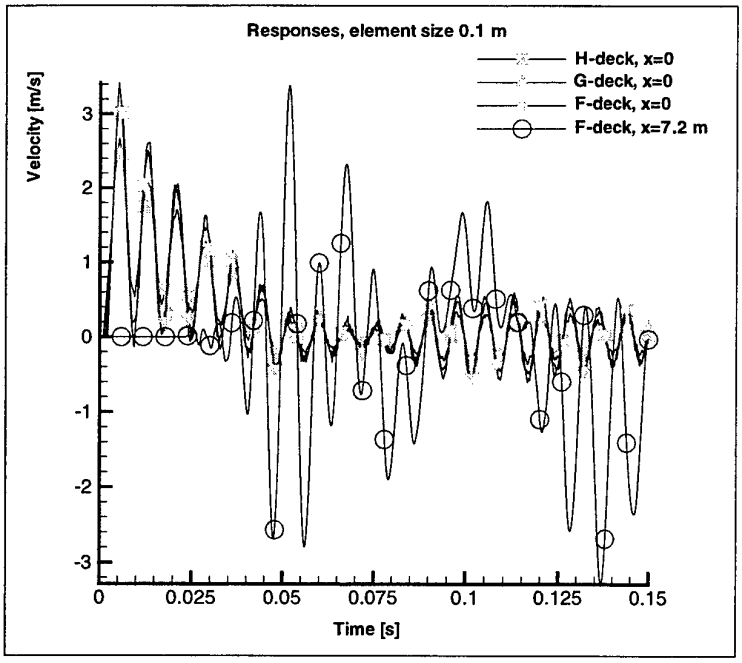

Figure 3.1 b) Velocity responses at the decks, element size 0.1 m

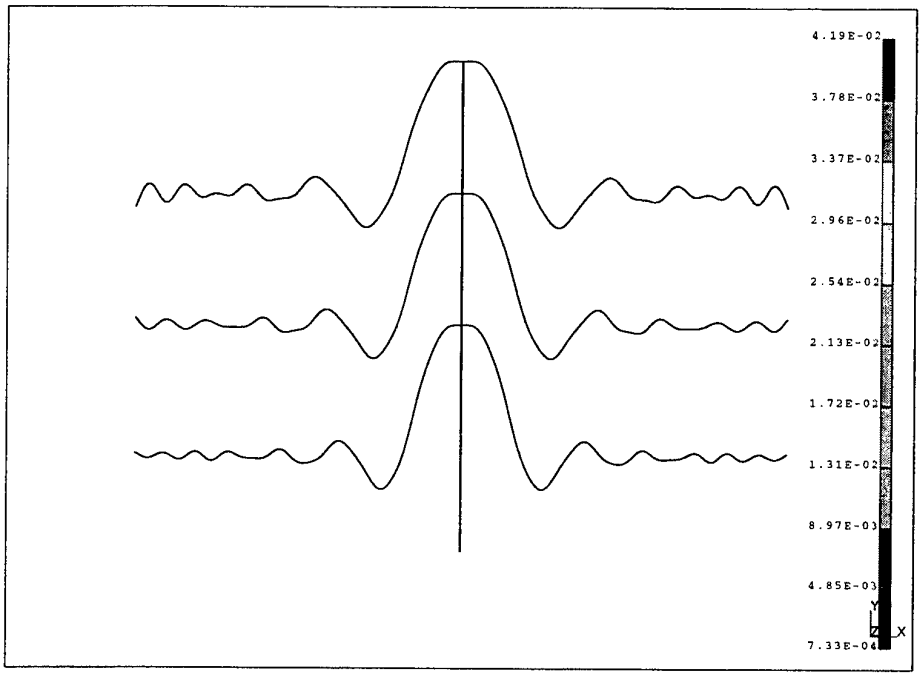

Figure 3.2 a) Deformed geometry at time 49.5 ms, element size 0.01 m

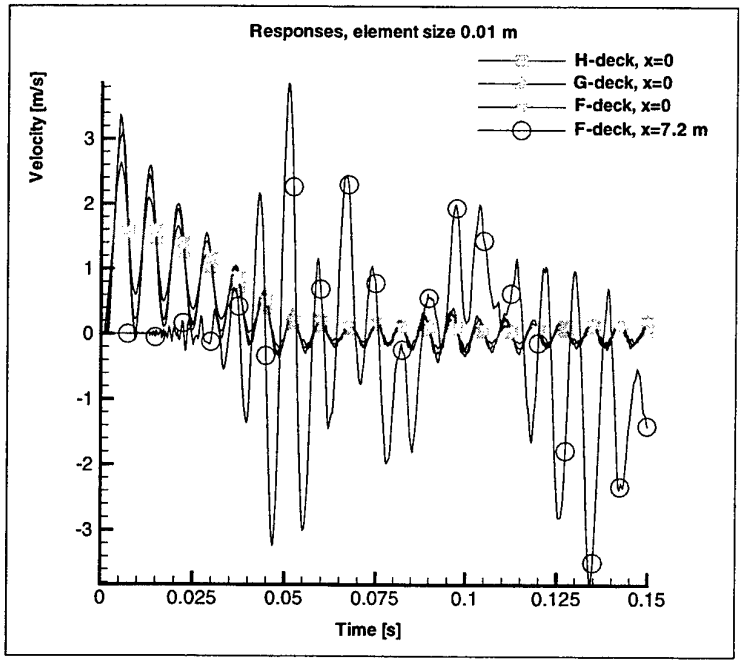

Figure 3.2 b) Velocity responses at the decks, element size 0.01 m

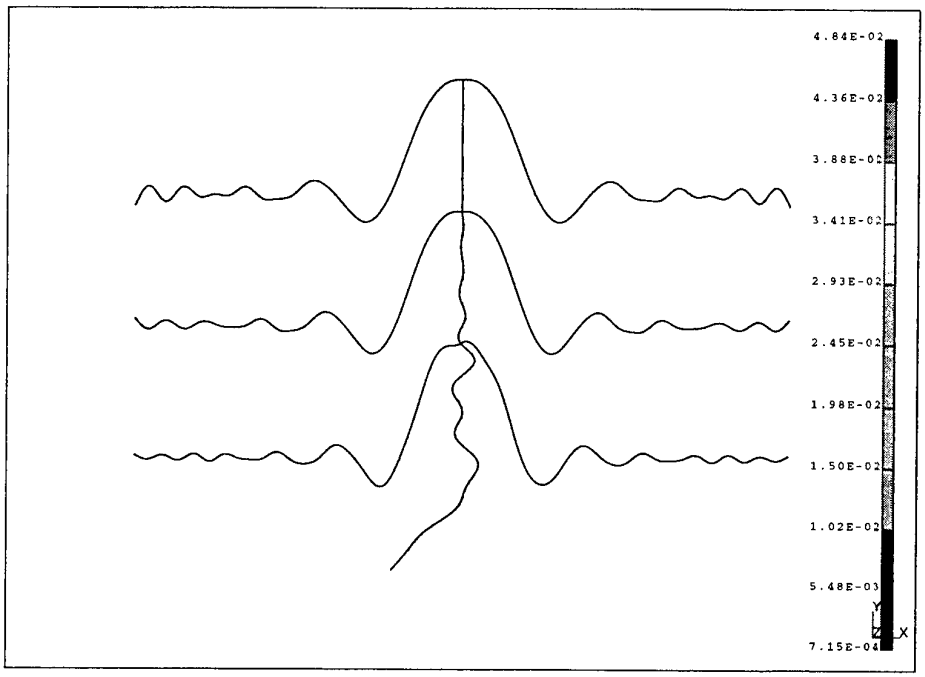

Figure 3.3 a) Deformed geometry at time 49.499 ms, element size 0.01 m, nonsymmetrical excitation

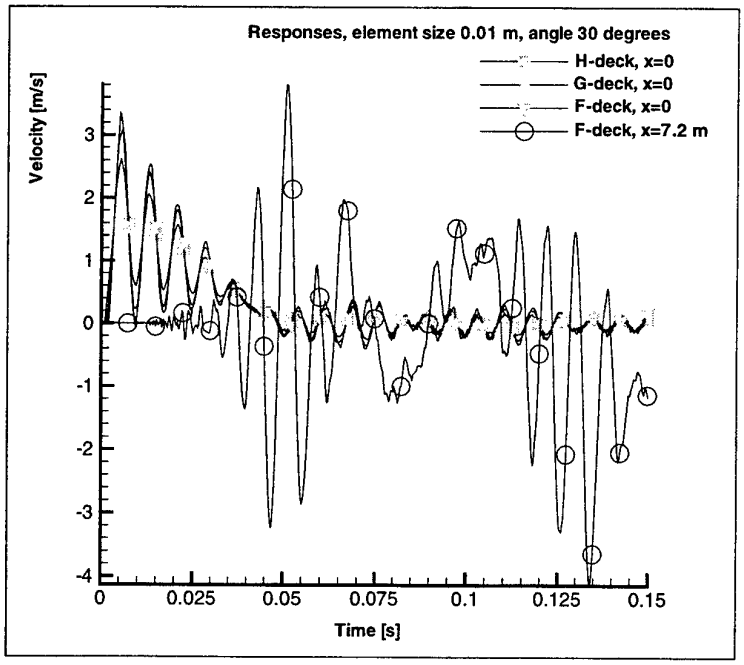

Figure 3.3 b) Velocity responses at the decks, element size 0.01 m, nonsymmetrical excitation

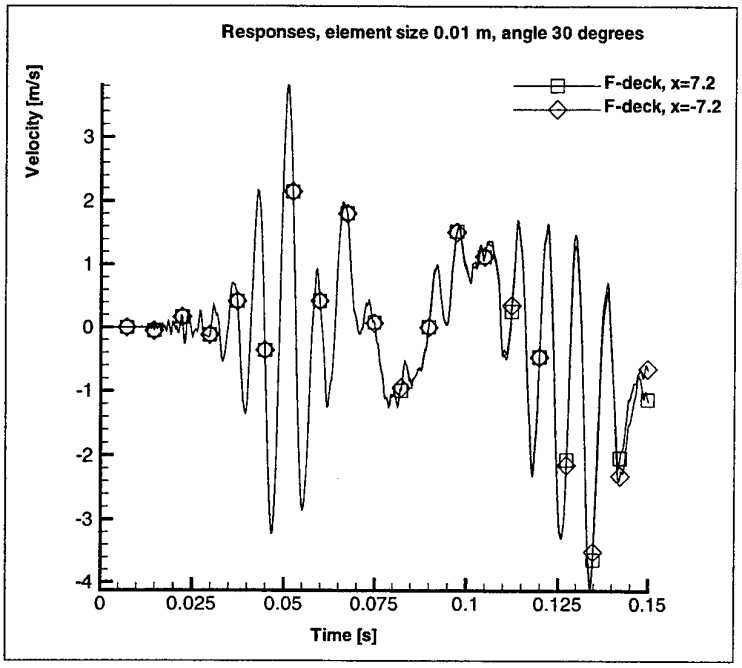

Figure 3.3 c) Velocity responses at the F-deck, element size 0.01 m, nonsymmetrical excitation

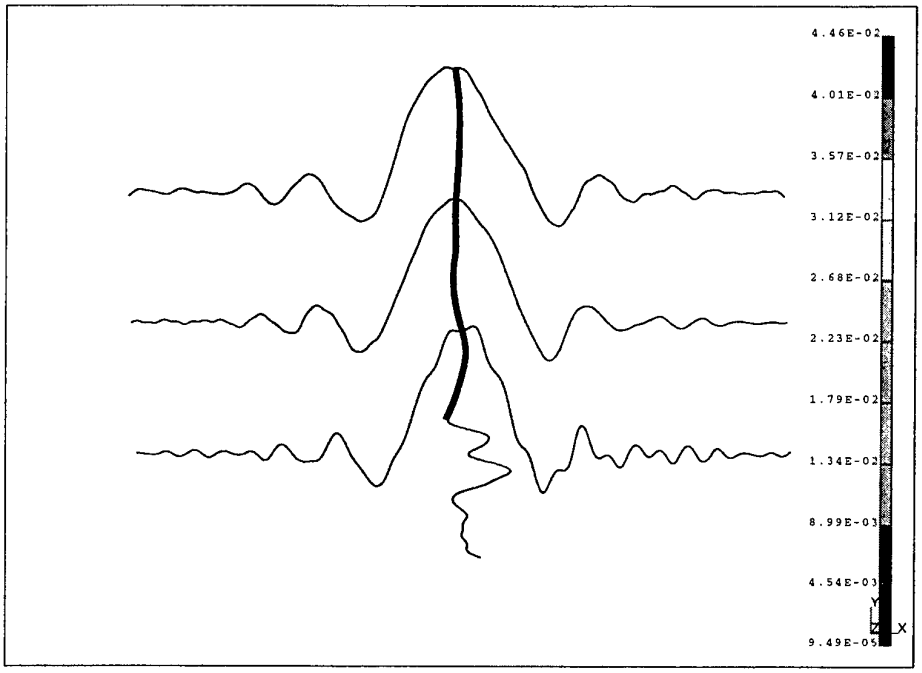

Figure 3.4 a) Deformed geometry at time 49.5 ms, element size 0.01 m, nonsymmetrical bulkhead

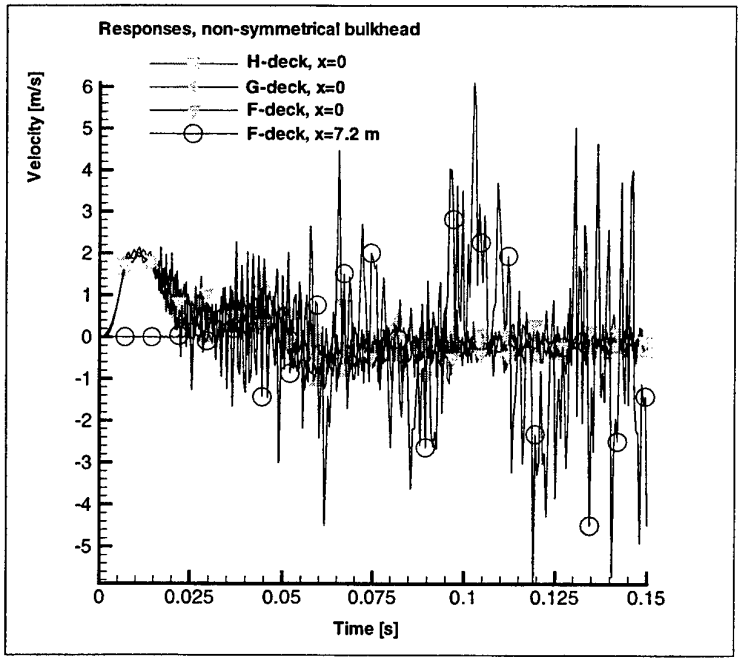

Figure 3.4 b) Velocity responses at the decks, element size 0.01 m, nonsymmetrical bulkhead

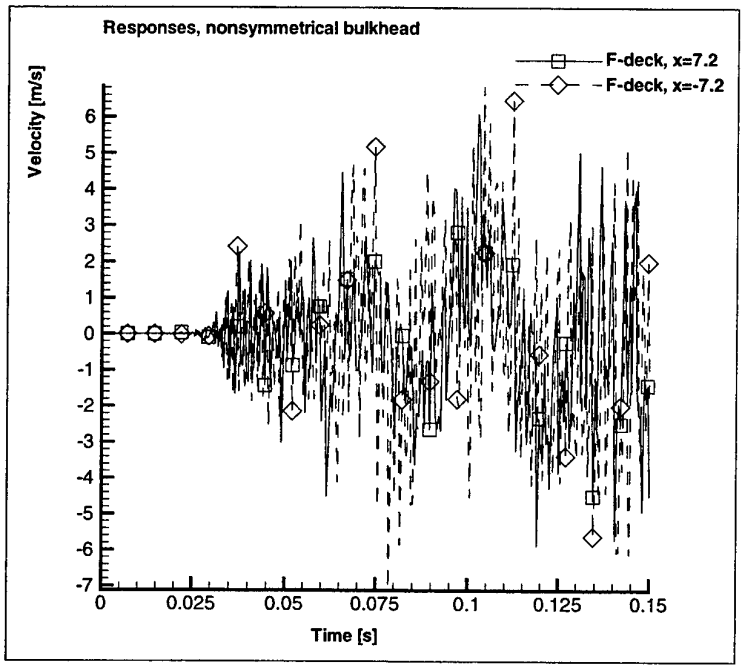

Figure 3.4 c) Velocity responses at the F-deck, element size 0.01 m, nonsymmetrical bulkhead

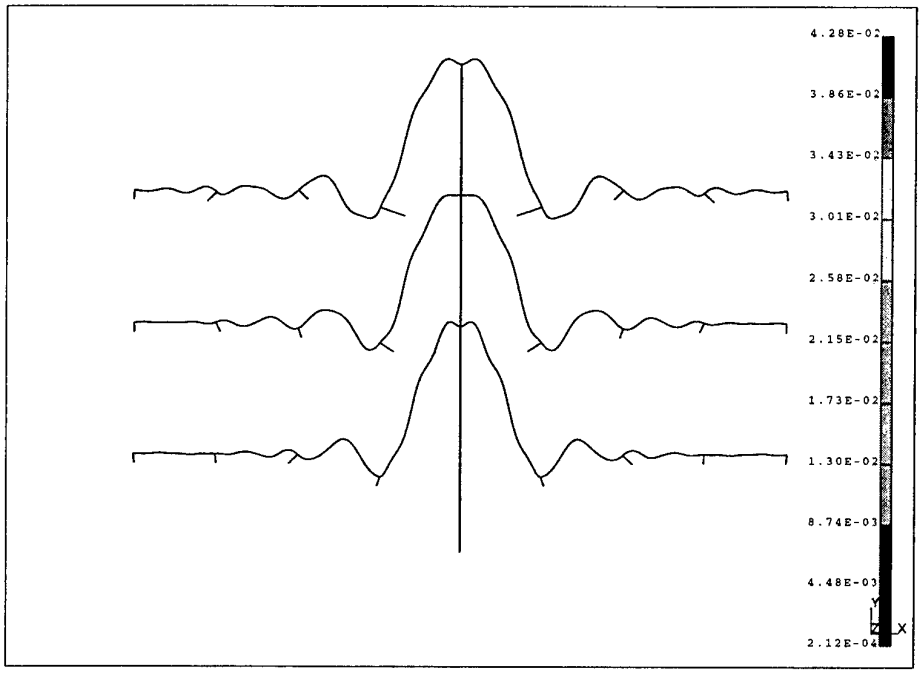

Figure 3.5 a) Deformed geometry at time 49.5 ms, element size 0.01 m, transverse frames included

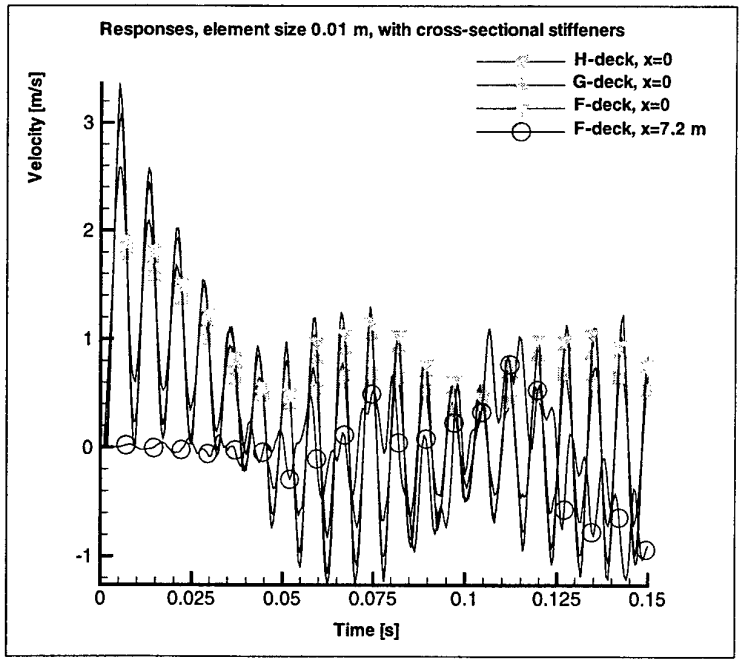

Figure 3.5 b) Velocity responses at the decks, element size 0.01 m, transverse frames included

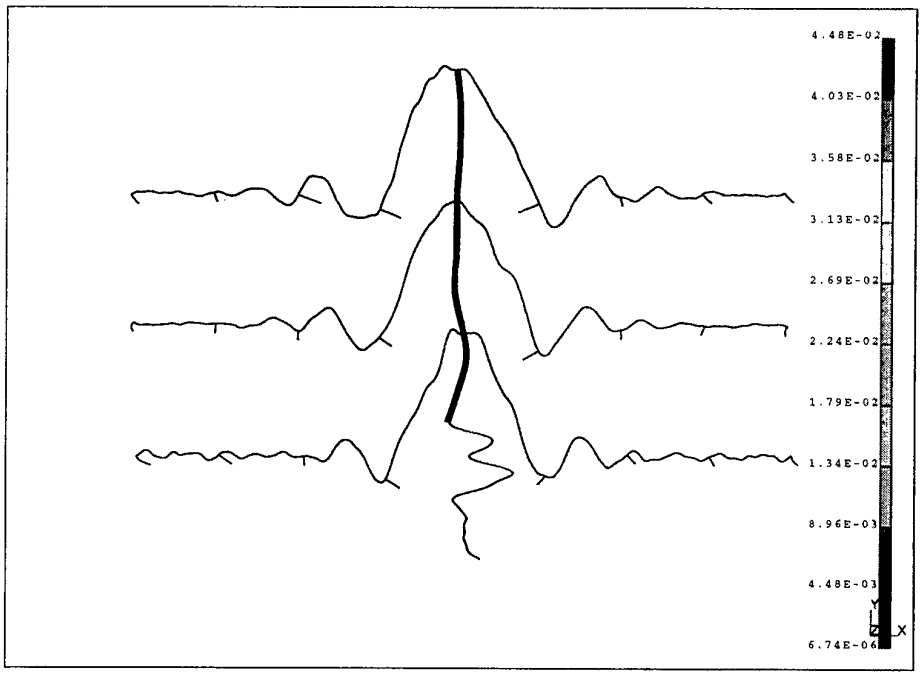

Figure 3.6 a) Deformed geometry at time 49.499 ms, element size 0.01 m, nonsymmetrical bulkhead

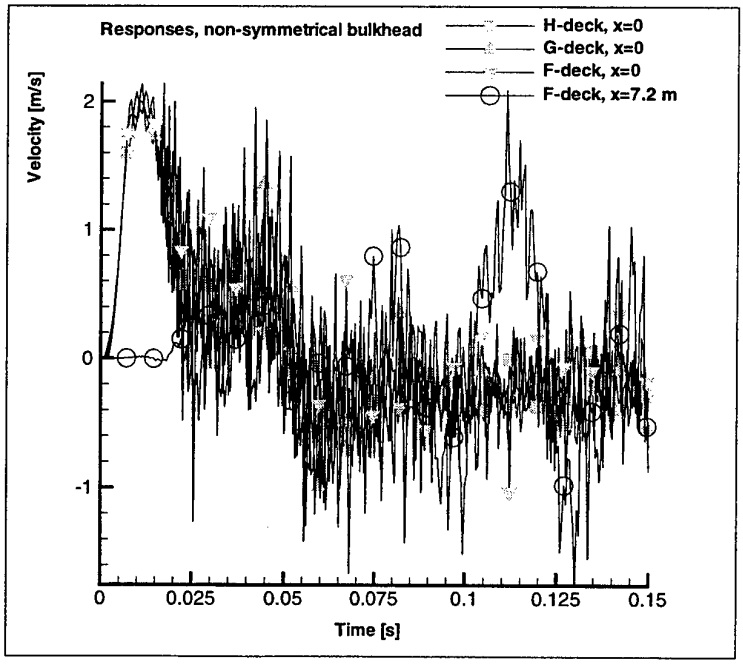

Figure 3.6 b) Velocity responses at the decks, element size 0.01 m, nonsymmetrical bulkhead

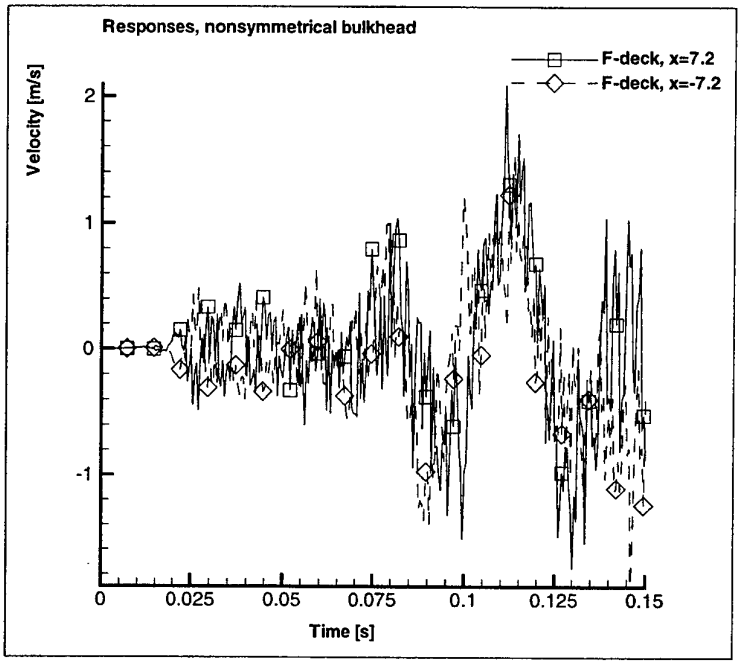

Figure 3.6 c) Velocity responses at the F-deck, element size 0.01 m, nonsymmetrical bulkhead

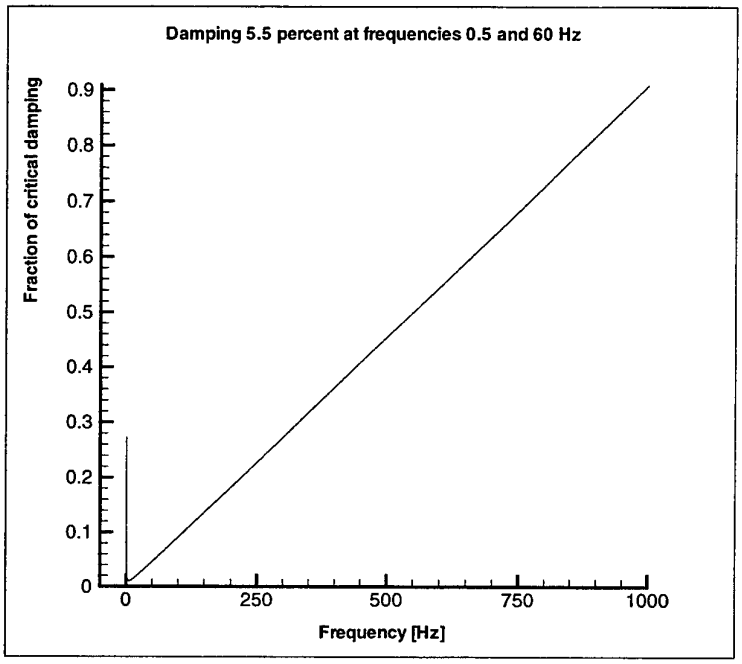

Figure 4.1 a) Rayleigh damping as used in ref. [6], based on 5.5 percent damping at 0.5 and 60 Hz

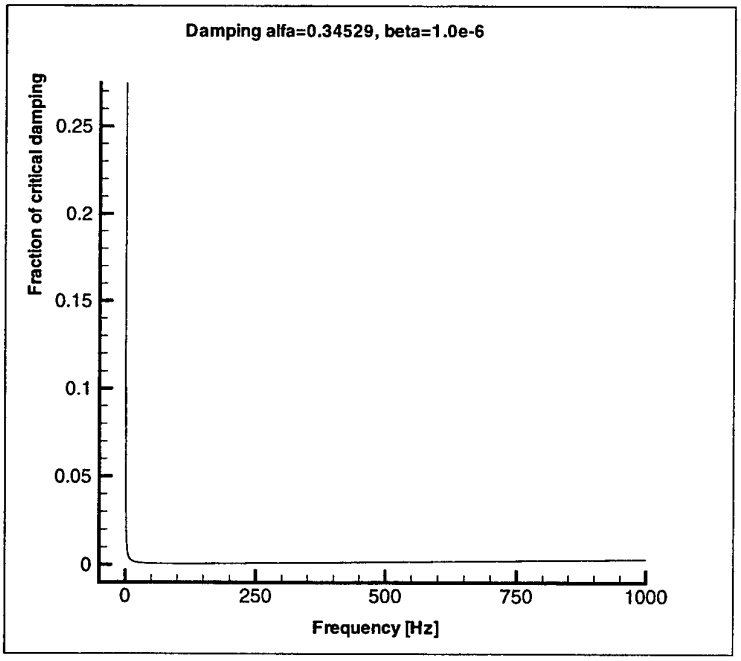

Figure 4.1 b) Modified Rayleigh damping, same a_0 (0.34529), modified a_1 (10^{-6})

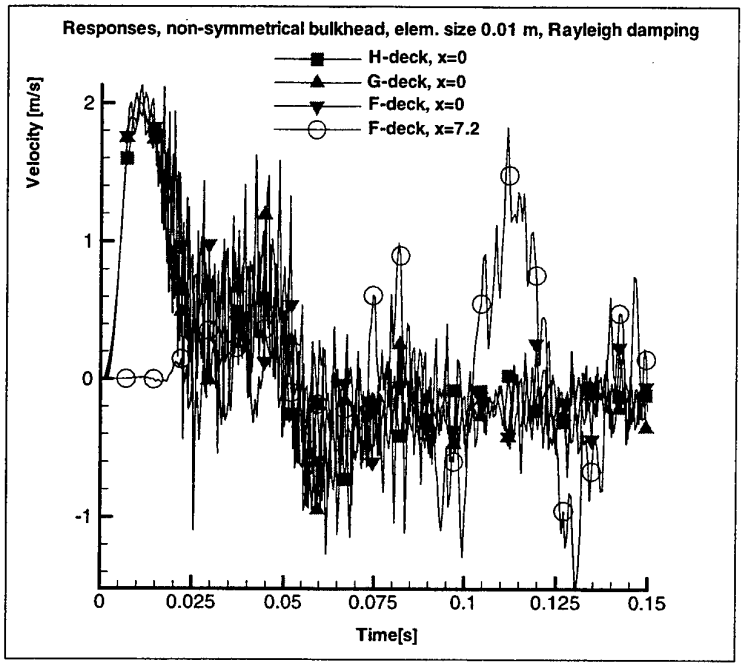

Figure 4.2 Velocity responses at the decks, element size 0.01 m, nonsymmetrical model, Rayleigh damping according to fig. 4.1 b) (compare fig. 3.6 b))

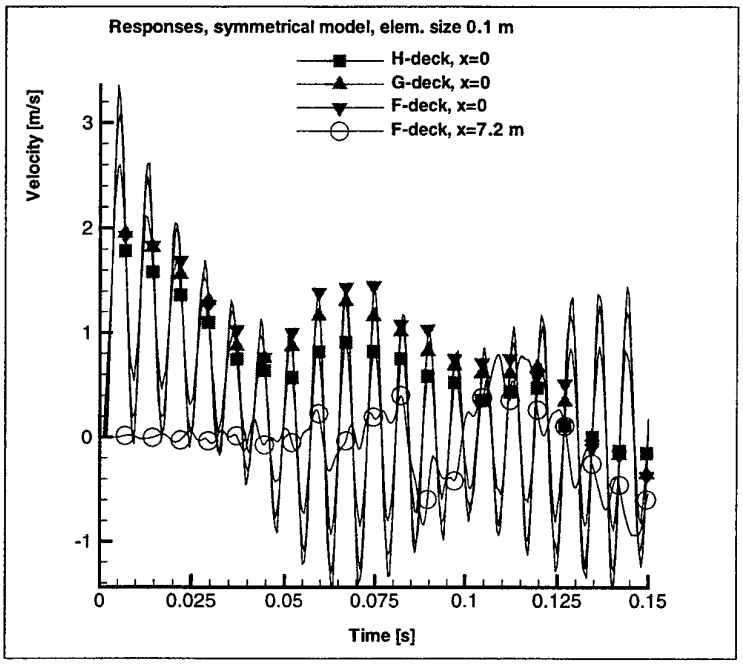

Figure 4.3 a) Velocity responses at the decks, element size 0.1 m, symmetrical model, no damping (compare fig. 3.5 b))

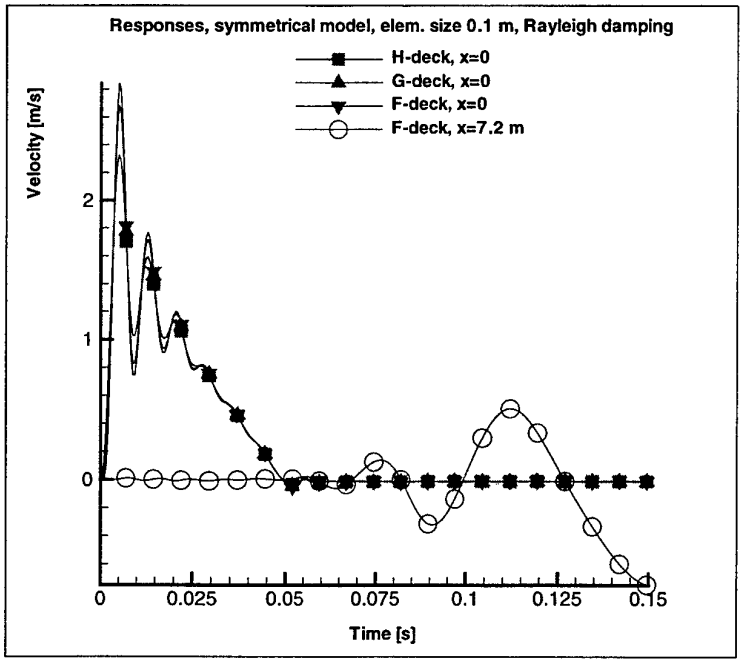

Figure 4.3 b) Velocity responses at the decks, element size 0.1 m, symmetrical model, Rayleigh damping according to fig. 4.1 a) (compare fig. 3.5 b))

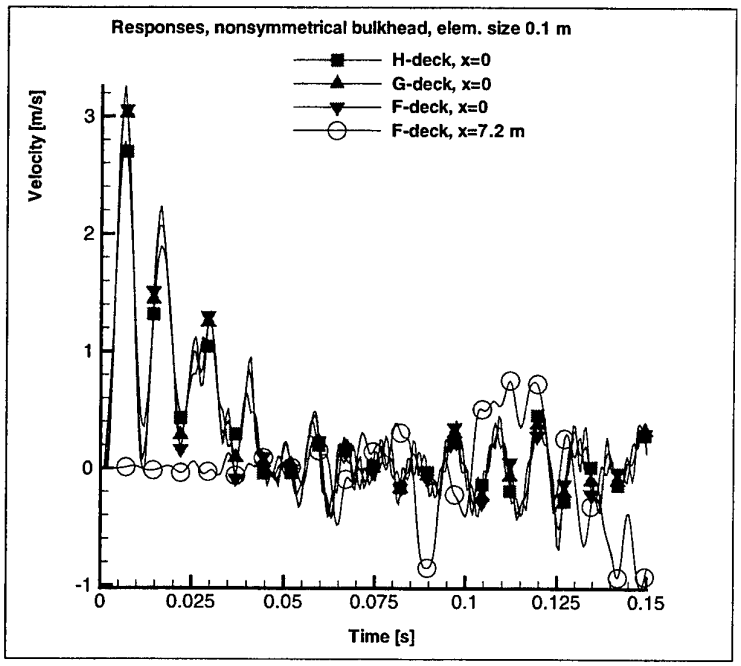

Figure 4.4 a) Velocity responses at the decks, element size 0.1 m, nonsymmetrical bulkhead, no damping (compare fig. 3.6 b))

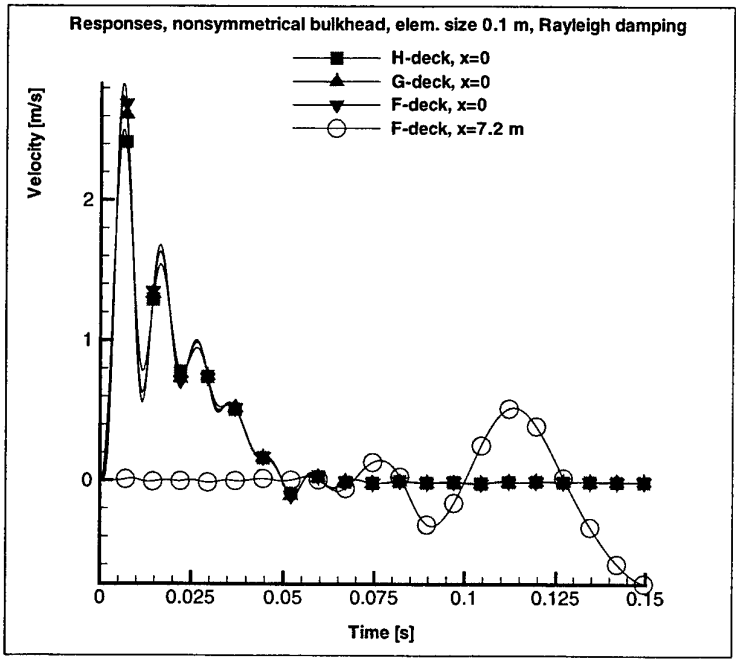

Figure 4.4 b) Velocity responses at the decks, element size 0.1 m, nonsymmetrical bulkhead, Rayleigh damping according to fig. 4.1 a) (compare fig. 3.6 b))

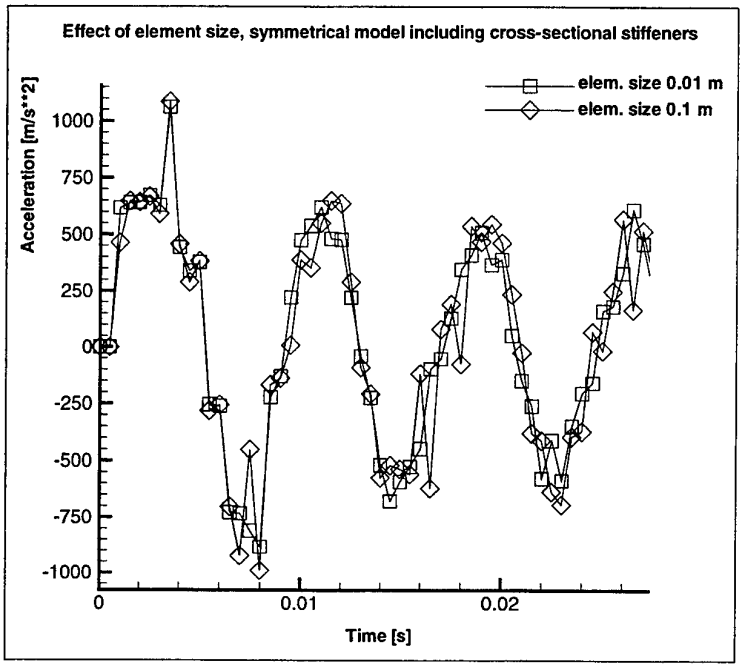

Figure 4.5 a) Comparison of accelerations at H-deck and x=0, symmetrical case, element sizes 0.1 and 0.01 m

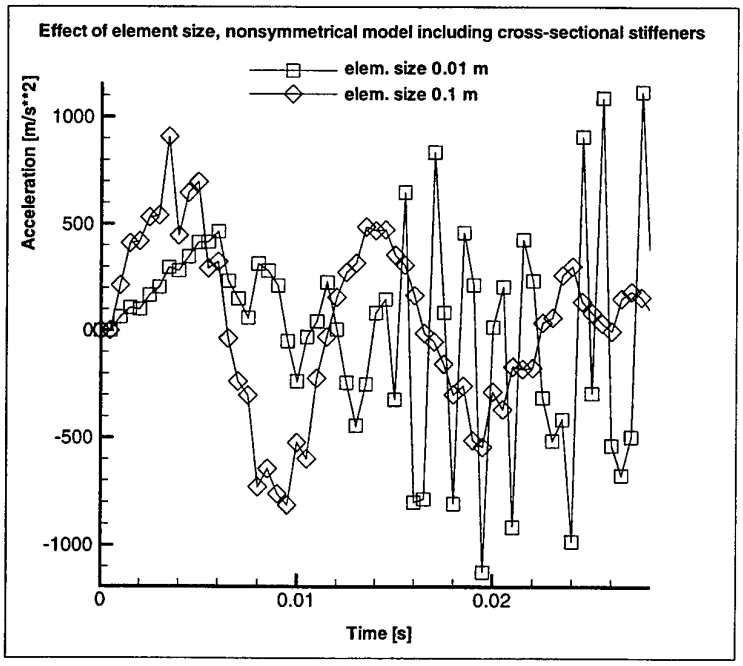

Figure 4.5 b) Comparison of accelerations at H-deck and x=0, nonsymmetrical bulkhead, element sizes 0.1 and 0.01 m

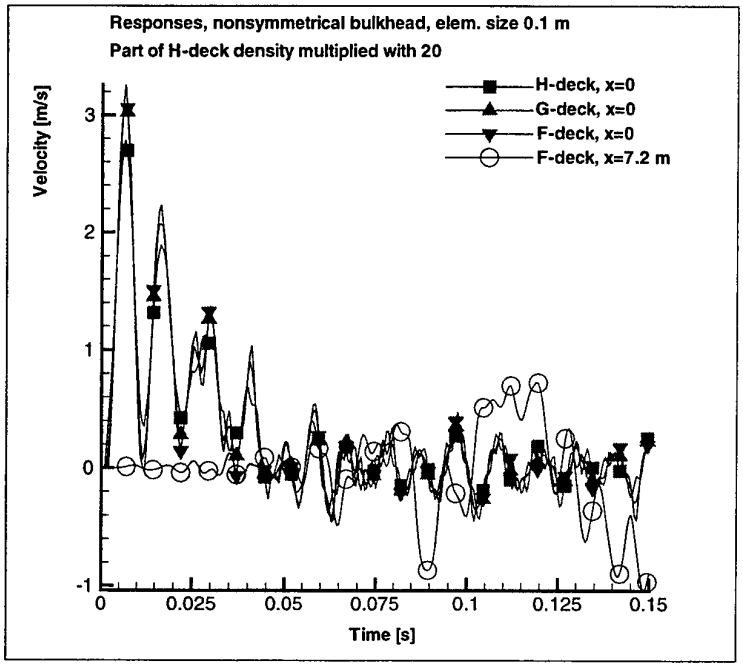

Figure 5.1 Velocity responses at the decks, element size 0.1 m, nonsymmetrical bulkhead, density of H-deck from x=-1.0 to -7.2 multiplied with a factor 20 (compare fig. 4.4 a))

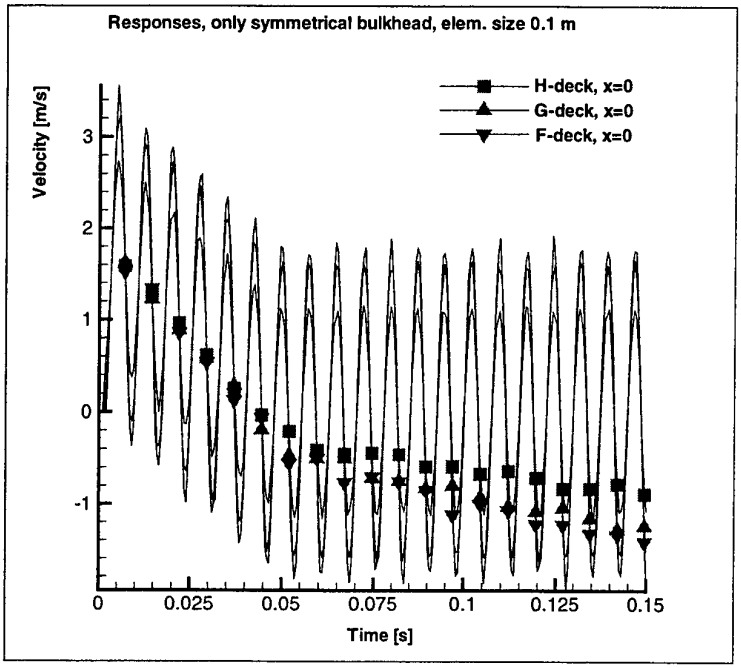

Figure 5.2 a) Velocity responses at deck levels, element size 0.1 m, model without decks (only symmetrical bulkhead), (compare fig. 4.3 a))

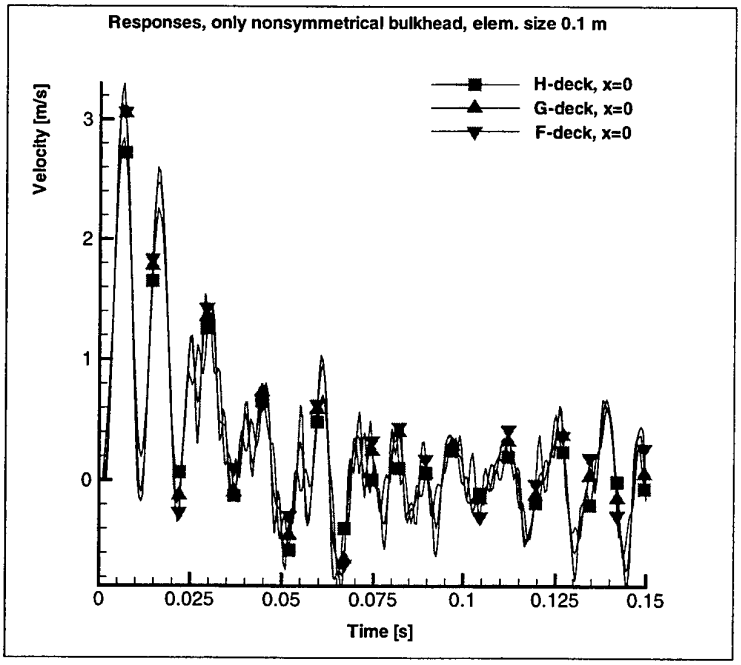

Figure 5.2 b) Velocity responses at deck levels, element size 0.1 m, model without decks (only nonsymmetrical bulkhead), (compare fig. 4.4 a))

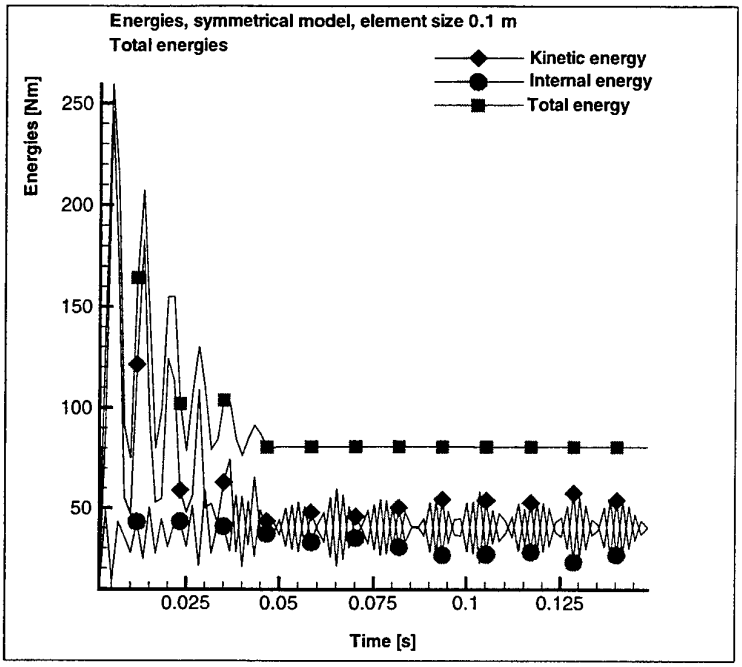

Figure 5.3 a) Total energy distribution, case with element size 0.1 m, symmetrical model

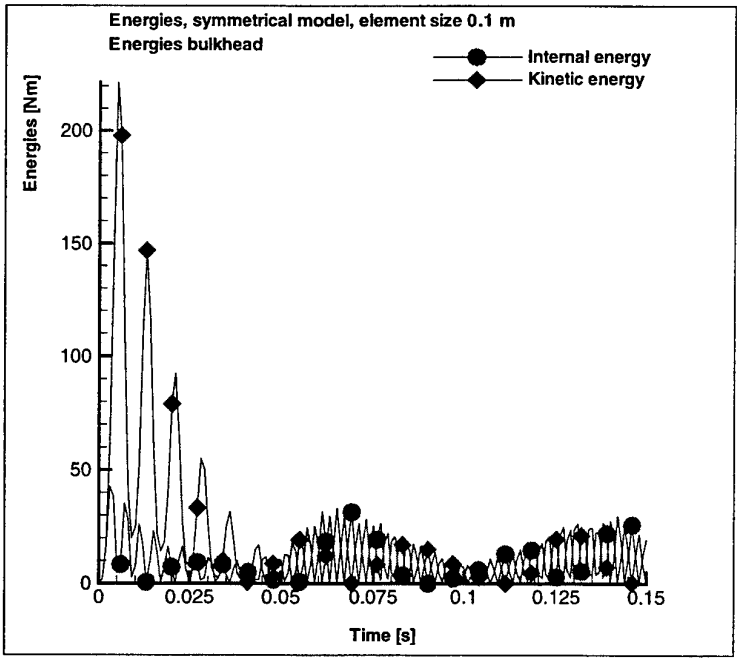

Figure 5.3 b) Energy distribution in bulkhead, case with element size 0.1 m, symmetrical model

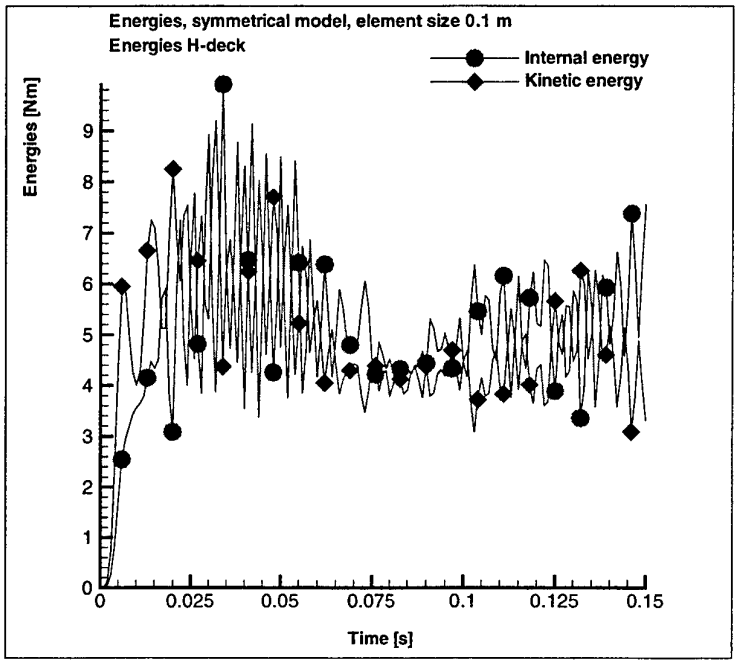

Figure 5.3 c) Energy distribution in H-deck, case with element size 0.1 m, symmetrical model

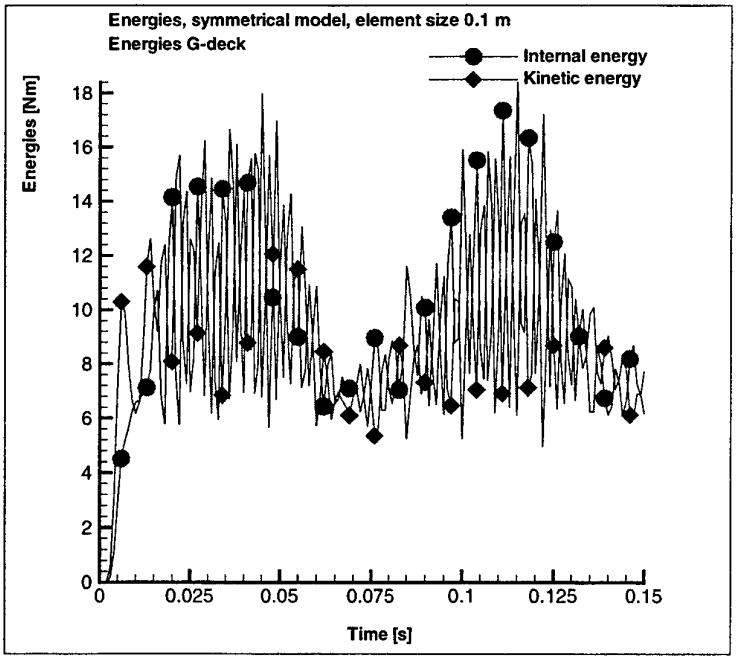

Figure 5.3 d) Energy distribution in G-deck, case with element size 0.1 m, symmetrical model

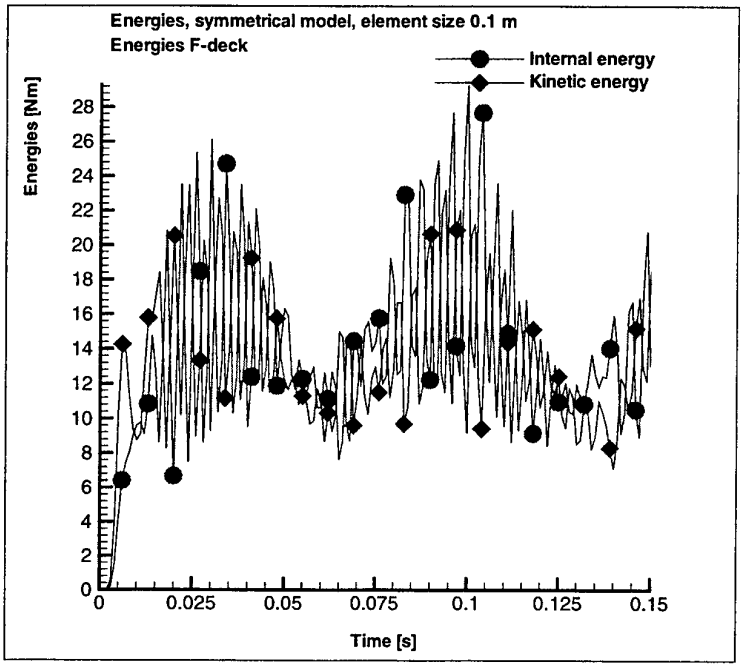

Figure 5.3 e) Energy distribution in F-deck, case with element size 0.1 m, symmetrical model

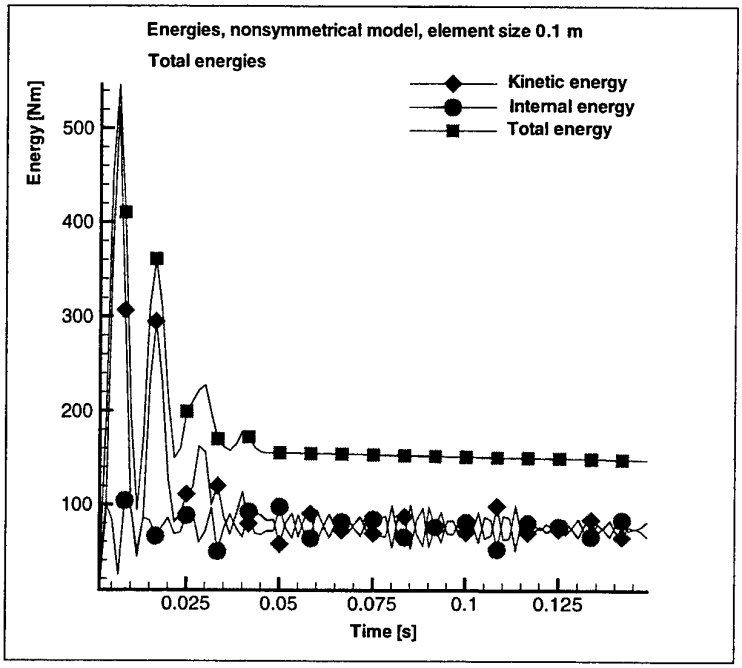

Figure 5.4 a) Total energy distribution, case with element size 0.1 m, nonsymmetrical bulkhead

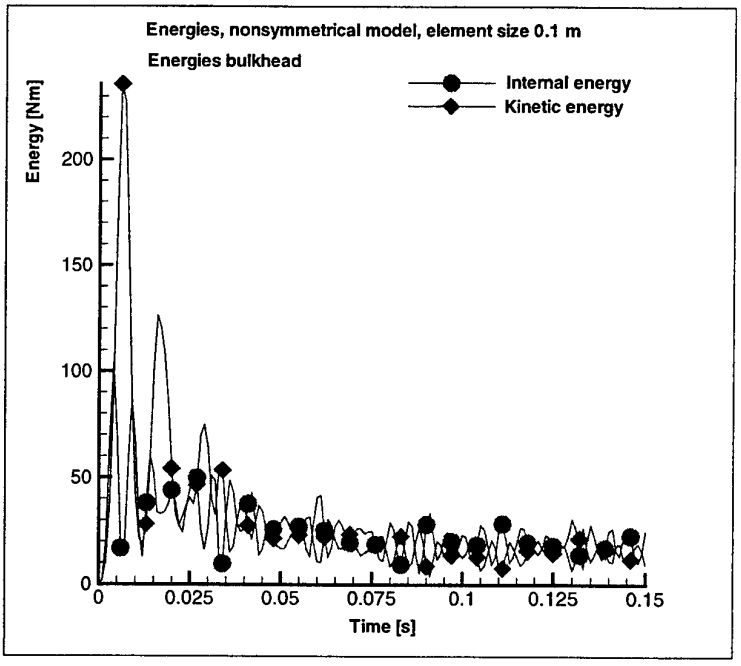

Figure 5.4 b) Energy distribution in bulkhead, case with element size 0.1 m, nonsymmetrical bulkhead

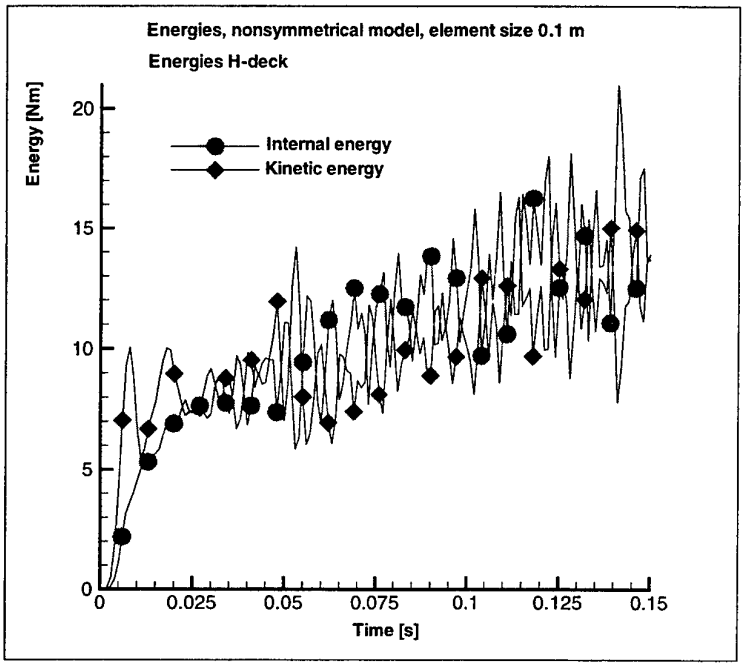

Figure 5.4 c) Energy distribution in H-deck, case with element size 0.1 m, nonsymmetrical bulkhead

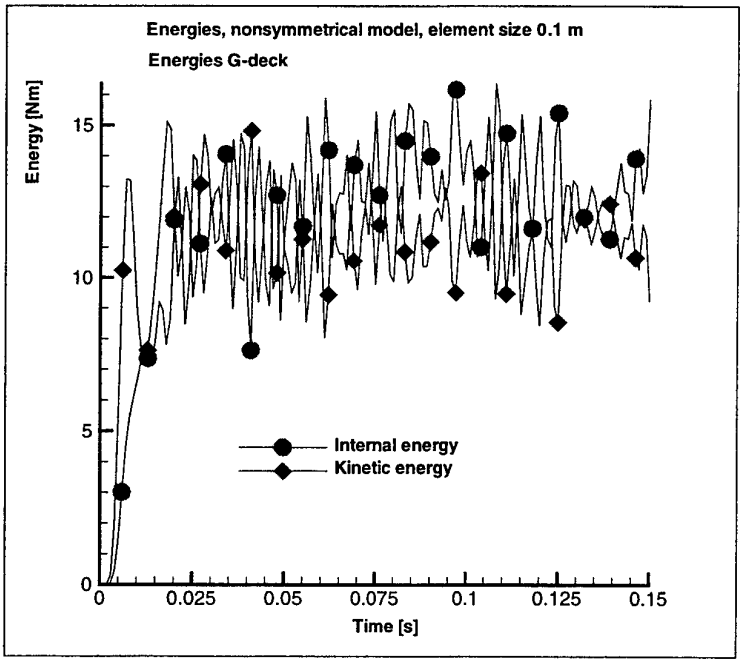

Figure 5.4 d) Energy distribution in G-deck, case with element size 0.1 m, nonsymmetrical bulkhead

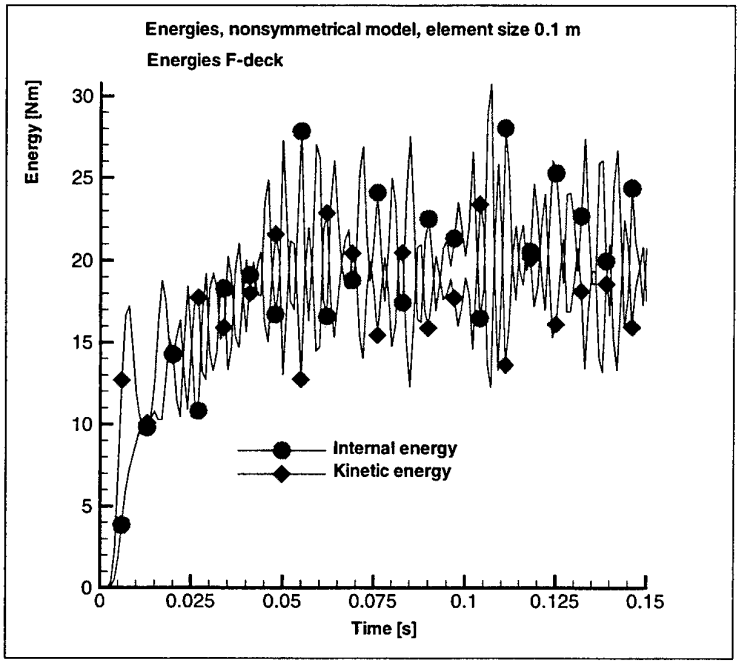

Figure 5.4 e) Energy distribution in F-deck, case with element size 0.1 m, nonsymmetrical bulkhead

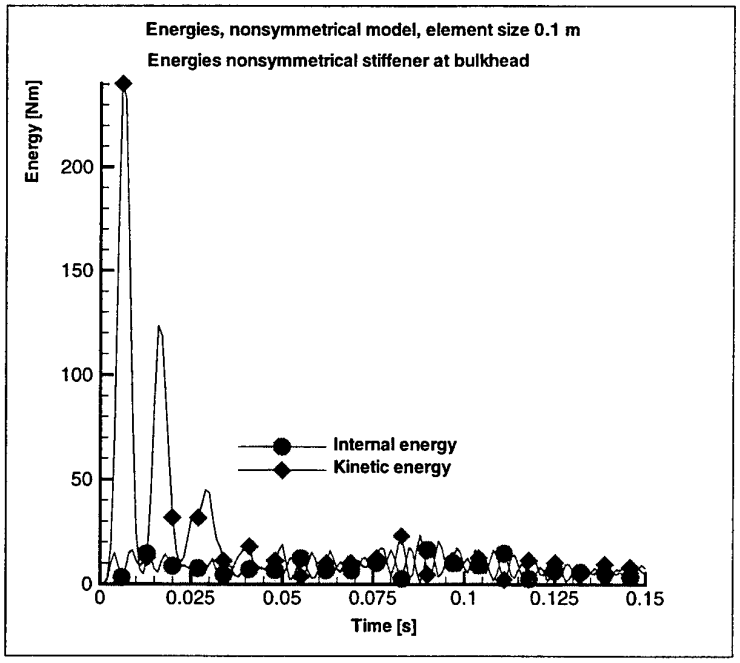

Figure 5.4 f) Energy distribution in nonsymmetrical stiffener at bulkhead, case with element size 0.1 m, nonsymmetrical bulkhead

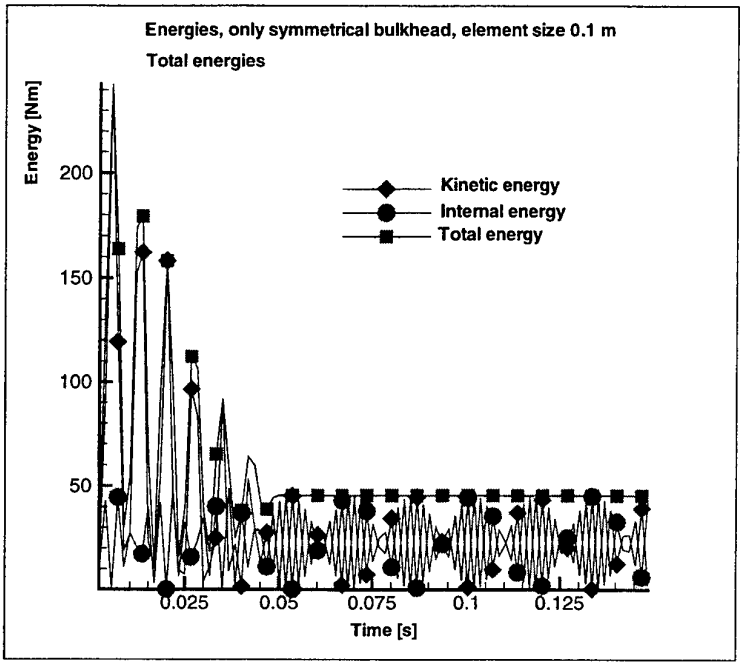

Figure 5.5 Total energy distribution, case with element size 0.1 m, model without decks, only symmetrical bulkhead

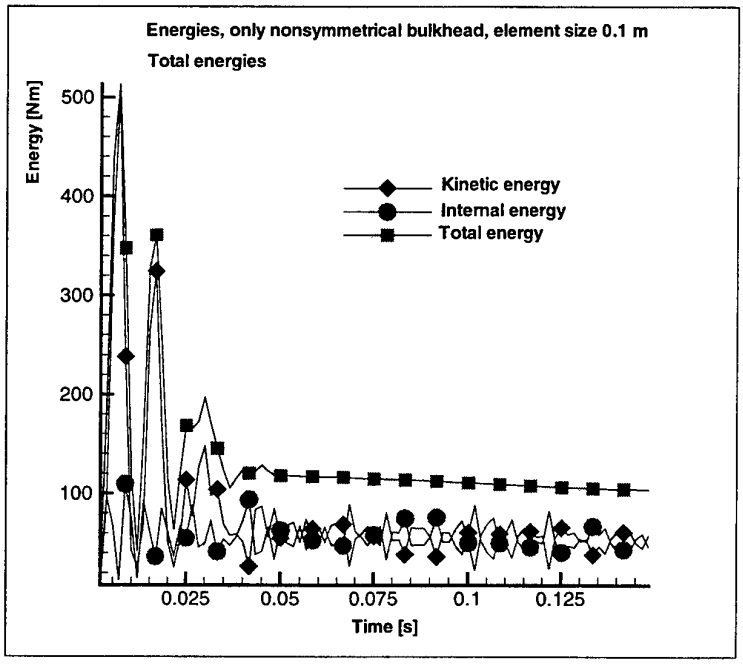

Figure 5.6 a) Total energy distribution, case with element size 0.1 m, model without decks, only nonsymmetrical bulkhead

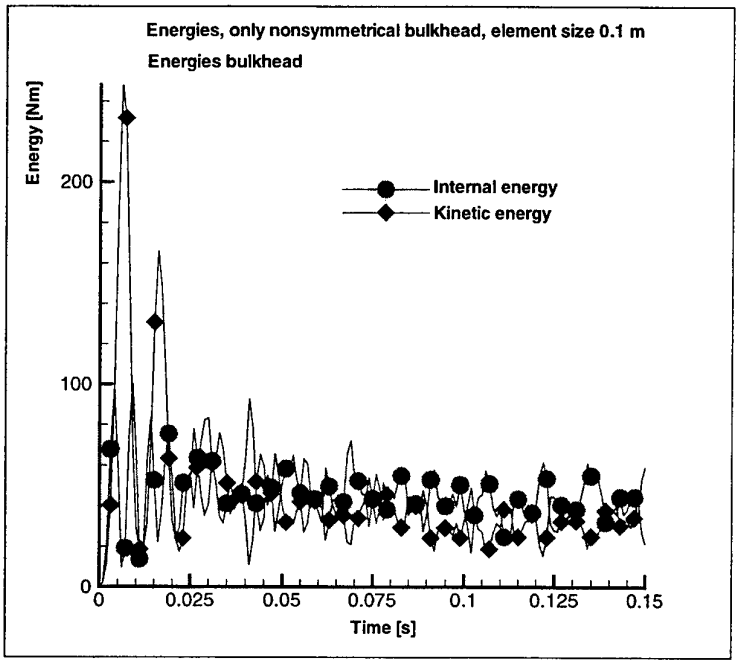

Figure 5.6 b) Energy distribution in bulkhead, case with element size 0.1 m, model without decks, only nonsymmetrical bulkhead

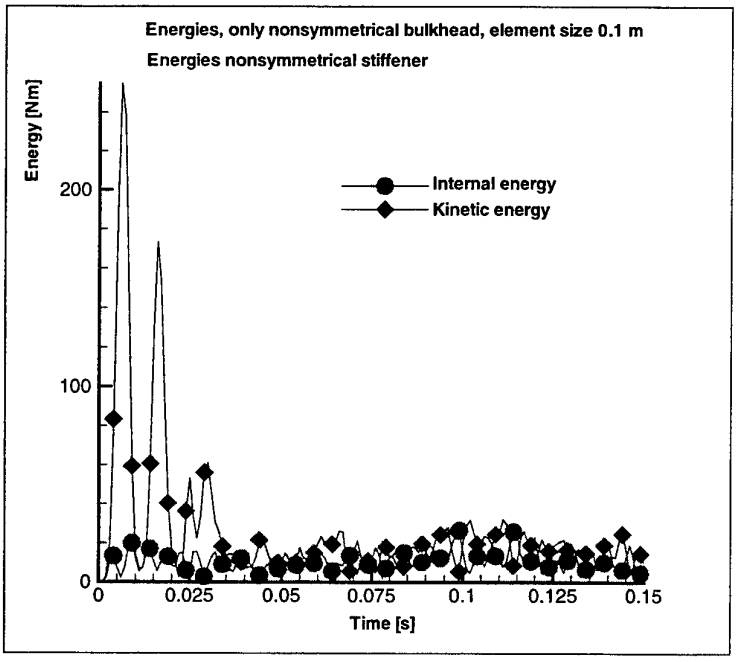

Figure 5.6 c) Energy distribution in nonsymmetrical stiffener at bulkhead, case with element size 0.1 m, model without decks, only nonsymmetrical bulkhead

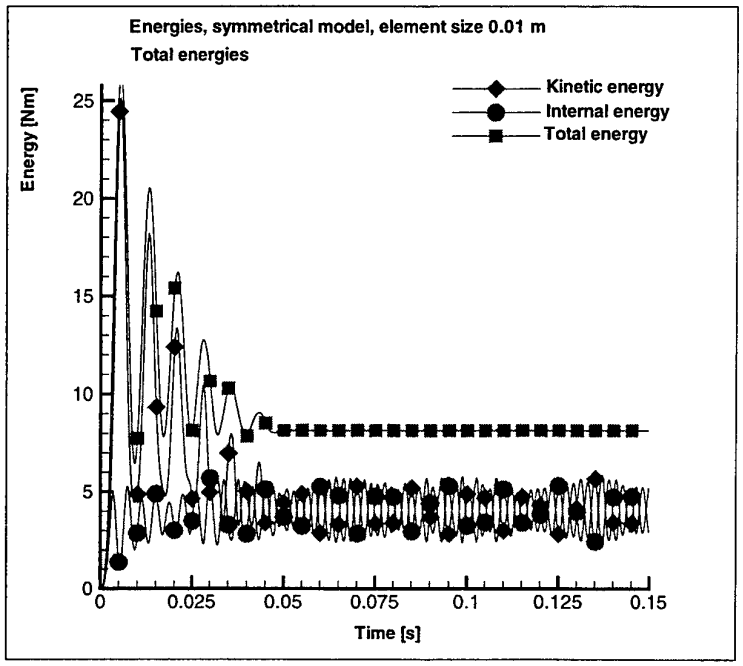

Figure 5.7 a) Total energy distribution, case with element size 0.01 m, symmetrical model

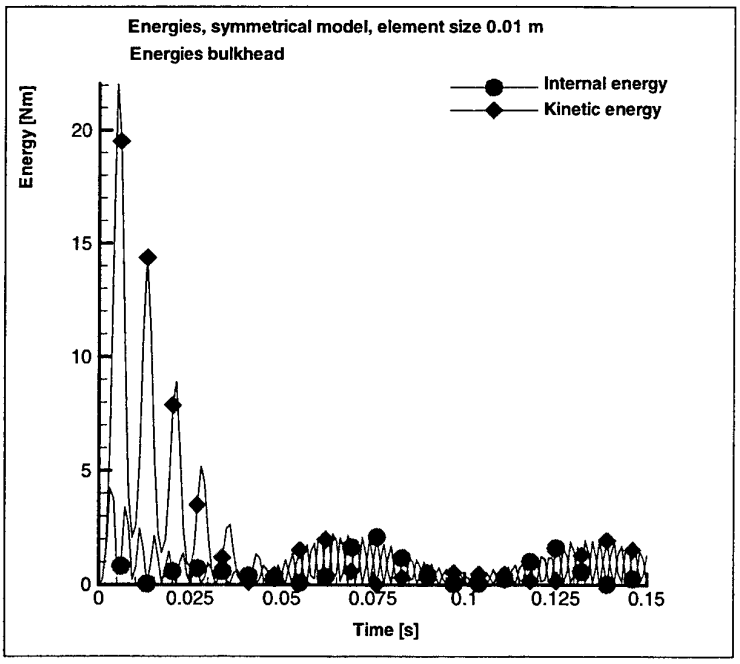

Figure 5.7 b) Energy distribution in bulkhead, case with element size 0.01 m, symmetrical model

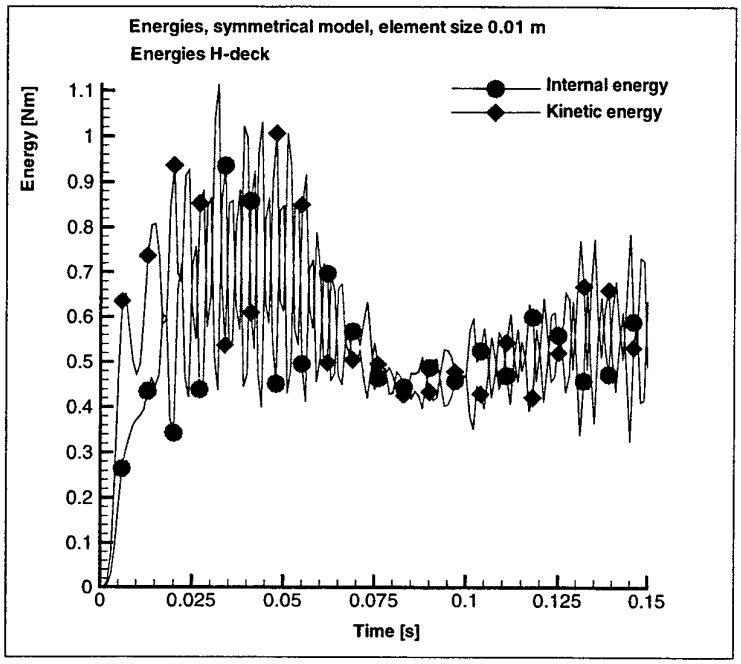

Figure 5.7 c) Energy distribution in H-deck, case with element size 0.01 m, symmetrical model

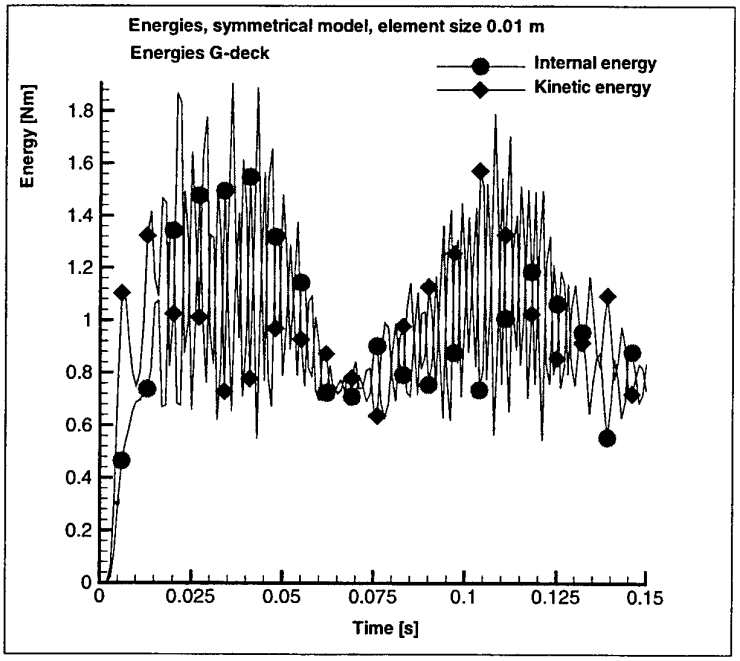

Figure 5.7 d) Energy distribution in G-deck, case with element size 0.01 m, symmetrical model

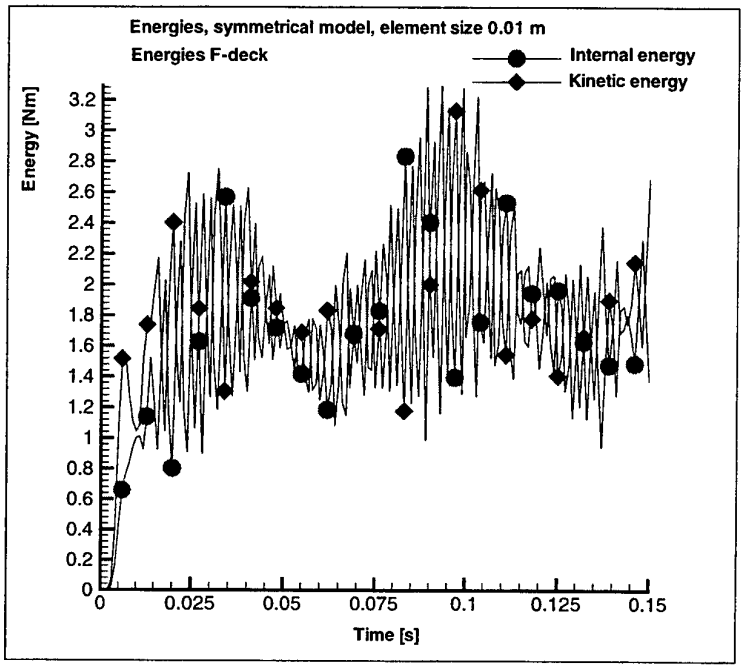

Figure 5.7 e) Energy distribution in F-deck, case with element size 0.01 m, symmetrical model

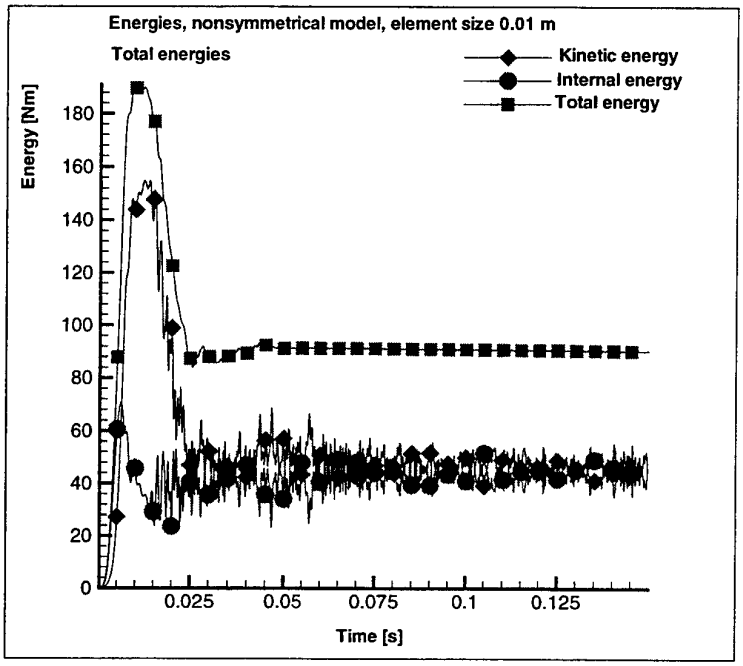

Figure 5.8 a) Total energy distribution, case with element size 0.01 m, nonsymmetrical bulkhead

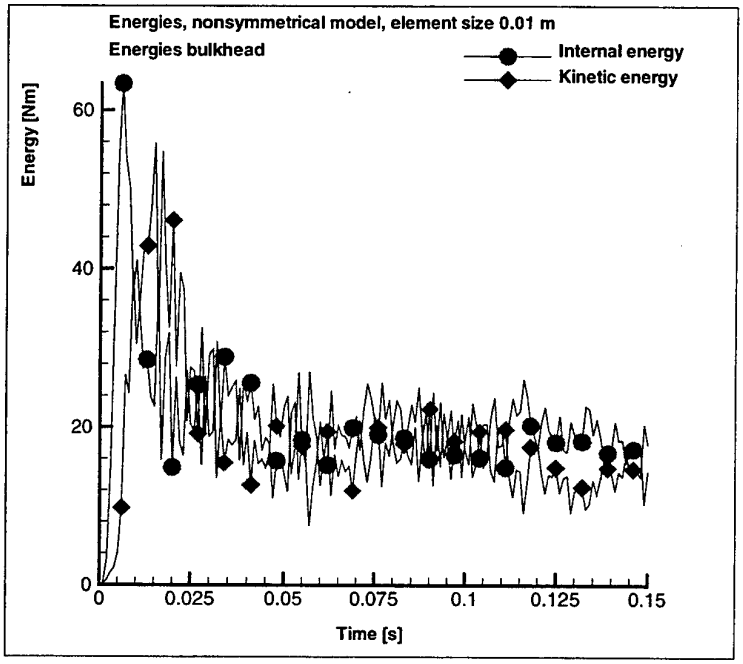

Figure 5.8 b) Energy distribution in bulkhead, case with element size 0.01 m, nonsymmetrical bulkhead

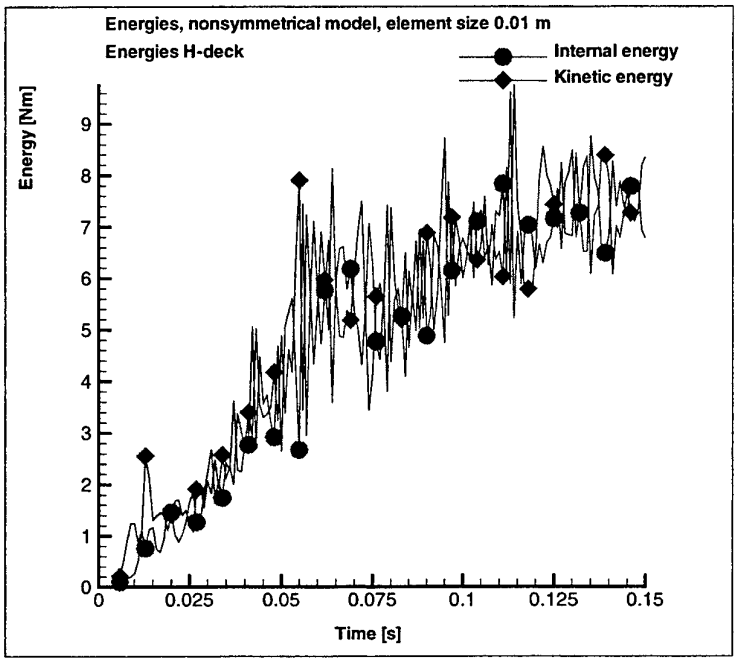

Figure 5.8 c) Energy distribution in H-deck, case with element size 0.01 m, nonsymmetrical bulkhead

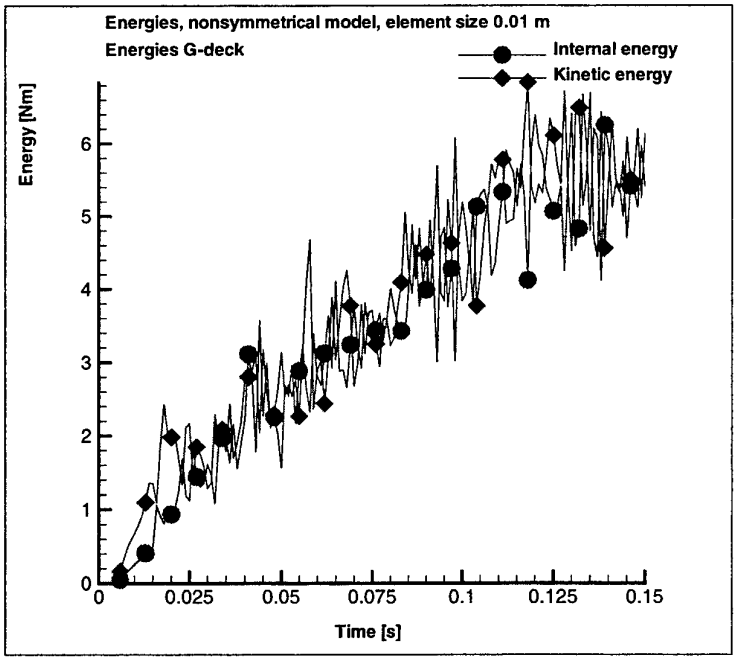

Figure 5.8 d) Energy distribution in G-deck, case with element size 0.01 m, nonsymmetrical bulkhead

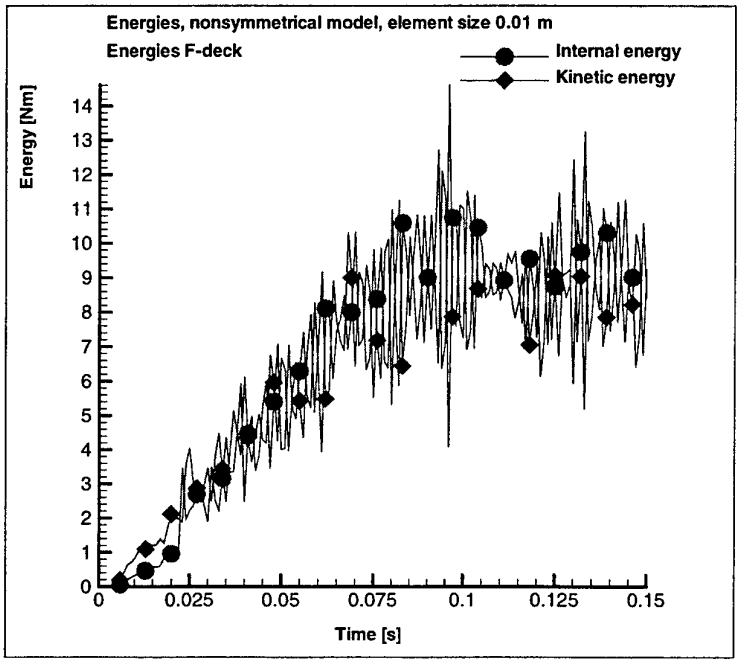

Figure 5.8 e) Energy distribution in F-deck, case with element size 0.01 m, nonsymmetrical bulkhead

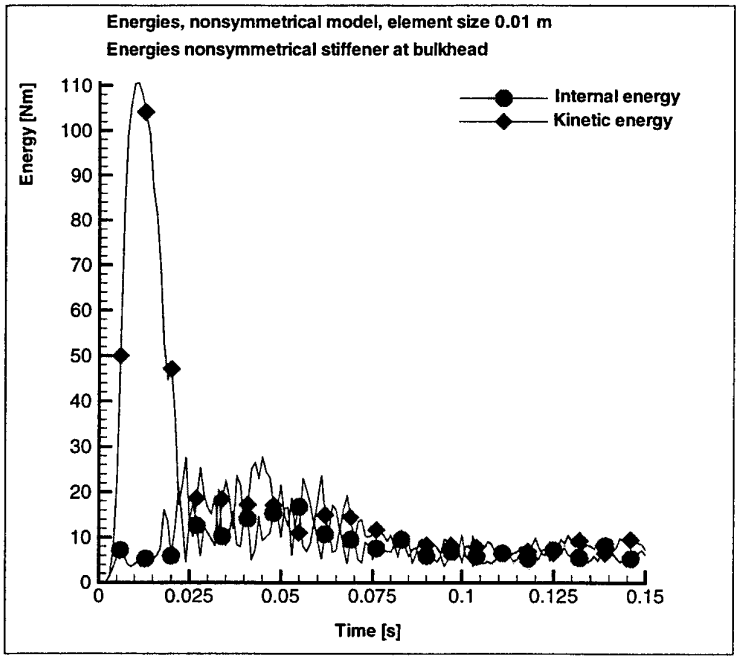

Figure 5.8 f) Energy distribution in nonsymmetrical stiffener at bulkhead, case with element size 0.01 m, nonsymmetrical bulkhead

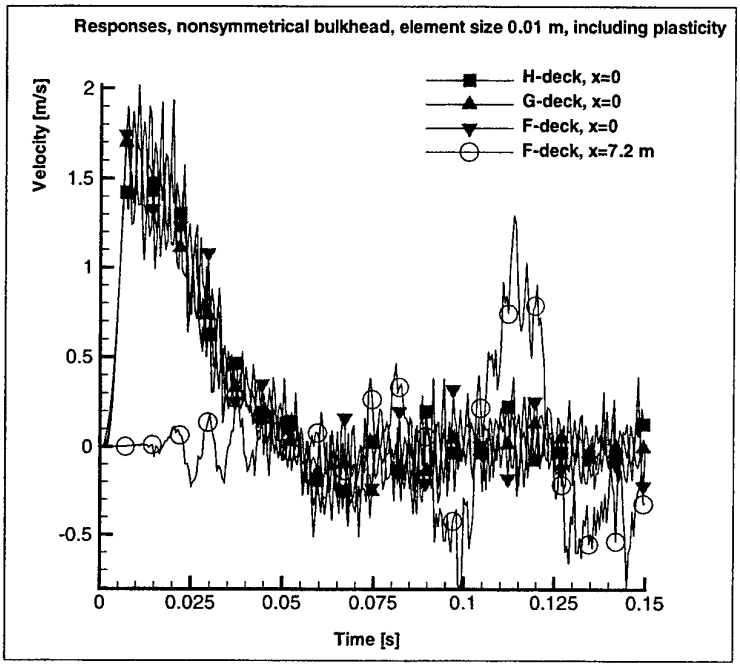

Figure 6.1 *Velocity responses at the decks, case with element size 0.01 m, nonsymmetrical bulkhead, including plasticity (compare fig. 3.6 b))*

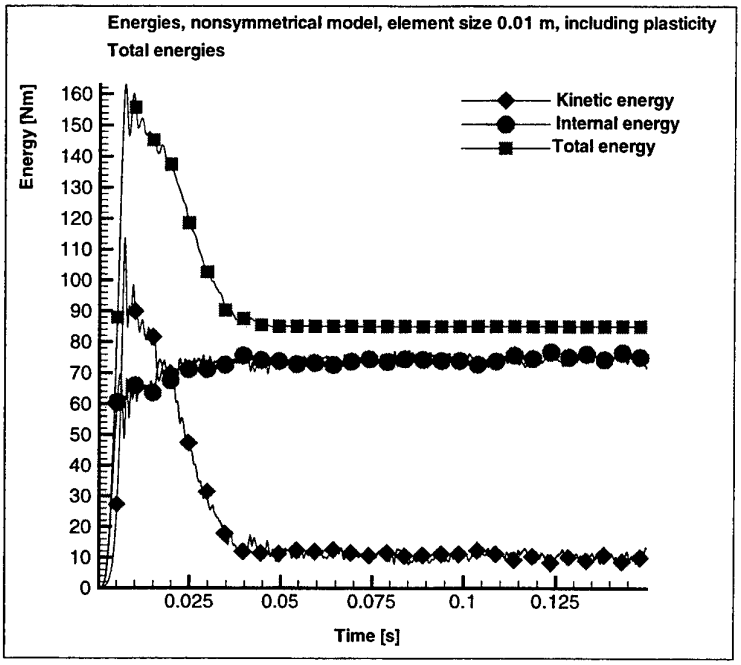

Figure 6.2 a) *Total energy distribution, case with element size 0.01 m, nonsymmetrical bulkhead, including plasticity*

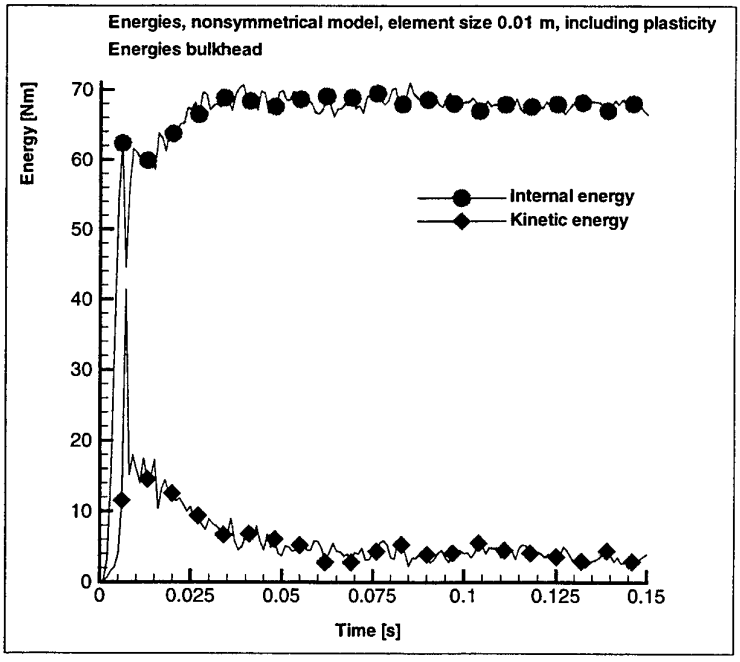

Figure 6.2 b) *Energy distribution in bulkhead, case with element size 0.01 m, nonsymmetrical bulkhead, including plasticity*

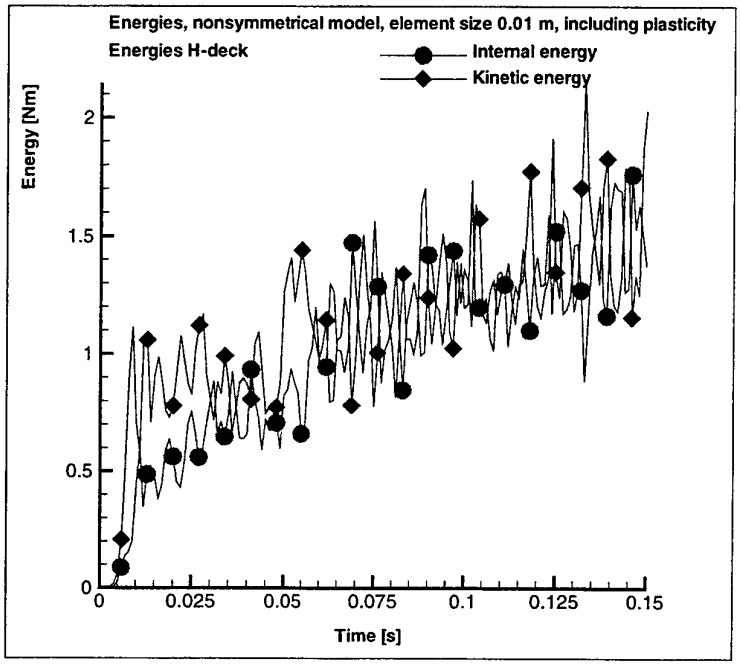

Figure 6.2 c) *Energy distribution in H-deck, case with element size 0.01 m, nonsymmetrical bulkhead, including plasticity*

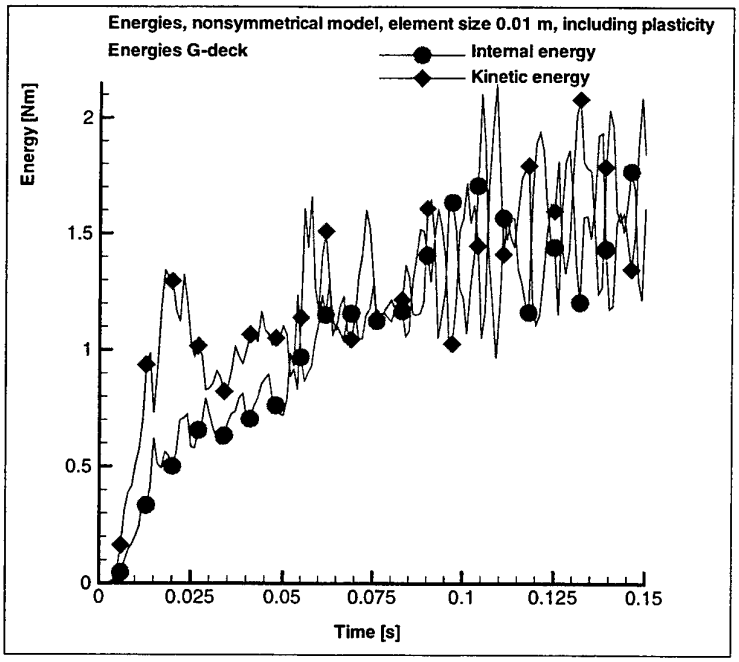

Figure 6.2 d) *Energy distribution in G-deck, case with element size 0.01 m, nonsymmetrical bulkhead, including plasticity*

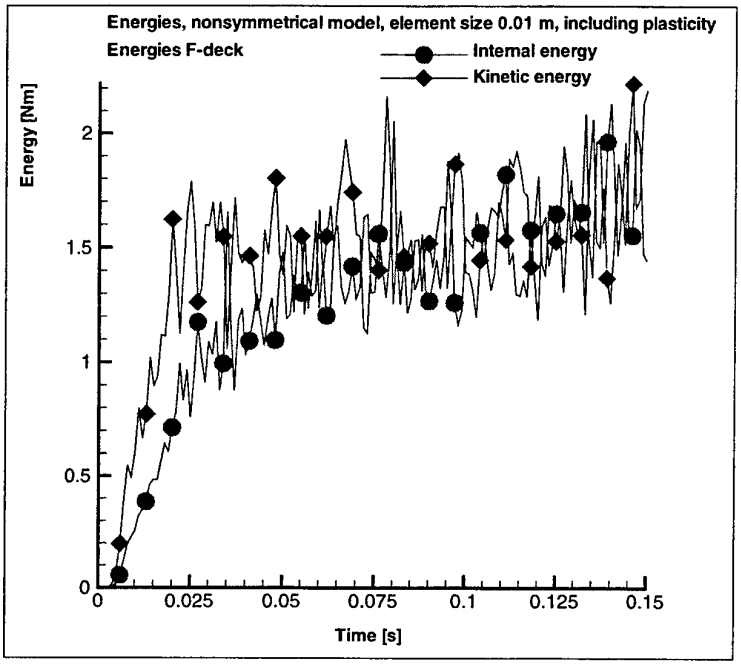

Figure 6.2 e) *Energy distribution in F-deck, case with element size 0.01 m, nonsymmetrical bulkhead, including plasticity*

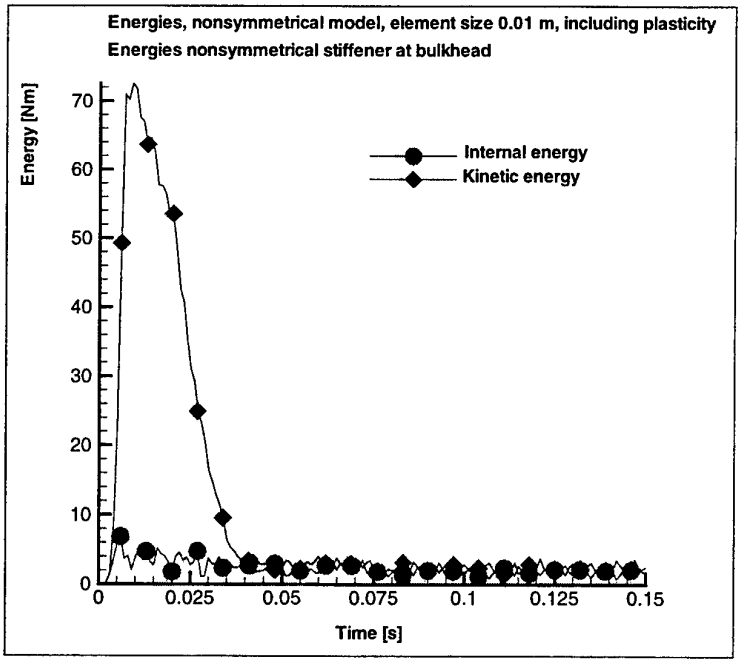

Figure 6.2 f) *Energy distribution in nonsymmetrical stiffener at bulkhead, case with element size 0.01 m, nonsymmetrical bulkhead, including plasticity*

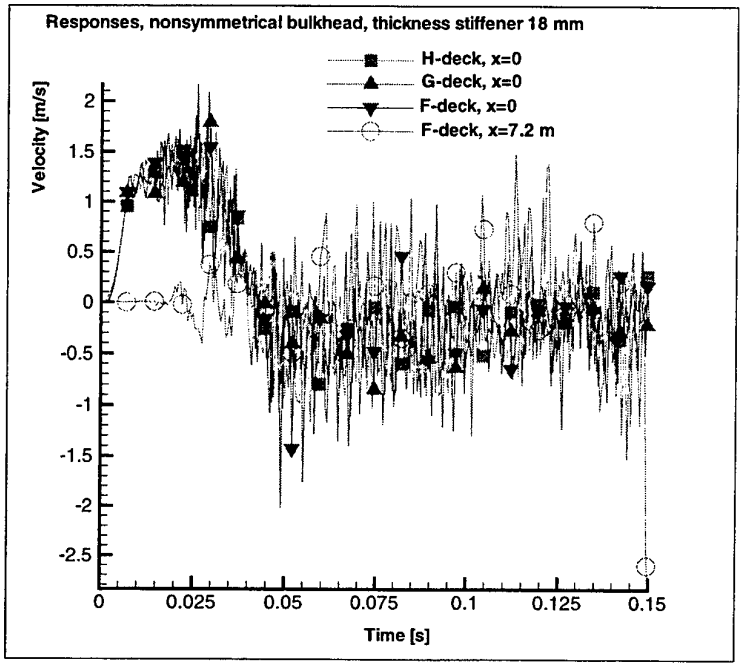

Figure 7.1 a) *Velocity responses at the decks, case with element size 0.01 m, nonsymmetrical bulkhead, elastic material, thickness of nonsymmetrical stiffener 18 mm (compare fig. 3.6 b))*

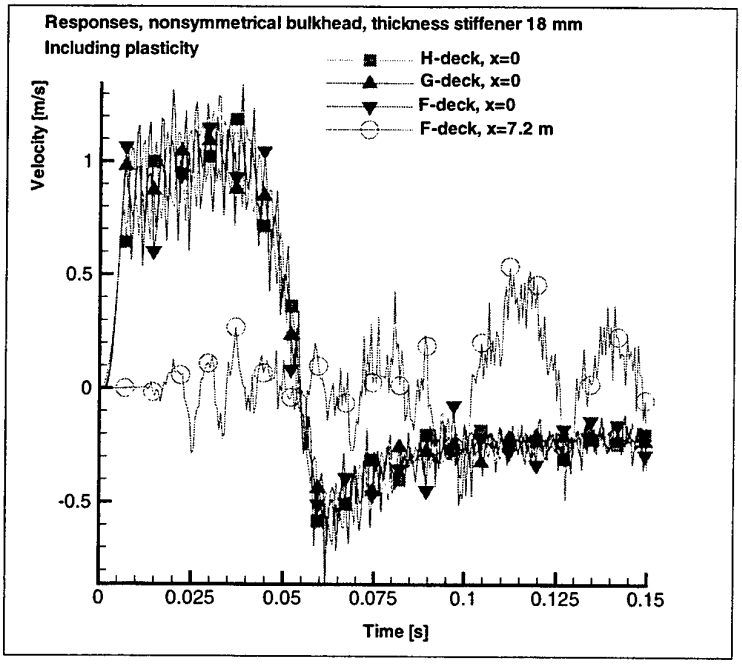

Figure 7.1 b) *Velocity responses at the decks, case with element size 0.01 m, nonsymmetrical bulkhead, elastic-plastic material, thickness of nonsymmetrical stiffener 18 mm*

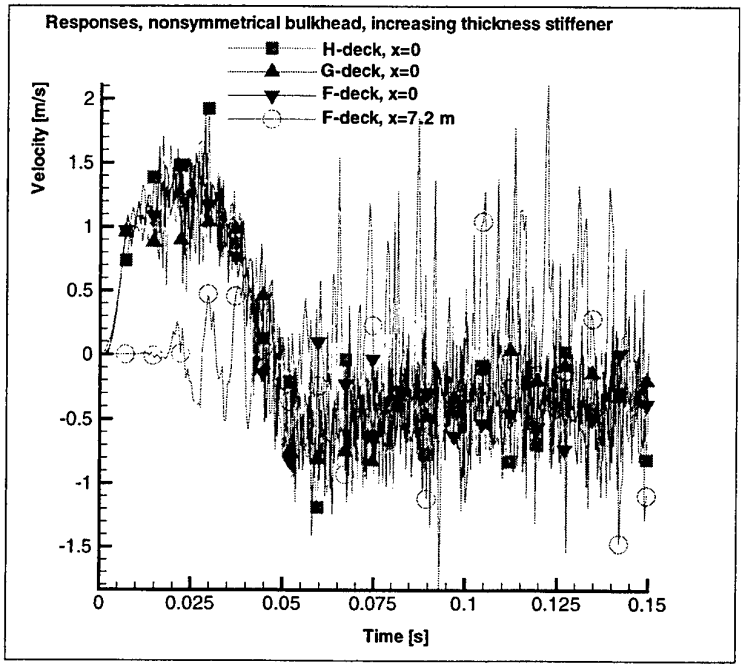

Figure 7.2 *Velocity responses at the decks, case with element size 0.01 m, nonsymmetrical bulkhead with increasing thickness, elastic material*

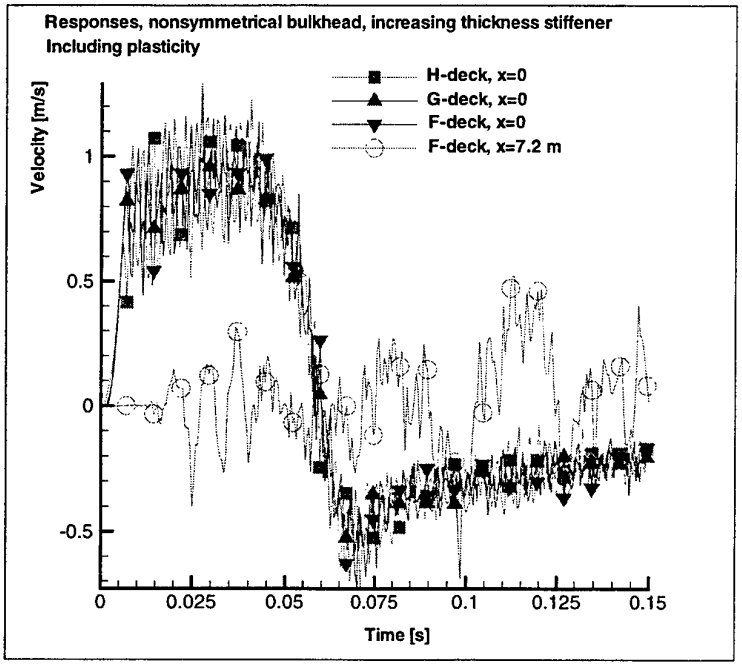

Figure 7.3 a) *Velocity responses at the decks, case with element size 0.01 m, nonsymmetrical bulkhead with increasing thickness, elastic-plastic material*

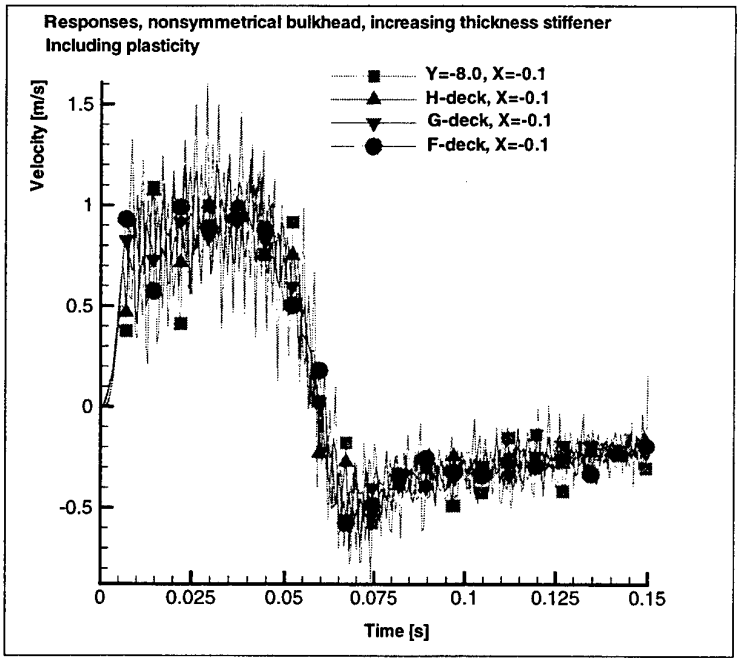

Figure 7.3 b) *Eccentric velocity responses at the nonsymmetrical stiffener, case with element size 0.01 m, nonsymmetrical bulkhead with increasing thickness, elastic-plastic material*

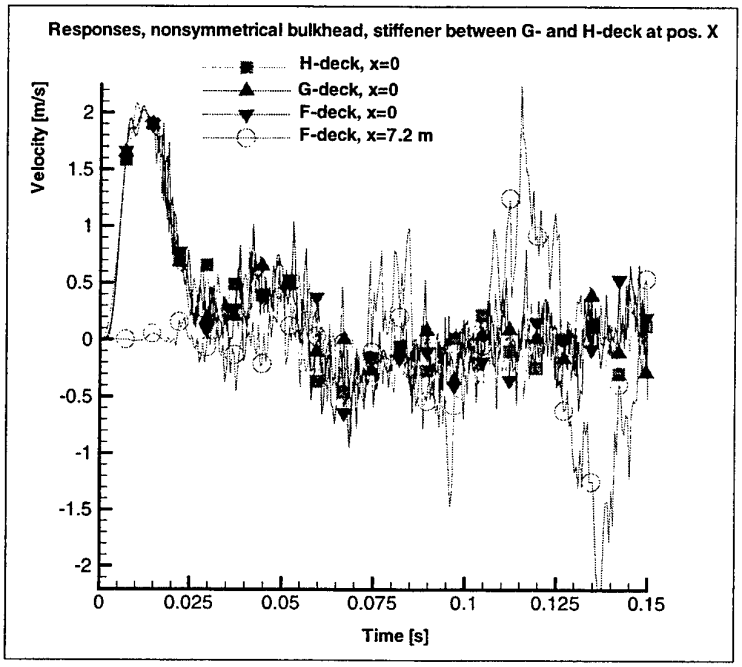

Figure 7.4 a) *Velocity responses at the decks, case with element size 0.01 m, nonsymmetrical bulkhead with nonsymmetrical stiffener between G- and H-deck at positive X-side, elastic material (compare fig. 3.6 b))*

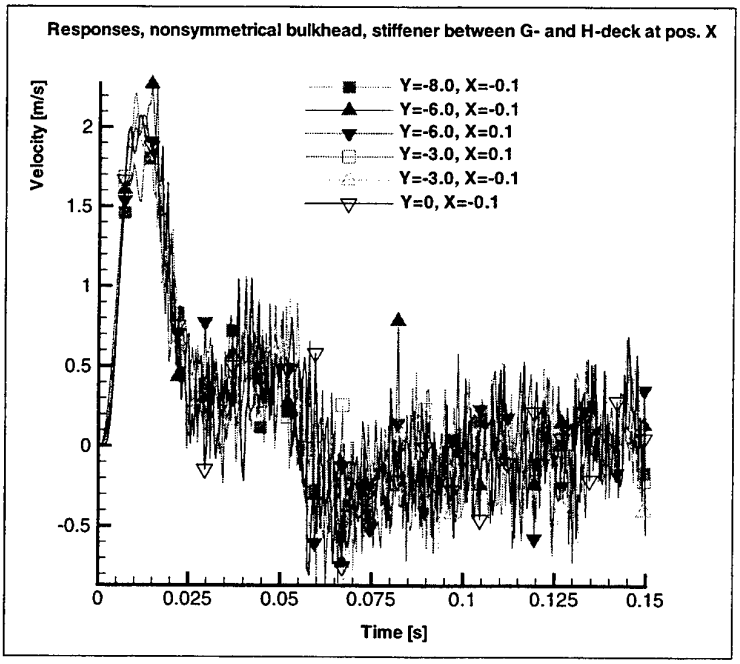

Figure 7.4 b) *Eccentric velocity responses at the nonsymmetrical stiffener, case with element size 0.01 m, nonsymmetrical bulkhead with nonsymmetrical stiffener between G- and H-deck at positive X-side, elastic material*

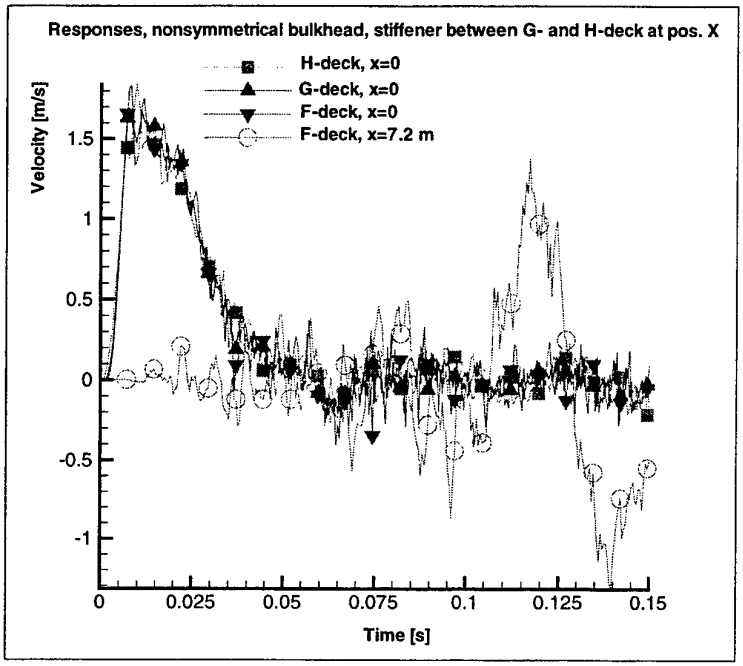

Figure 7.5 a) *Velocity responses at the decks, case with element size 0.01 m, nonsymmetrical bulkhead with nonsymmetrical stiffener between G- and H-deck at positive X-side, elastic-plastic material*

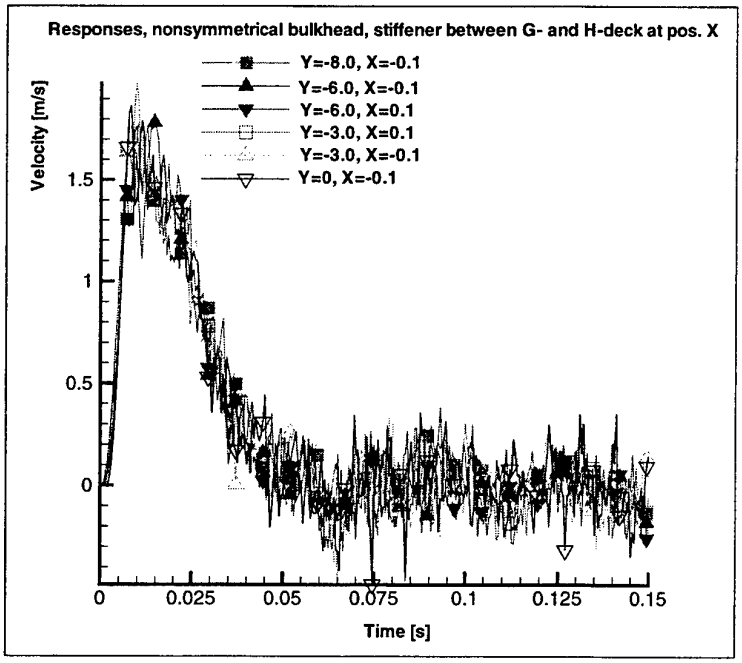

Figure 7.5 b) *Eccentric velocity responses at the nonsymmetrical stiffener, case with element size 0.01 m, nonsymmetrical bulkhead with nonsymmetrical stiffener between G- and H-deck at positive X-side, elastic-plastic material*

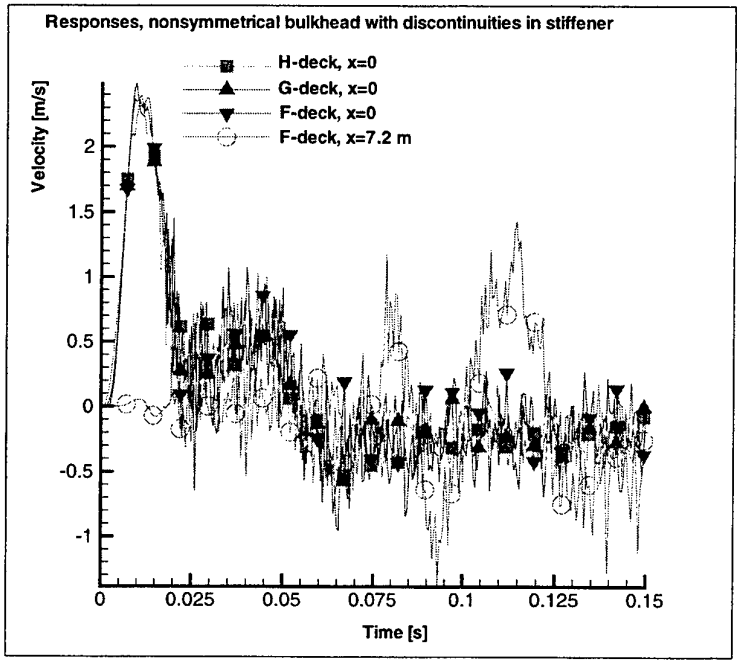

Figure 7.6 *Velocity responses at the decks, case with element size 0.01 m, nonsymmetrical bulkhead with discontinuities at Y=-1.5 m, -4.5 m and -7.5 m, elastic material*

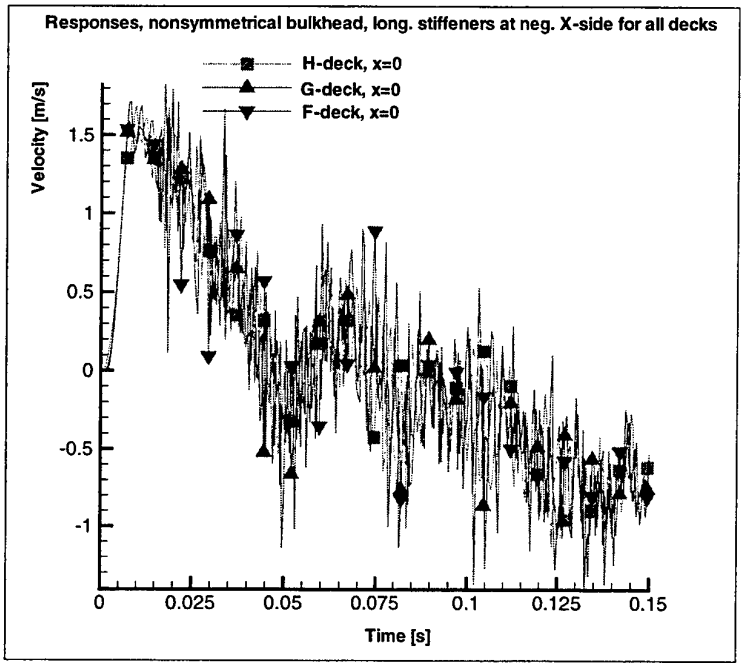

Figure 7.7 a) *Velocity responses at the decks, case with element size 0.01 m, nonsymmetrical bulkhead with longitudinal girders at negative X-side of the decks, elastic material*

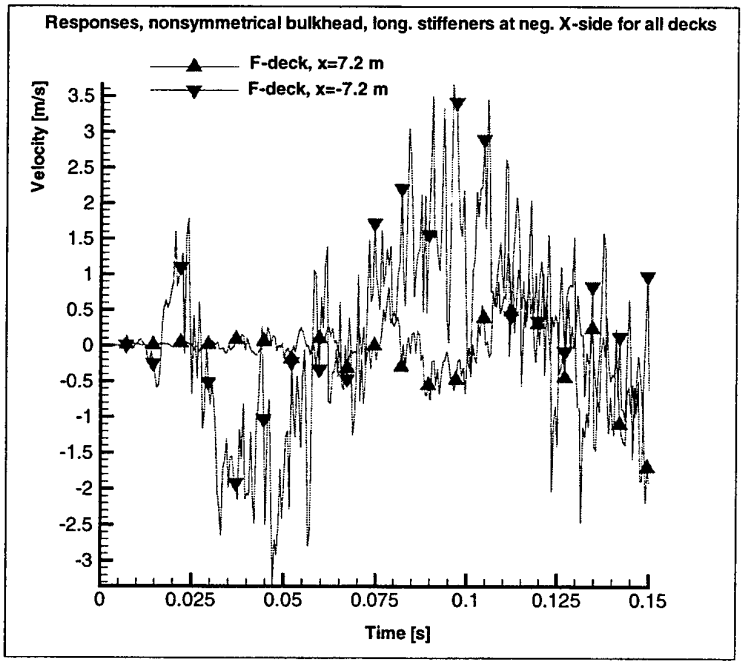

Figure 7.7 b) *Eccentric velocity responses at the nonsymmetrical stiffener, case with element size 0.01 m, nonsymmetrical bulkhead with longitudinal girders at negative X-side of the decks, elastic material*

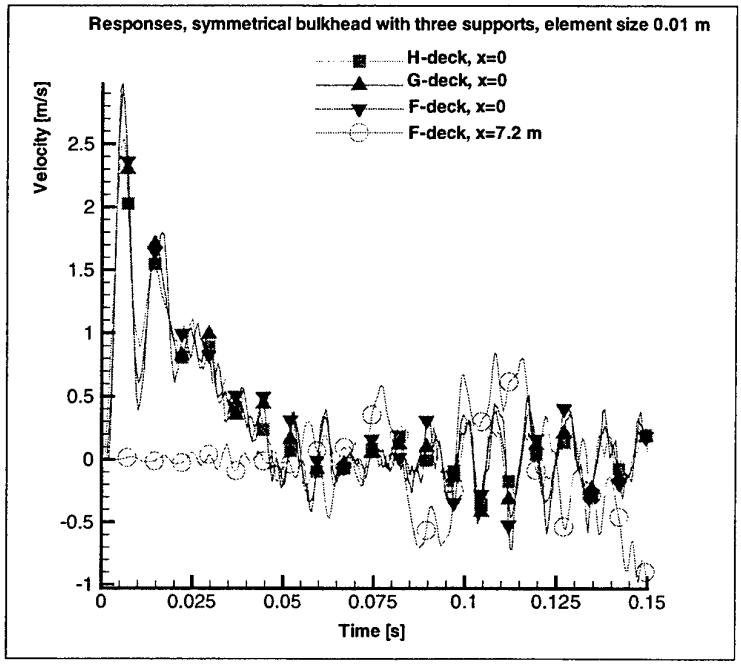

Figure 7.8 a) *Velocity responses at the decks, case with element size 0.01 m, symmetrical bulkhead with struts at Y=-8.0, -4.5 and -1.5 m, elastic material*

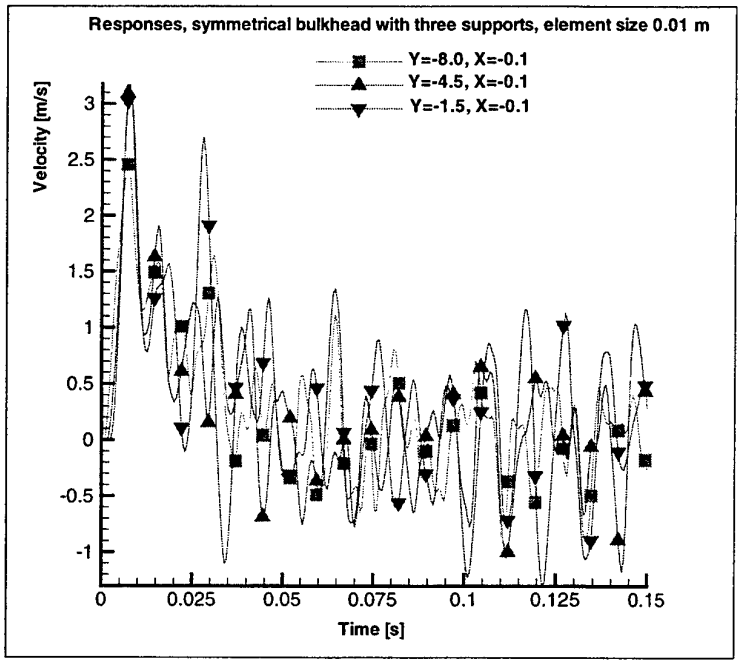

Figure 7.8 b) *Eccentric velocity responses at the struts at X=-0.1 m, case with element size 0.01 m, symmetrical bulkhead with struts at Y=-8.0, -4.5 and -1.5 m, elastic material*

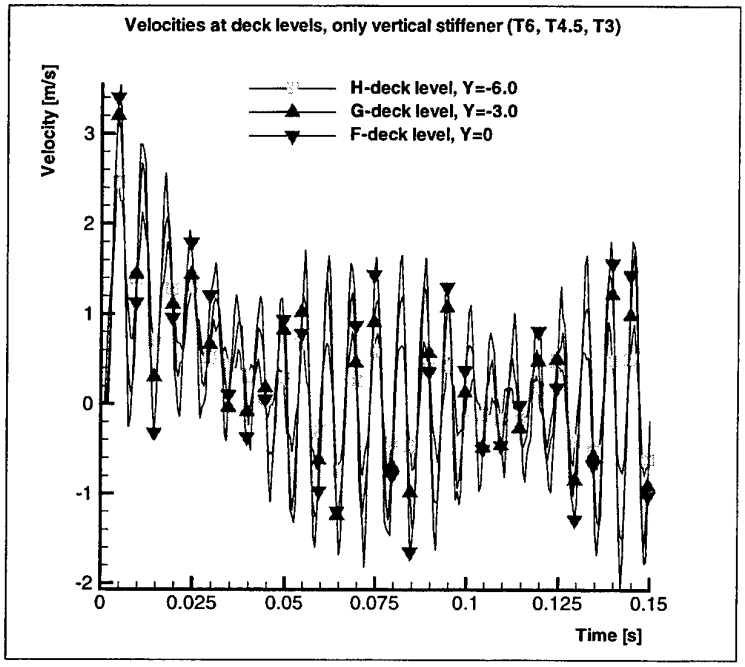

Figure 9.1 *Velocity responses at the deck levels, model with only vertical stiffener built up from profiles T6, T4.5 and T3*

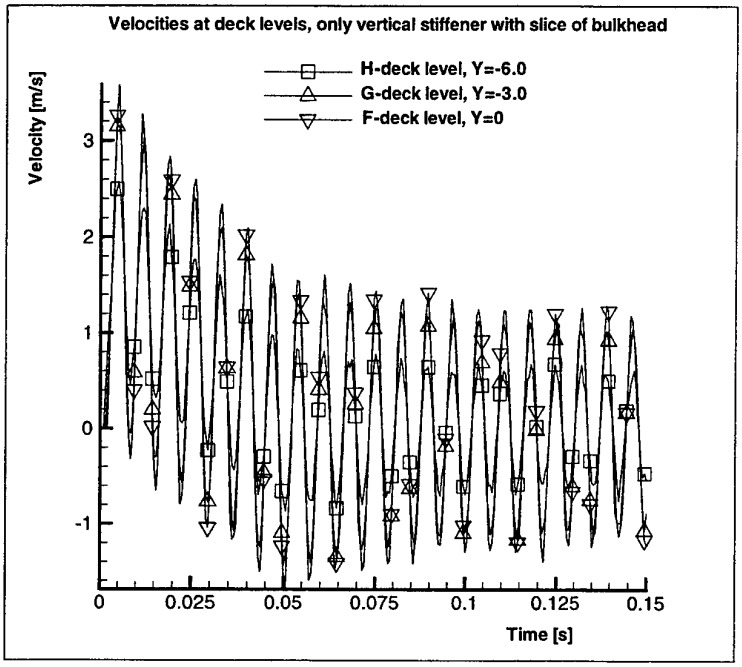

Figure 9.2 a) *Velocity responses at the deck levels, model with only vertical stiffener built up from profiles T6, T4.5 and T3, and slice of bulkhead*

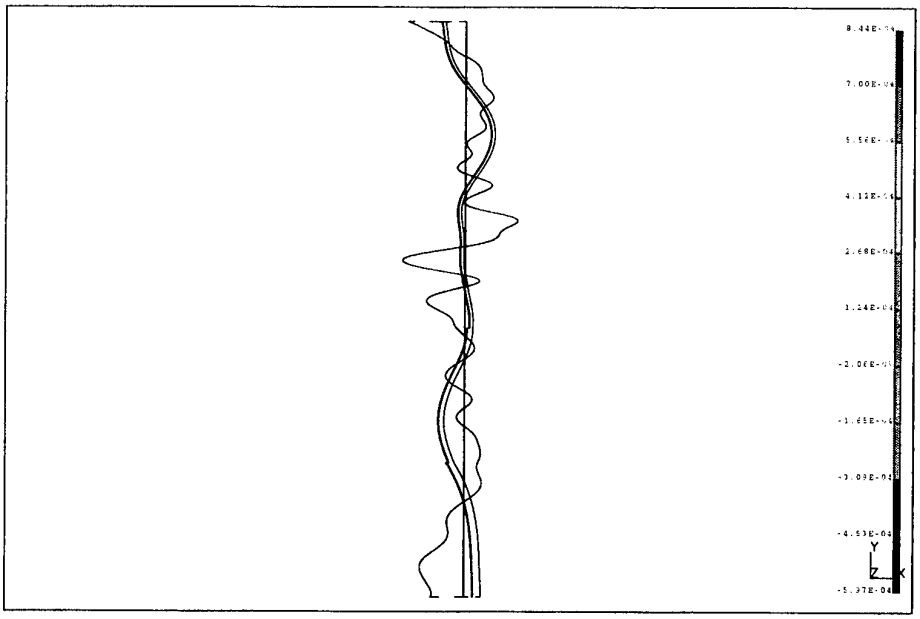

Figure 9.2 b) *Deformation at time is 49.498 ms, only X-component, model with only vertical stiffener built up from profiles T6, T4.5 and T3, and slice of bulkhead*

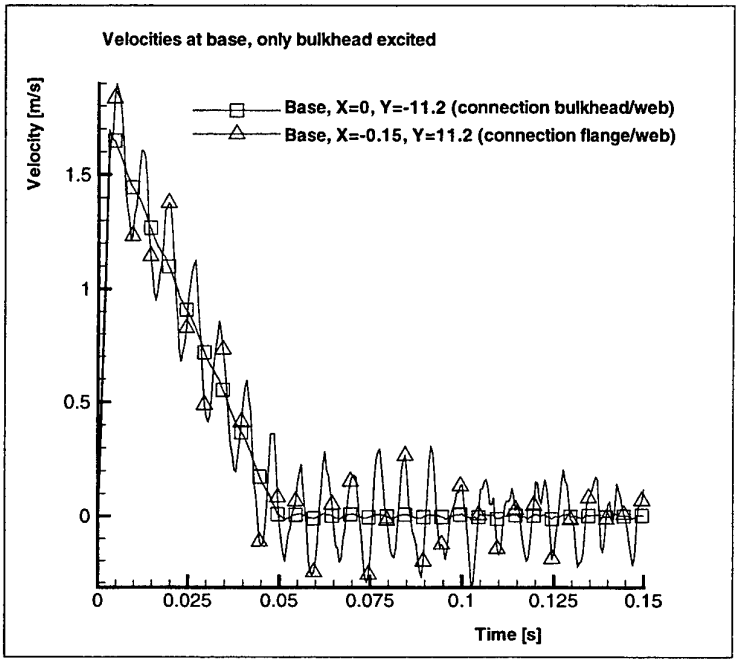

Figure 9.3 a) *Velocities at Y=-11.2 m, model with only vertical stiffener built up from profiles T6, T4.5 and T3, and slice of bulkhead; Excitation at bulkhead only*

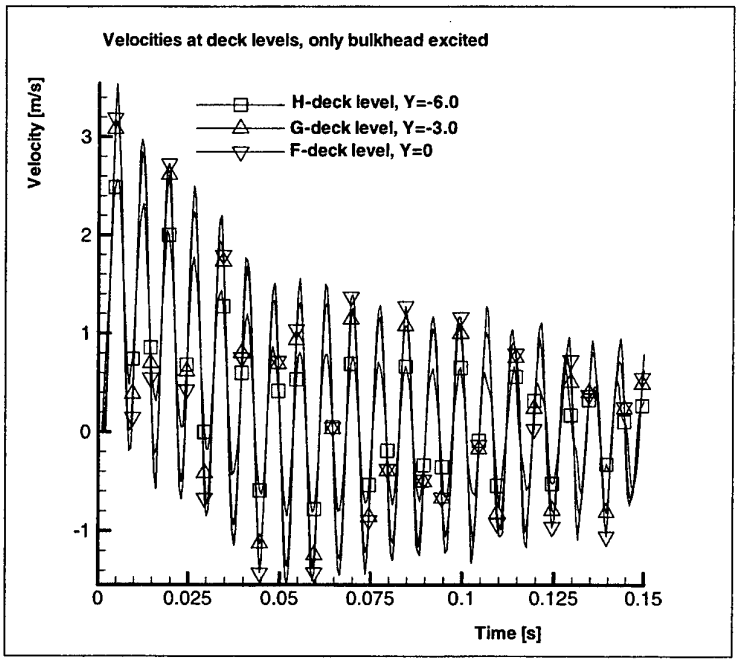

Figure 9.3 b) *Velocity responses at the deck levels, model with only vertical stiffener built up from profiles T6, T4.5 and T3, and slice of bulkhead; Excitation at bulkhead only*

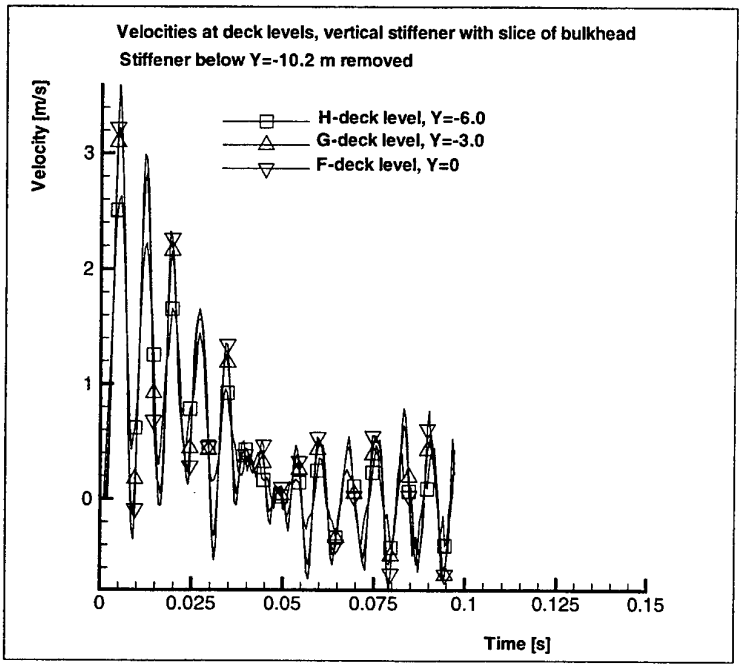

Figure 9.4 *Velocity responses at the deck levels, model with only vertical stiffener built up from profiles T6, T4.5 and T3, and slice of bulkhead; No stiffener from Y=-10.2 to Y=-11.2 m*

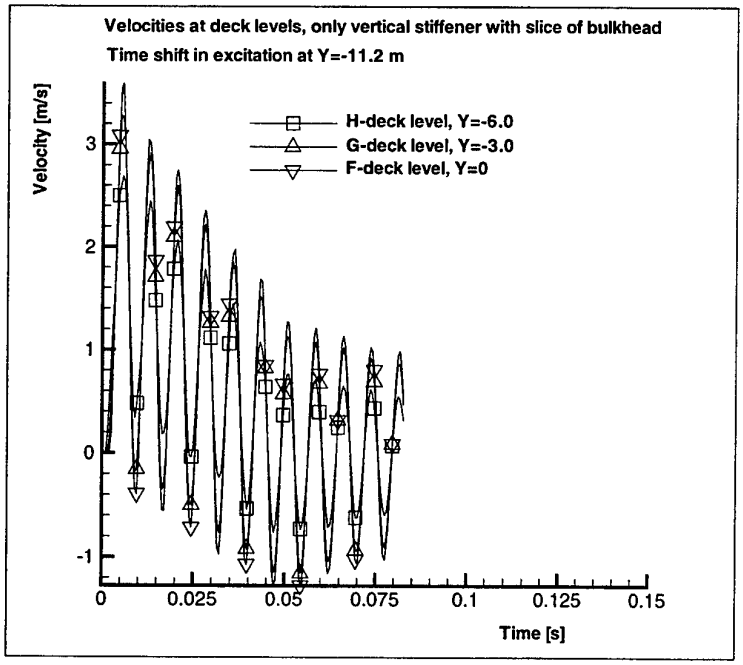

Figure 9.5 *Velocity responses at the deck levels, model with only vertical stiffener built up from profiles T6, T4.5 and T3, and slice of bulkhead; Time shift in excitation at Y=-11.2 m*

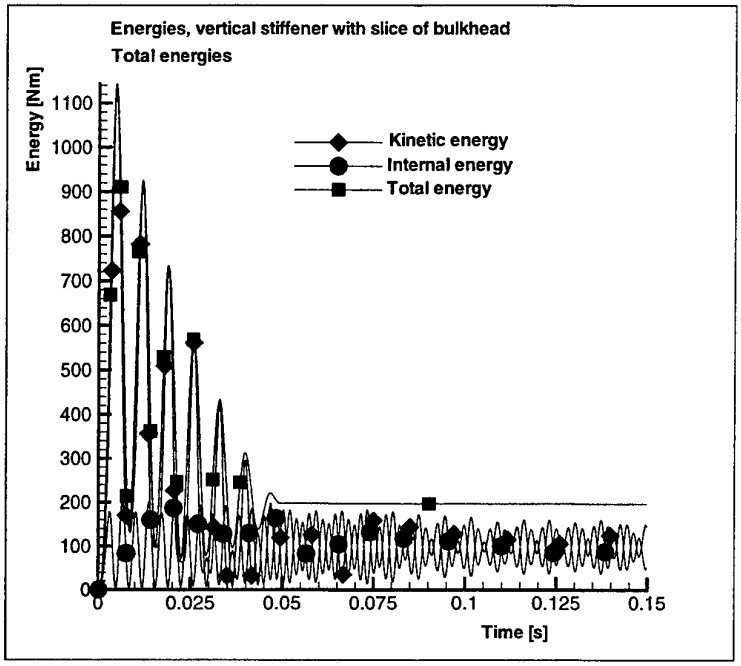

Figure 9.6 a) *Total energy distribution, model with only vertical stiffener built up from profiles T6, T4.5 and T3, and slice of bulkhead (case from fig. 9.2)*

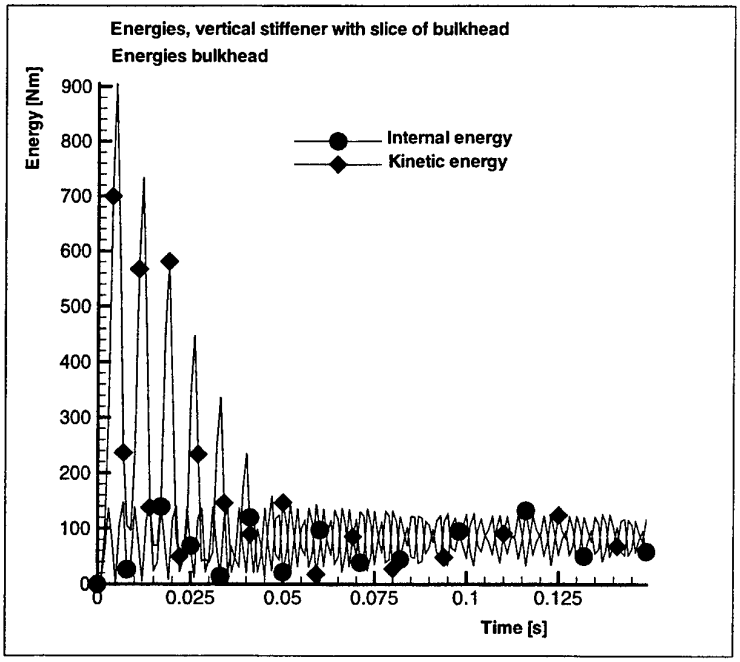

Figure 9.6 b) *Energy distribution in bulkhead, model with only vertical stiffener built up from profiles T6, T4.5 and T3, and slice of bulkhead (case from fig. 9.2)*

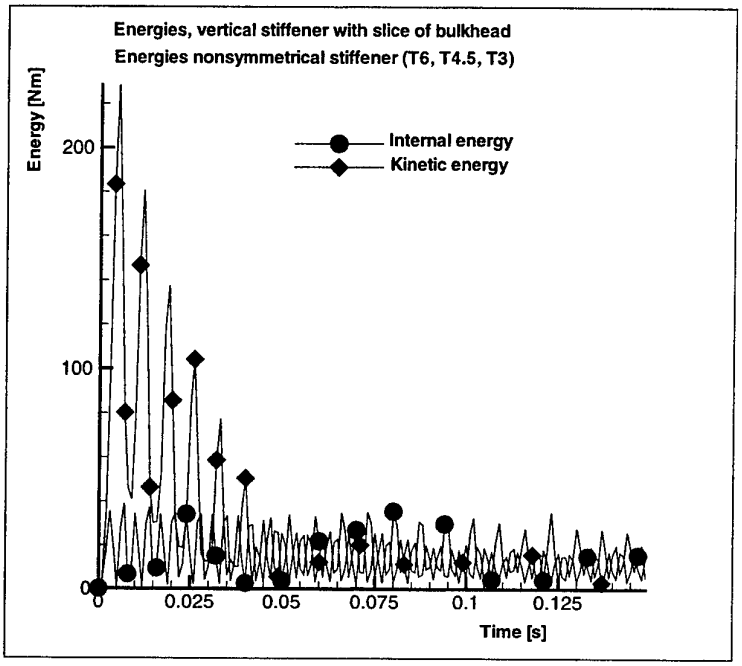

Figure 9.6 c) *Energy distribution in stiffener, model with only vertical stiffener built up from profiles T6, T4.5 and T3, and slice of bulkhead (case from fig. 9.2)*

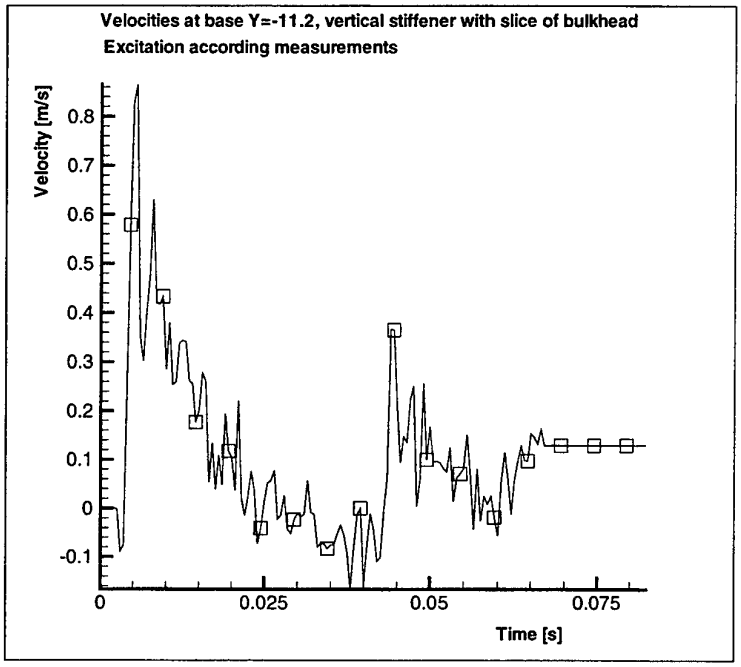

Figure 9.7 a) *Velocity at base Y=-11.2 m, model with vertical stiffener and slice of bulkhead; Excited by measured signal*

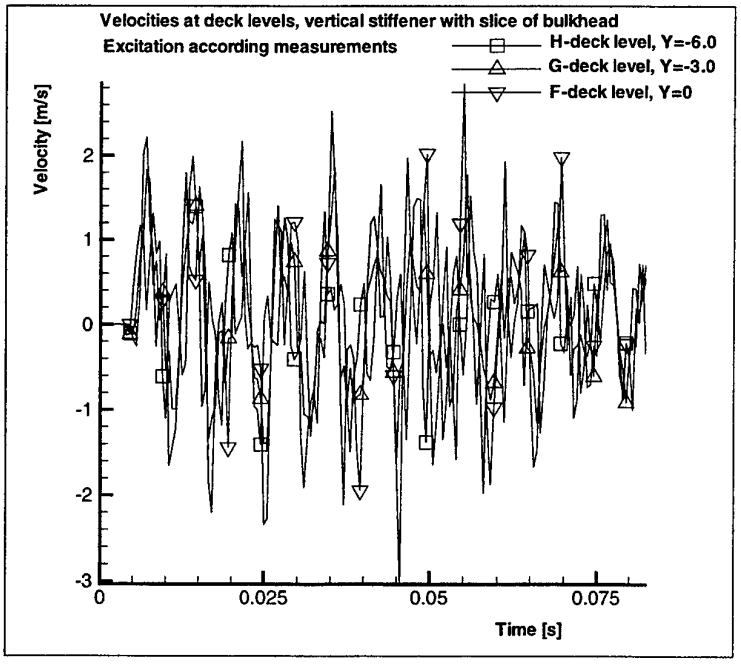

Figure 9.7 b) *Velocity responses at the deck levels, model with vertical stiffener and slice of bulkhead; Excited by measured signal*

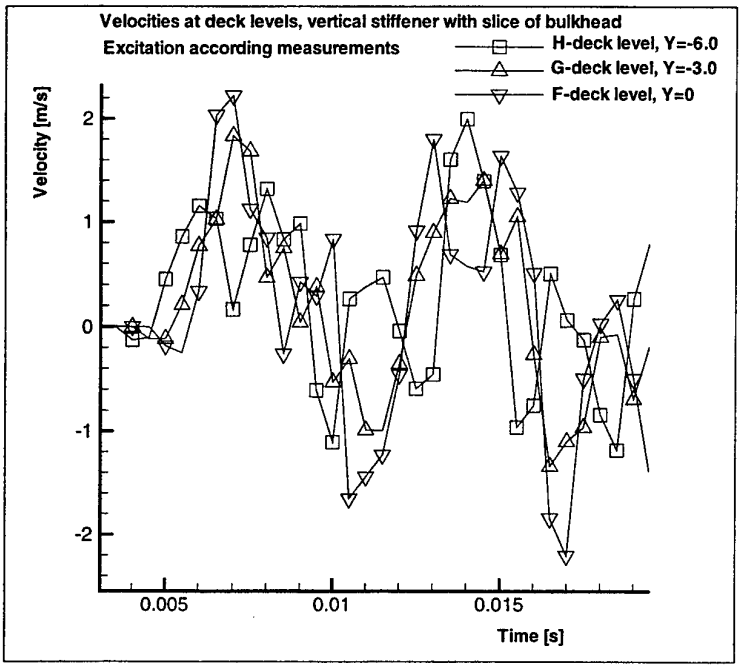

Figure 9.7 c) *Velocity responses at the deck levels, model with vertical stiffener and slice of bulkhead; Excited by measured signal (zoomed time scale)*

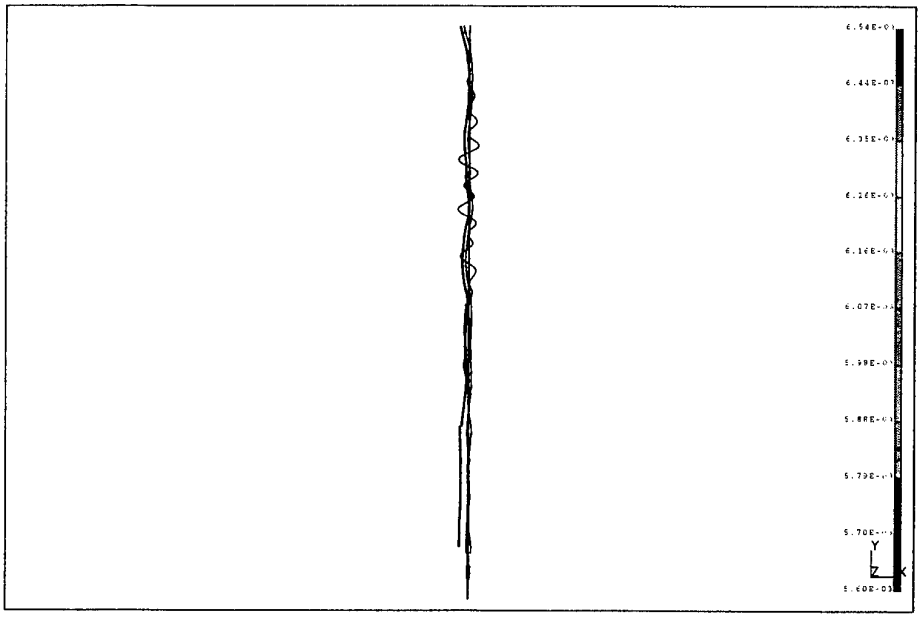

Figure 9.7 d) *Deformation at time is 49.498 ms, model with vertical stiffener and slice of bulkhead; Excited by measured signal*

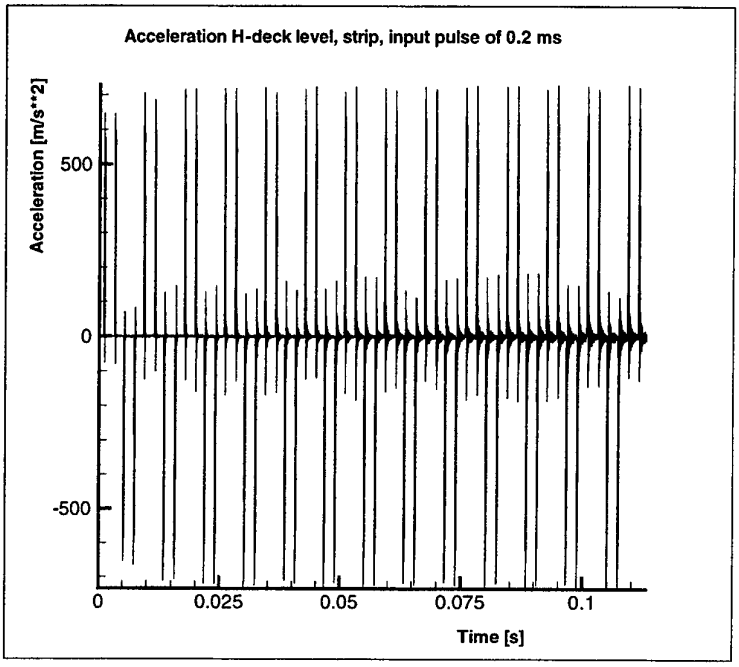

Figure 9.8 a) *Acceleration response at the H-deck level, only slice of bulkhead with thickness 7 mm; Excited by block function, duration 0.2 ms*

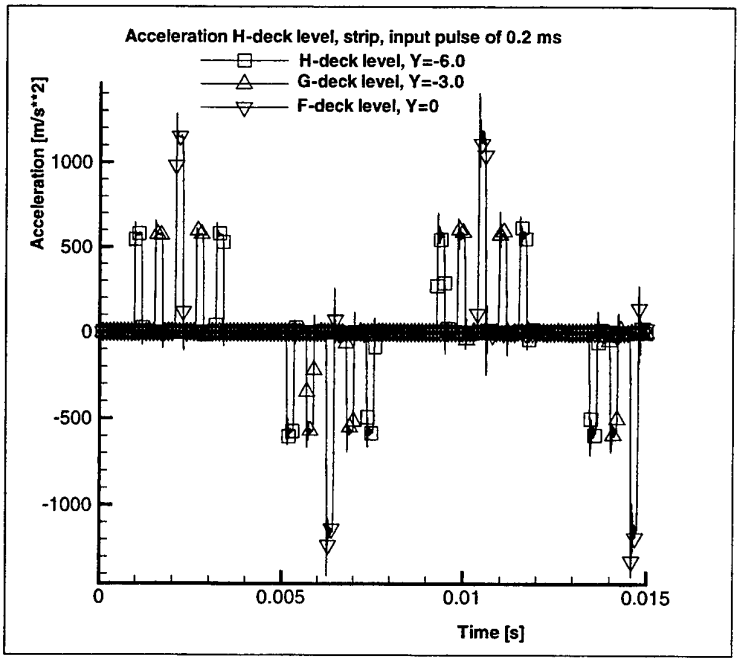

Figure 9.8 b) *Acceleration responses at the deck levels, only slice of bulkhead with thickness 7 mm; Excited by block function, duration 0.2 ms*

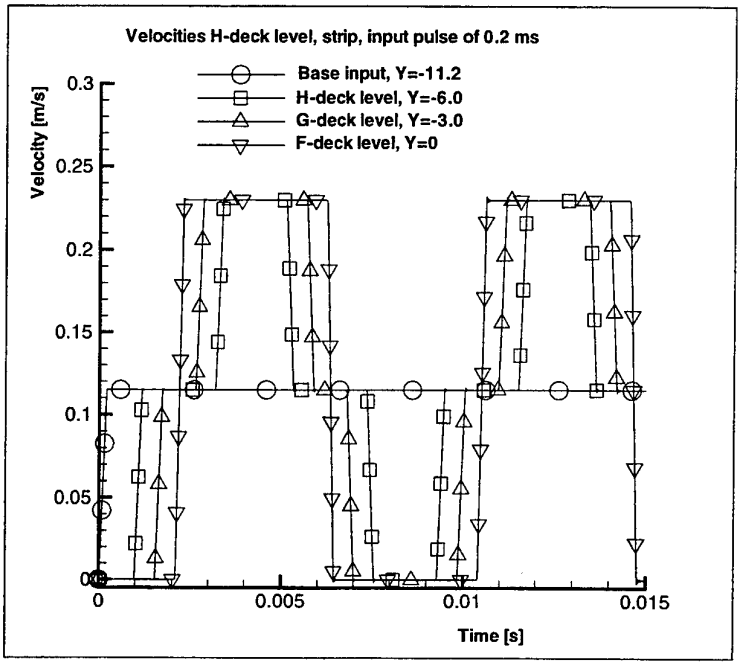

Figure 9.8 c) *Velocity responses at the deck levels, only slice of bulkhead with thickness 7 mm; Excited by block function, duration 0.2 ms*

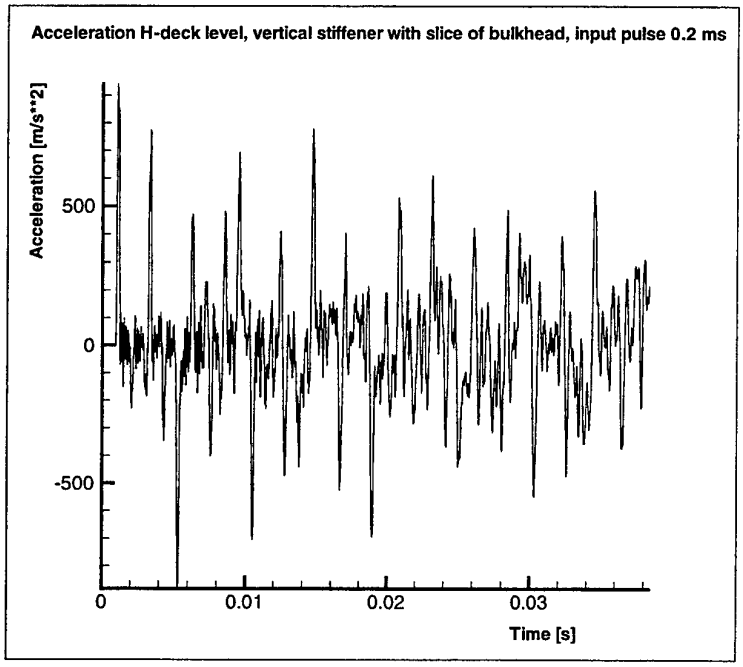

Figure 9.9 a) *Acceleration response at the H-deck level, vertical stiffener with slice of bulkhead; Excited by block function, duration 0.2 ms*

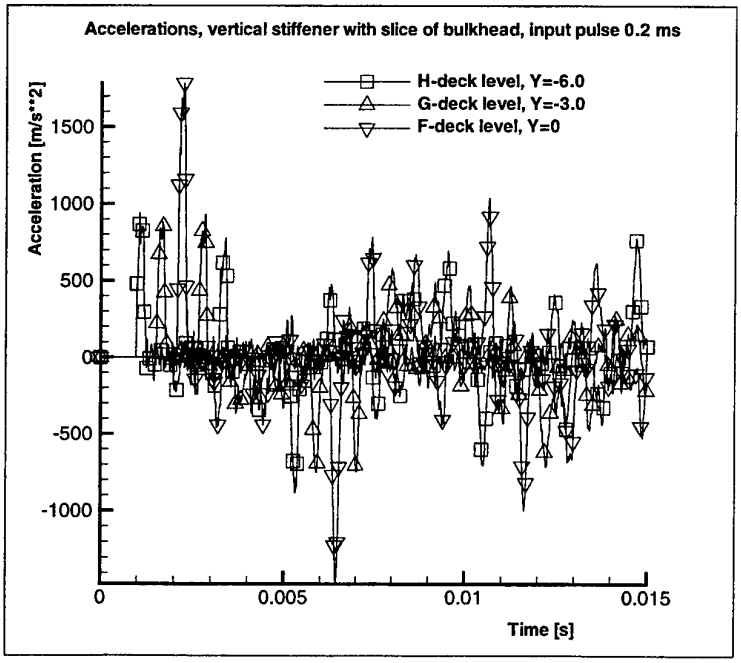

Figure 9.9 b) *Acceleration responses at the deck levels, vertical stiffener with slice of bulkhead; Excited by block function, duration 0.2 ms*

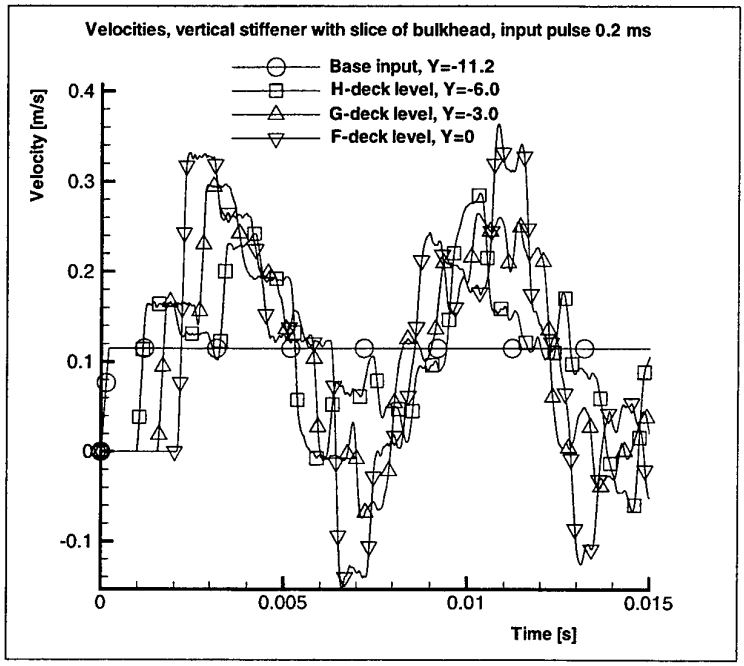

Figure 9.9 c) *Velocity responses at the deck levels, vertical stiffener with slice of bulkhead; Excited by block function, duration 0.2 ms*

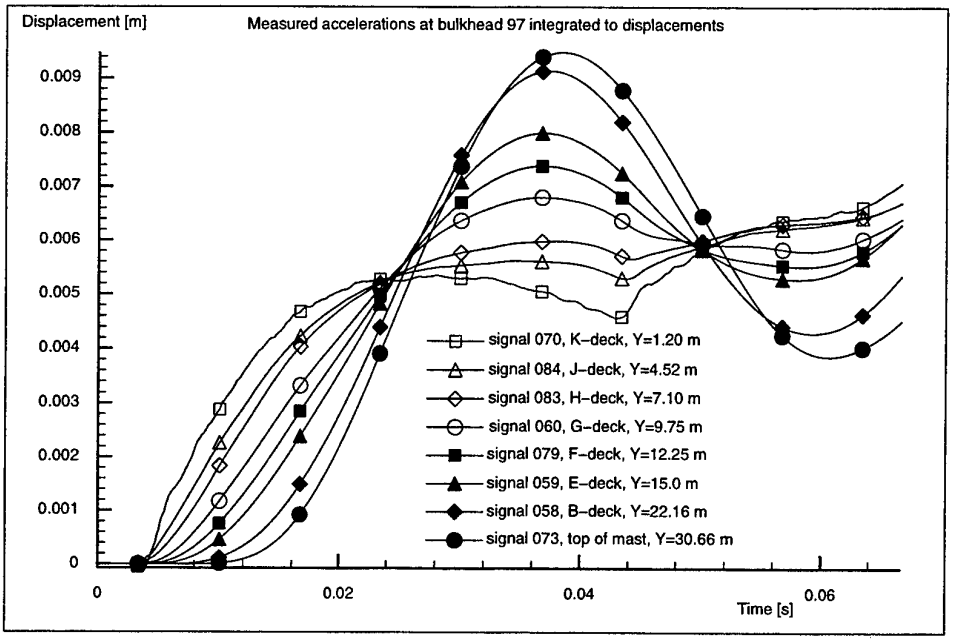

Figure 11.1 a) *Displacements as integrated from measured accelerations at the centerline of bulkhead 97, different deck levels, shock trials M-frigate, shot number two*

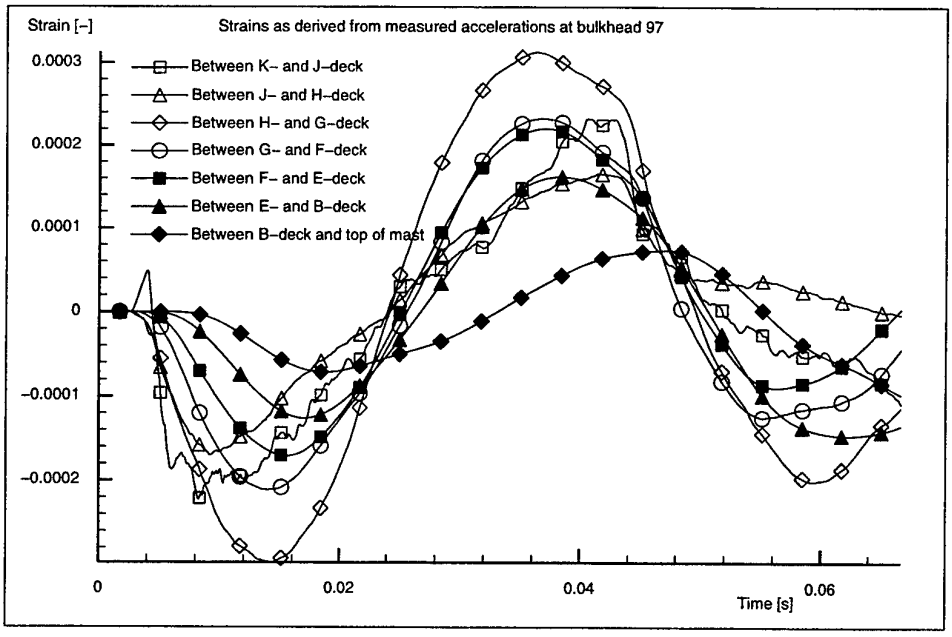

Figure 11.1 b) *Strains as derived from the measured signals at the centerline of bulkhead 97, different deck levels, shock trials M-frigate, shot number two*

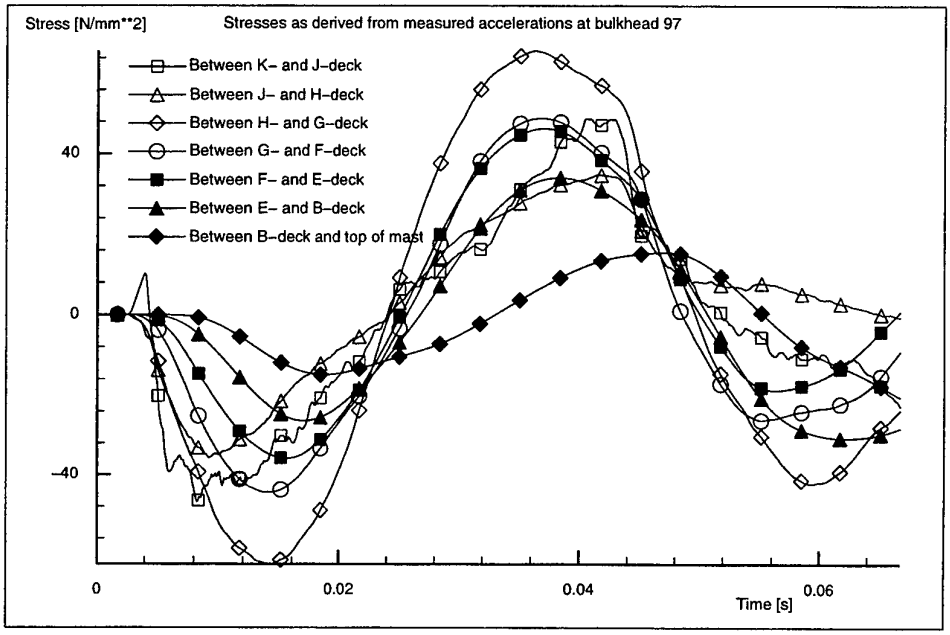

Figure 11.1 c) Stresses as derived from the measured signals at the centerline of bulkhead 97, different deck levels, shock trials M-frigate, shot number two

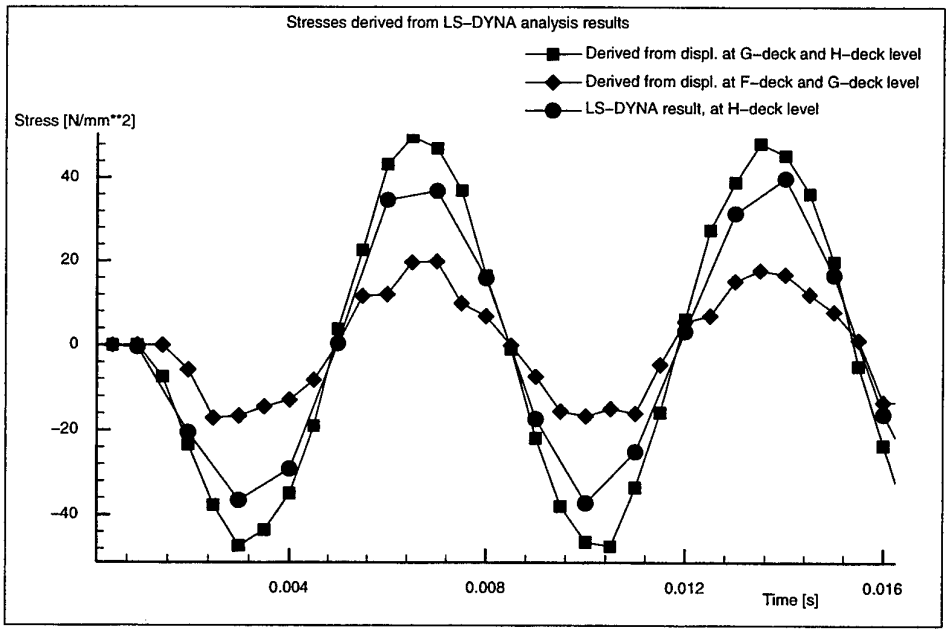

Figure 11.2 Stresses as derived from analysis results, model with only vertical stiffener built up from profiles T6, T4.5 and T3, and slice of bulkhead (case from fig. 9.2)

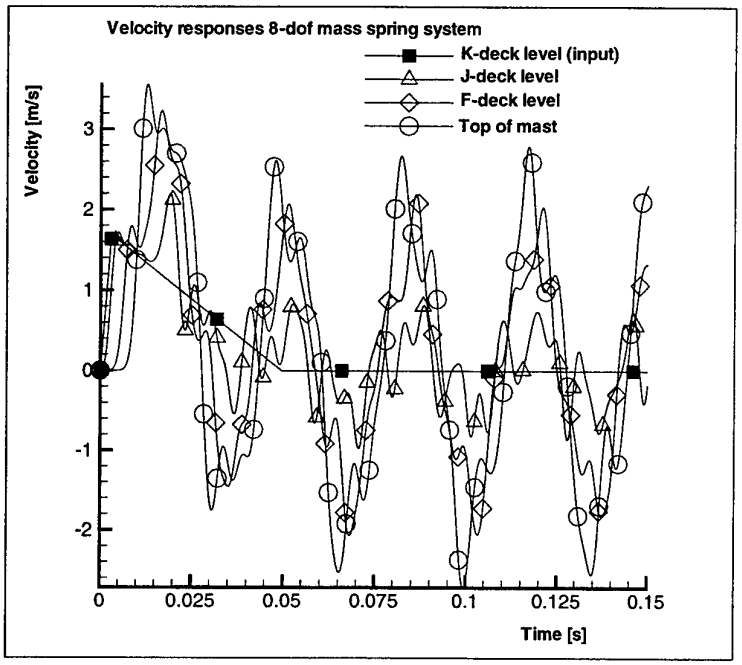

Figure 11.3 *Velocity responses as calculated using 8-dof mass-spring system; Equal spring stiffness ($1.32 \cdot 10^9$ N/m) and masses (1656 kg)*

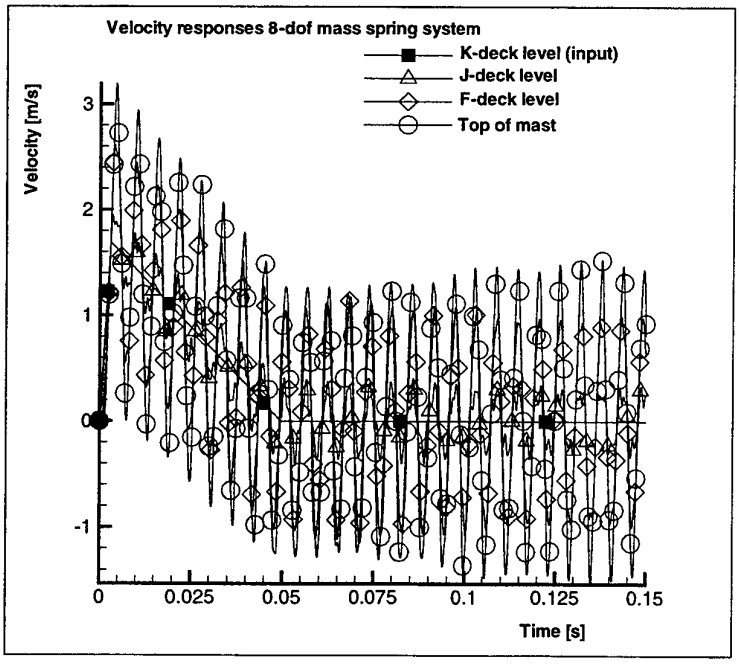

Figure 11.4 *Velocity responses as calculated using 8-dof mass-spring system; Equal spring stiffness ($2.1 \cdot 10^{11}$ N/m) and masses (7800 kg)*

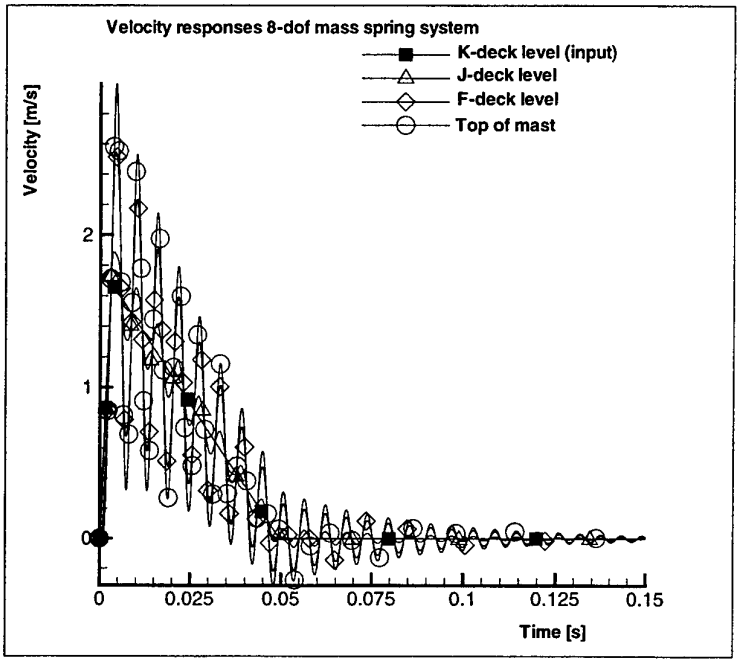

Figure 11.5 a) Velocity responses as calculated using 8-dof mass-spring system; Equal spring stiffness ($2.1 \cdot 10^{11}$ N/m) and masses (7800 kg); Effect of damping, all damping $1.0 \cdot 10^{7}$ Ns/m

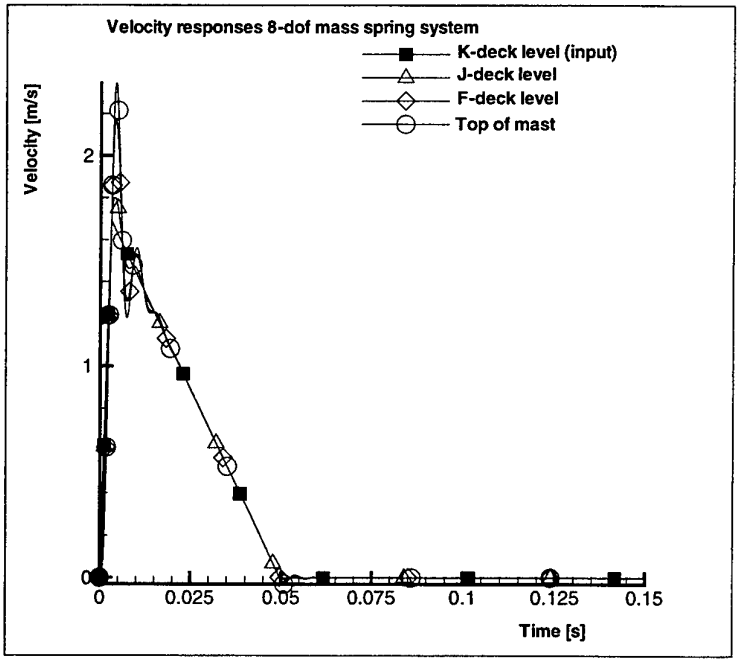

Figure 11.5 b) Velocity responses as calculated using 8-dof mass-spring system; Equal spring stiffness ($2.1 \cdot 10^{11}$ N/m) and masses (7800 kg)); Effect of damping, all damping $1.0 \cdot 10^{8}$ Ns/m

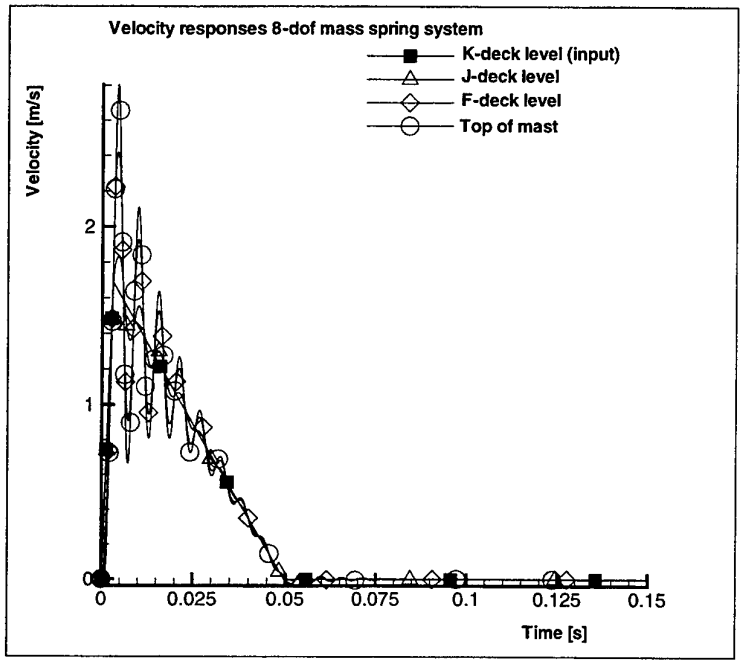

Figure 11.5 c) Velocity responses as calculated using 8-dof mass-spring system; Equal spring stiffness ($2.1 \cdot 10^{11}$ N/m) and masses (7800 kg)); Effect of damping, first damping value $1.0 \cdot 10^{8}$ Ns/m, remaining damping $1.0 \cdot 10^{7}$ Ns/m

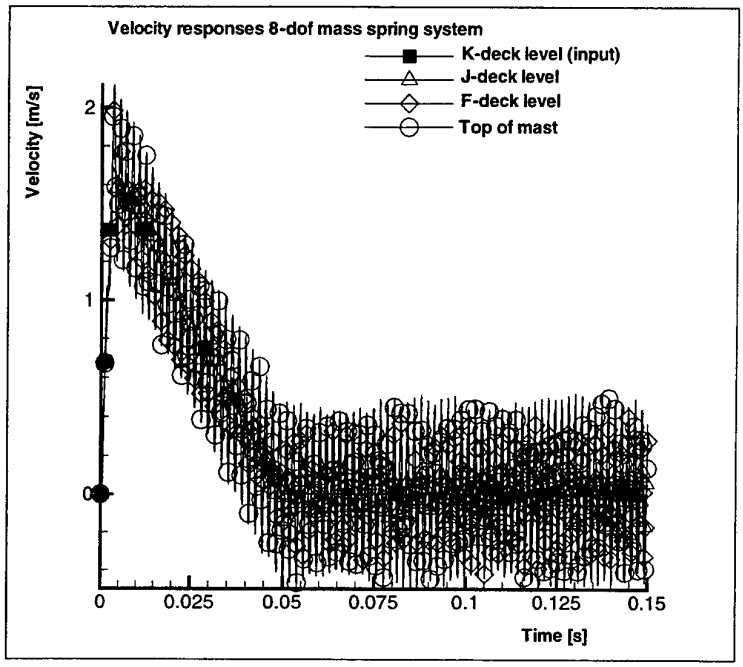

Figure 11.6 a) *Velocity responses as calculated using 8-dof mass-spring system; Equal spring stiffness ($2.1 \cdot 10^{11}$ N/m); No damping; All masses reduced to 780 kg*

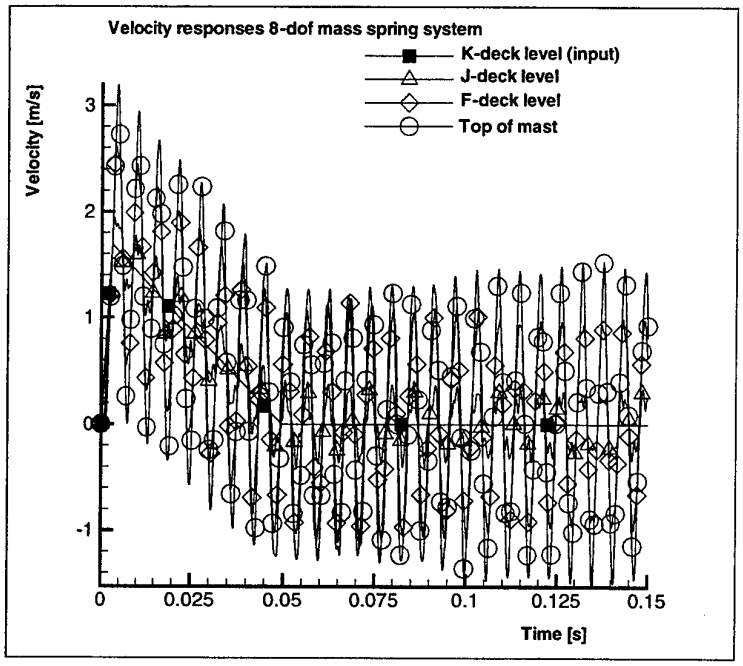

Figure 11.6 b) *Velocity responses as calculated using 8-dof mass-spring system; Equal spring stiffness ($2.1 \cdot 10^{11}$ N/m); No damping; First mass increased to 78000 kg, all remaining masses 7800 kg*

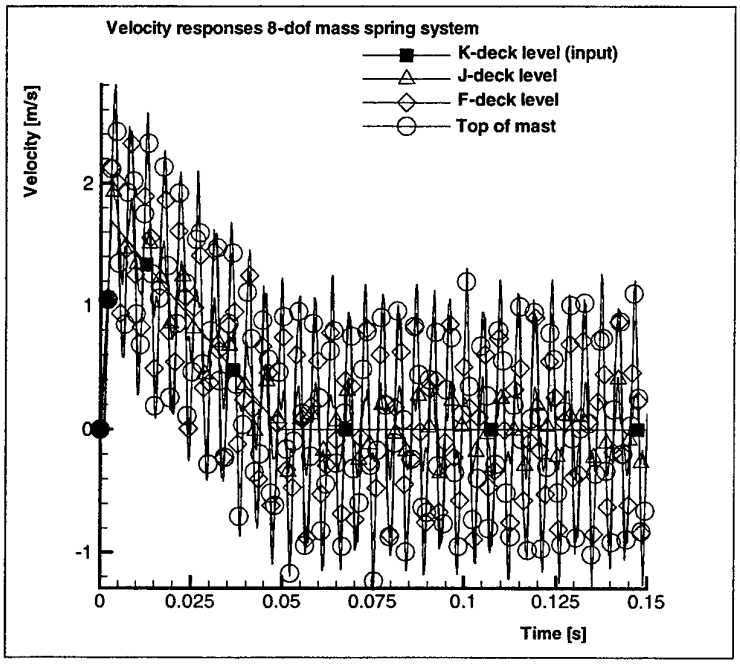

Figure 11.6 c) Velocity responses as calculated using 8-dof mass-spring system; Equal spring stiffness ($2.1 \cdot 10^{11}$ N/m); No damping; Same total mass, linear distributed (13840 kg at K-deck level, 1730 kg at top of mast level)

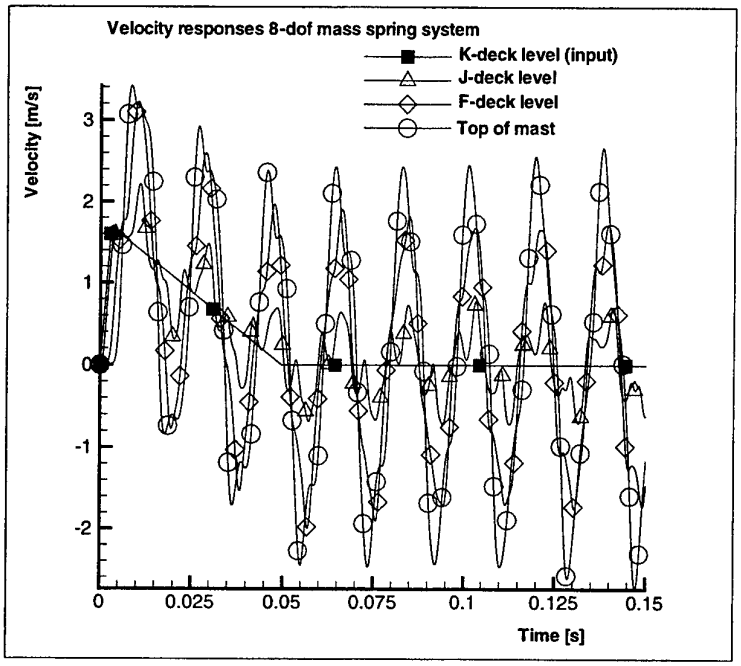

Figure 11.7 a) *Velocity responses as calculated using 8-dof mass-spring system; Equal masses (7800 kg); No damping; All spring stiffnesses reduced to $2.1 \cdot 10^{10}$ N/m*

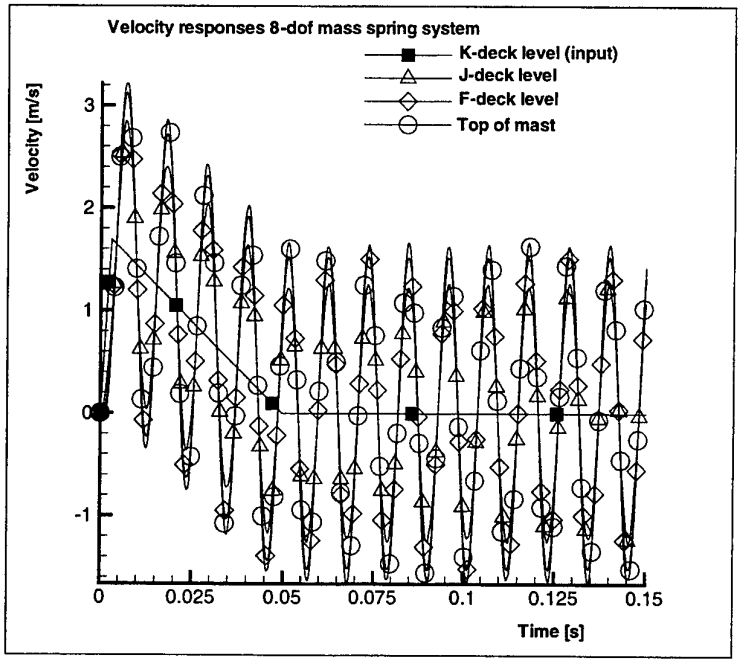

Figure 11.7 b) *Velocity responses as calculated using 8-dof mass-spring system; Equal masses (7800 kg); No damping; First spring stiffness reduced to $2.1 \cdot 10^{10}$ N/m, all other spring stiffnesses at $2.1 \cdot 10^{11}$ N/m*

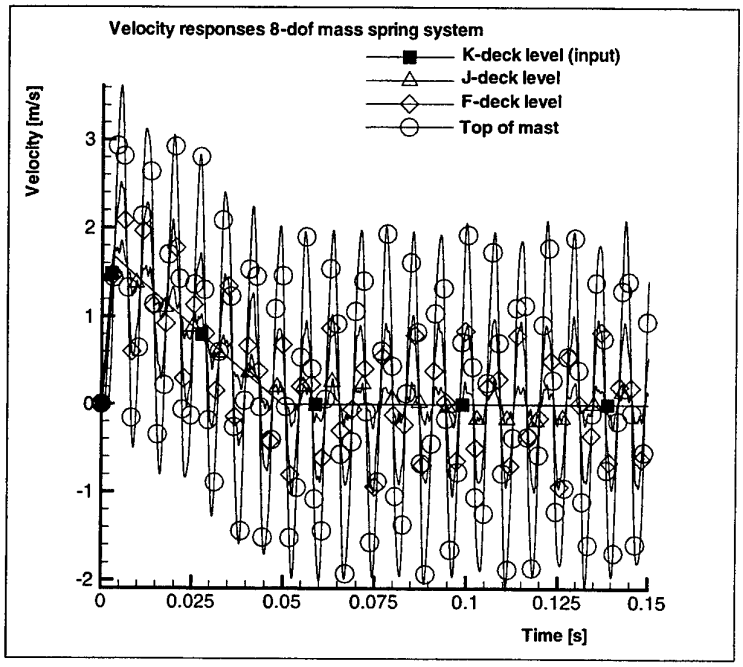

Figure 11.7 c) *Velocity responses as calculated using 8-dof mass-spring system; Equal masses (7800 kg); No damping; Linear varying spring stiffness from $2.1 \cdot 10^{11}$ N/m between K- and J-deck, upto $3.0 \cdot 10^{10}$ N/m between B-deck and top of mast*

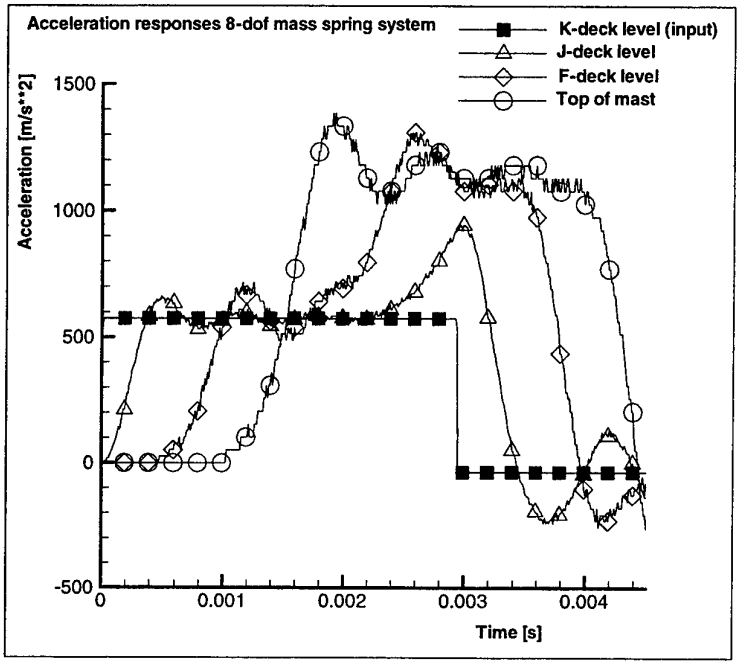

Figure 11.8 a) *Acceleration responses as calculated using 8-dof mass-spring system; Equal masses (7800 kg); No damping; Equal spring stiffness ($2.1 \cdot 10^{11}$ N/m); Case from fig. 11.4*

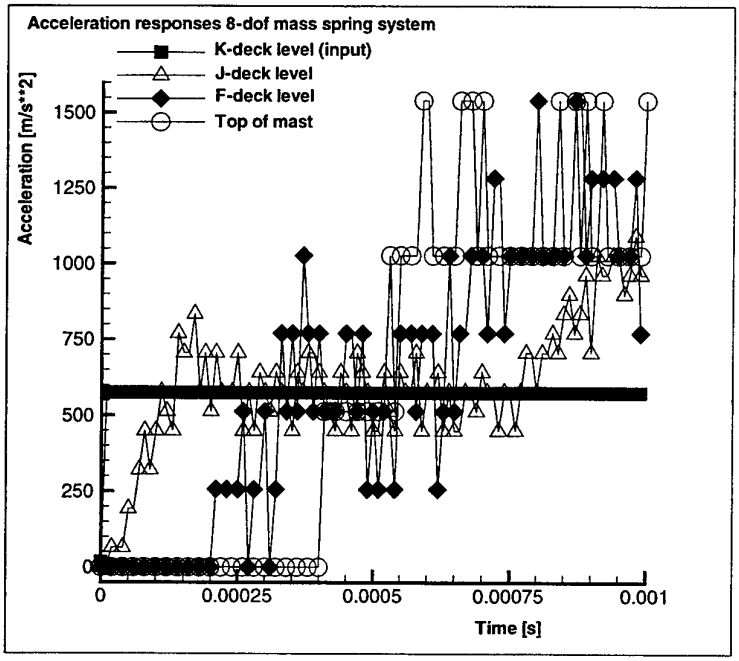

Figure 11.8 b) *Acceleration responses as calculated using 8-dof mass-spring system; Equal masses (780 kg); No damping; Equal spring stiffness ($2.1 \cdot 10^{11}$ N/m); Case from fig. 11.6 a)*

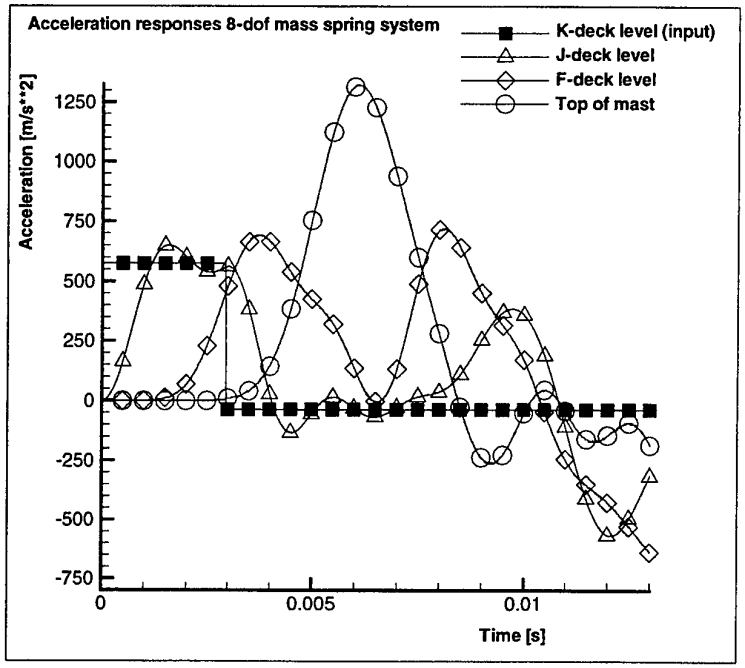

Figure 11.8 c) *Acceleration responses as calculated using 8-dof mass-spring system; Equal masses (7800 kg); No damping; Equal spring stiffness ($2.1 \cdot 10^{10}$ N/m); Case from fig. 11.7 a)*

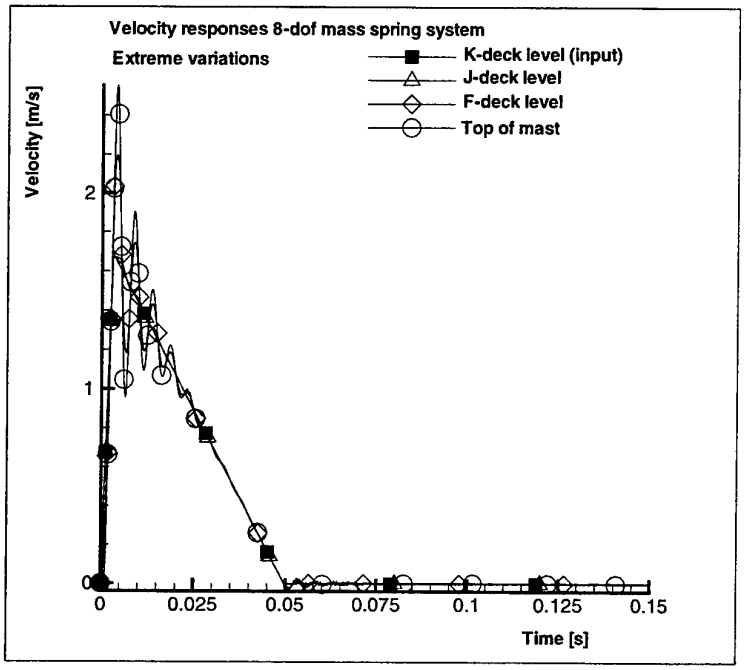

Figure 11.9 a) *Velocity responses for 8-dof mass-spring system; Equal springs ($2.1 \cdot 10^{11}$ N/m); Equal masses of 7800 kg; Extreme damping variation ($1.0 \cdot 10^{9}$ Ns/m above K-deck upto $1.0 \cdot 10^{3}$ Ns/m below top of mast)*

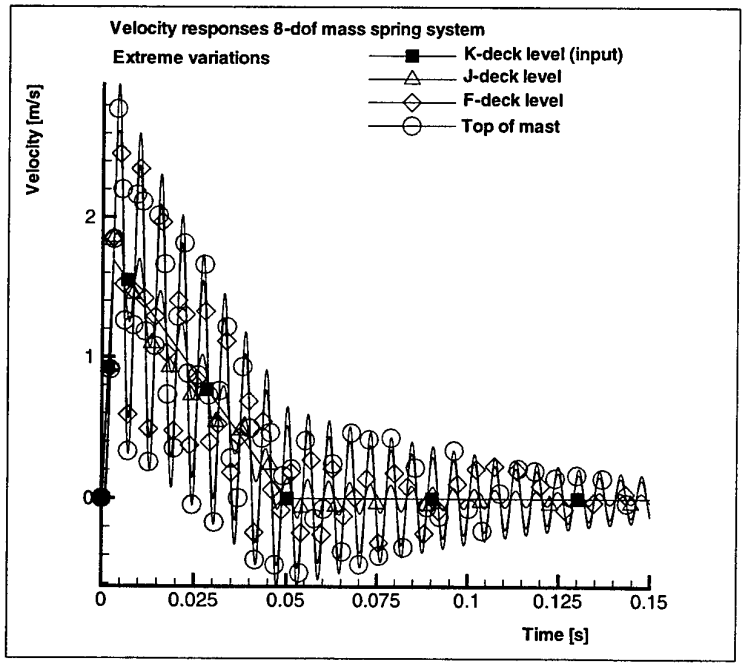

Figure 11.9 b) *Velocity responses for 8-dof mass-spring system; Equal springs ($2.1 \cdot 10^{11}$ N/m); Equal masses of 7800 kg; Extreme damping variation ($1.0 \cdot 10^{3}$ Ns/m above K-deck upto $1.0 \cdot 10^{9}$ Ns/m below top of mast)*

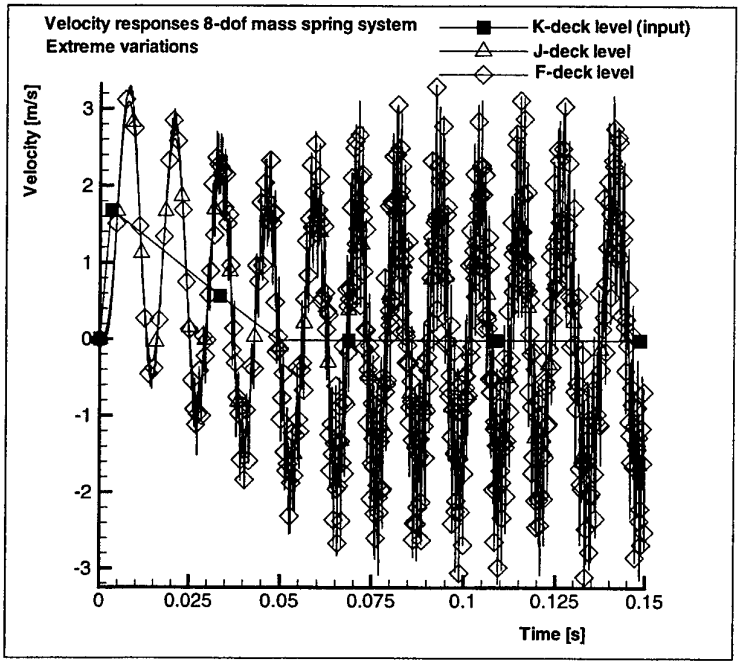

Figure 11.10 a) Velocity responses as calculated using 8-dof mass-spring system; Equal spring stiffnesses of $2.1 \cdot 10^{11}$ N/m; No damping; Extreme mass variation ($7.8 \cdot 10^{6}$ kg at K-deck level upto $7.8 \cdot 10^{-1}$ kg at top of mast level)

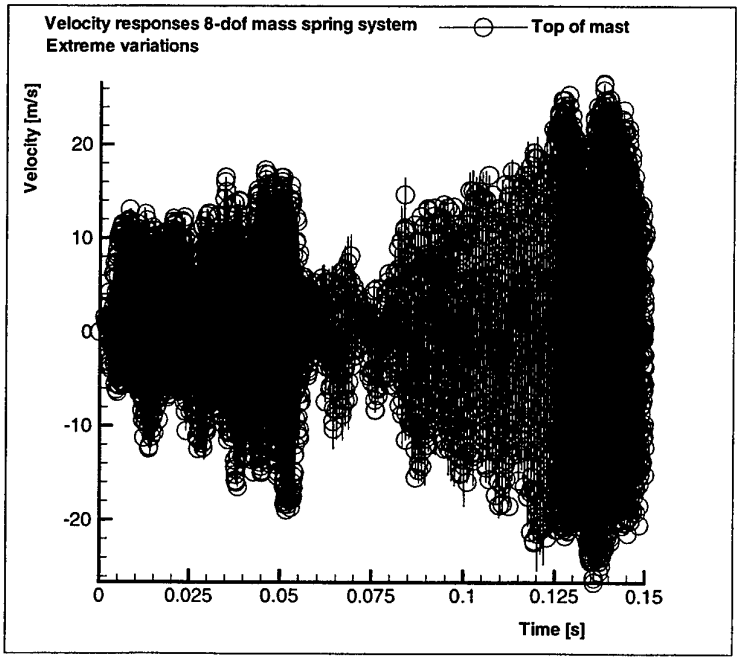

Figure 11.10 b) Velocity responses as calculated using 8-dof mass-spring system; Equal spring stiffnesses of $2.1 \cdot 10^{11}$ N/m; No damping; Extreme mass variation ($7.8 \cdot 10^{6}$ kg at K-deck level upto $7.8 \cdot 10^{-1}$ kg at top of mast level)

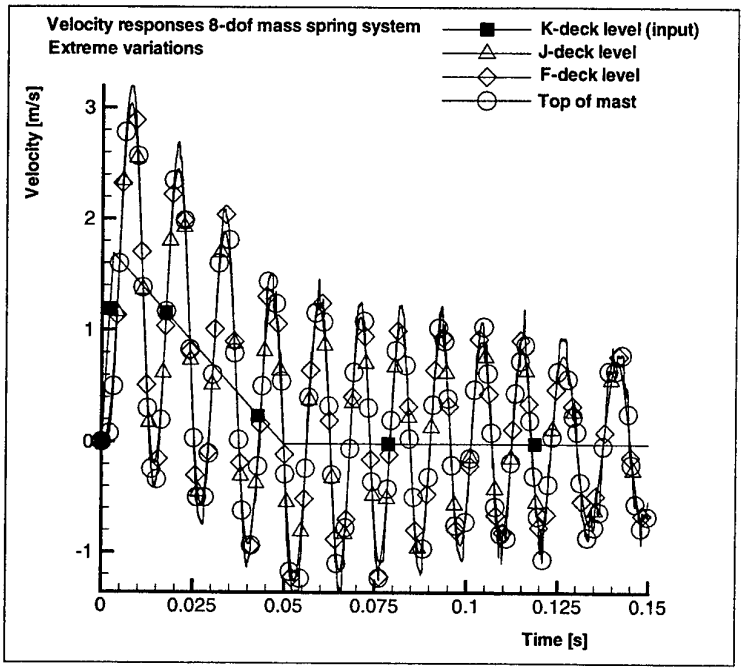

Figure 11.10 c) Velocity responses as calculated using 8-dof mass-spring system; Equal spring stiffnesses of $2.1 \cdot 10^{11}$ N/m; Equal damping of $1.0 \cdot 10^{7}$ Ns/m; Extreme mass variation ($7.8 \cdot 10^{6}$ kg at K-deck level upto $7.8 \cdot 10^{-1}$ kg at top of mast level)

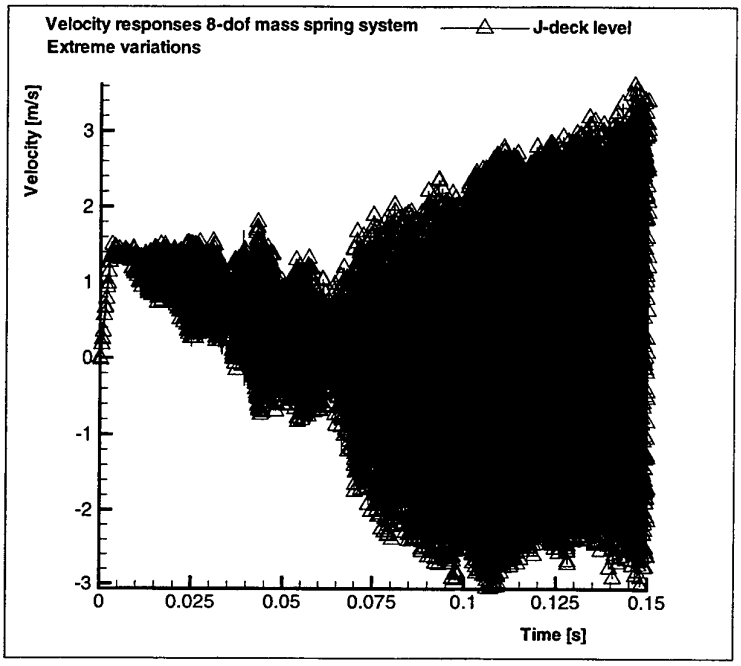

Figure 11.11 a) Velocity responses as calculated using 8-dof mass-spring system; Equal spring stiffnesses of $2.1 \cdot 10^{11}$ N/m; No damping; Extreme mass variation ($7.8 \cdot 10^{-1}$ kg at K-deck level upto $7.8 \cdot 10^{6}$ kg at top of mast level)

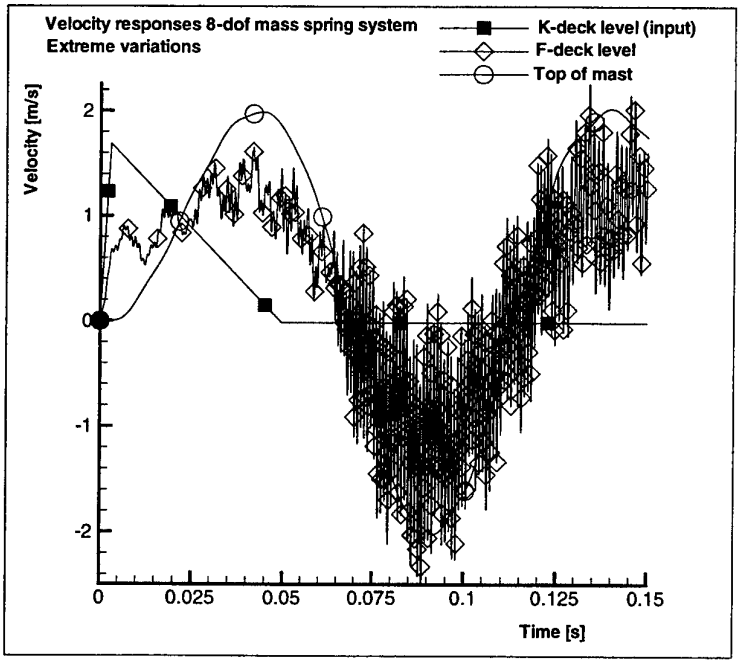

Figure 11.11 b) Velocity responses as calculated using 8-dof mass-spring system; Equal spring stiffnesses of $2.1 \cdot 10^{11}$ N/m; No damping; Extreme mass variation ($7.8 \cdot 10^{-1}$ kg at K-deck level upto $7.8 \cdot 10^{6}$ kg at top of mast level)

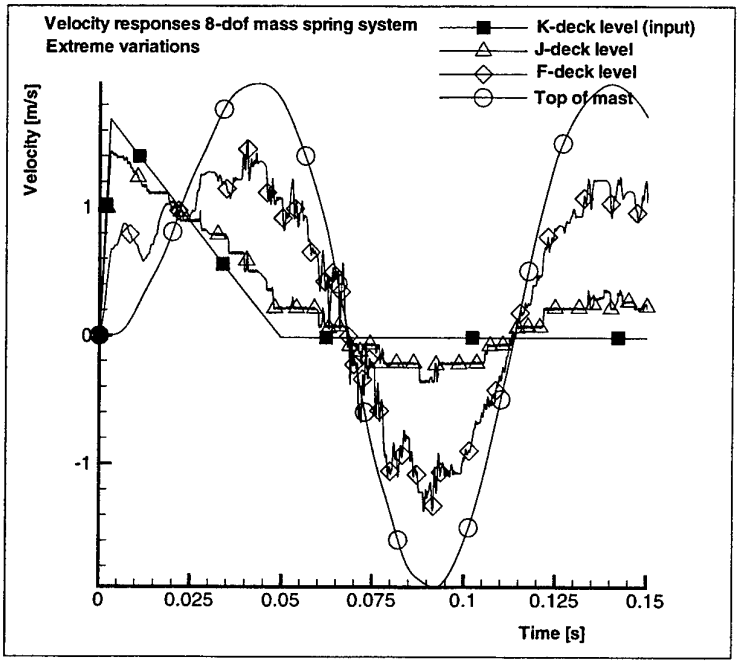

Figure 11.11 c) Velocity responses as calculated using 8-dof mass-spring system; Equal spring stiffnesses of $2.1 \cdot 10^{11}$ N/m; Equal damping of $1.0 \cdot 10^{7}$ Ns/m; Extreme mass variation ($7.8 \cdot 10^{-1}$ kg at K-deck level upto $7.8 \cdot 10^{6}$ kg at top of mast level)

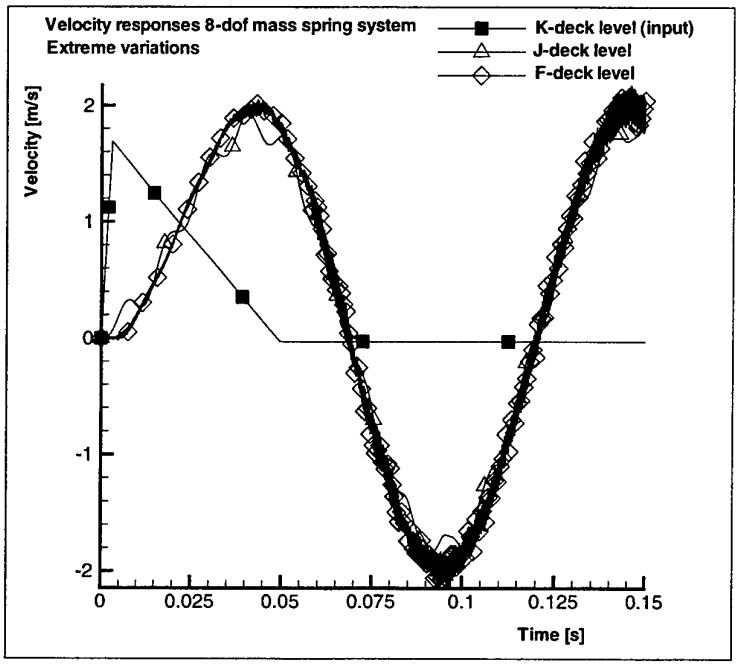

Figure 11.12 a) Velocity responses for 8-dof mass-spring system; Equal masses of 7800 kg; No damping; Extreme variation of springs ($2.1 \cdot 10^8$ N/m between K-deck and J-deck upto $2.1 \cdot 10^{14}$ N/m between B-deck and top of mast level)

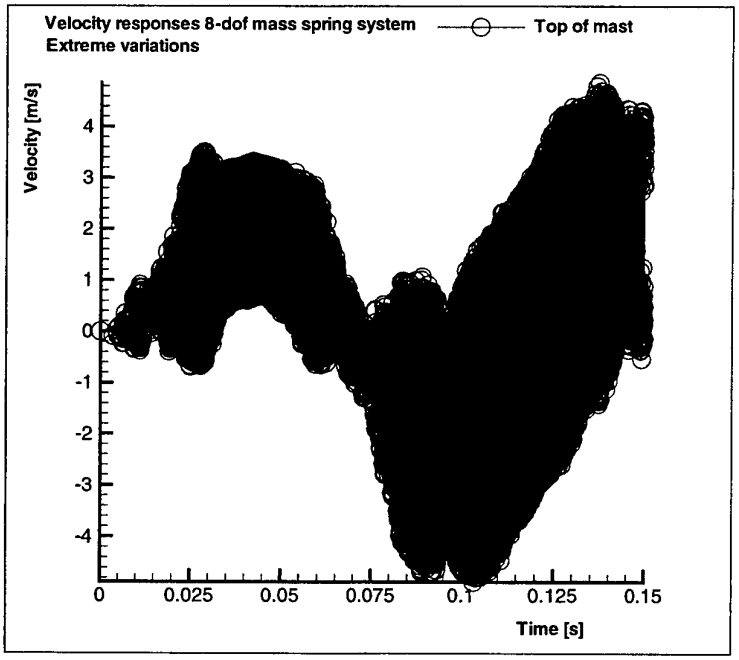

Figure 11.12 b) Velocity responses for 8-dof mass-spring system; Equal masses of 7800 kg; No damping; Extreme variation of springs ($2.1 \cdot 10^8$ N/m between K-deck and J-deck upto $2.1 \cdot 10^{14}$ N/m between B-deck and top of mast level)

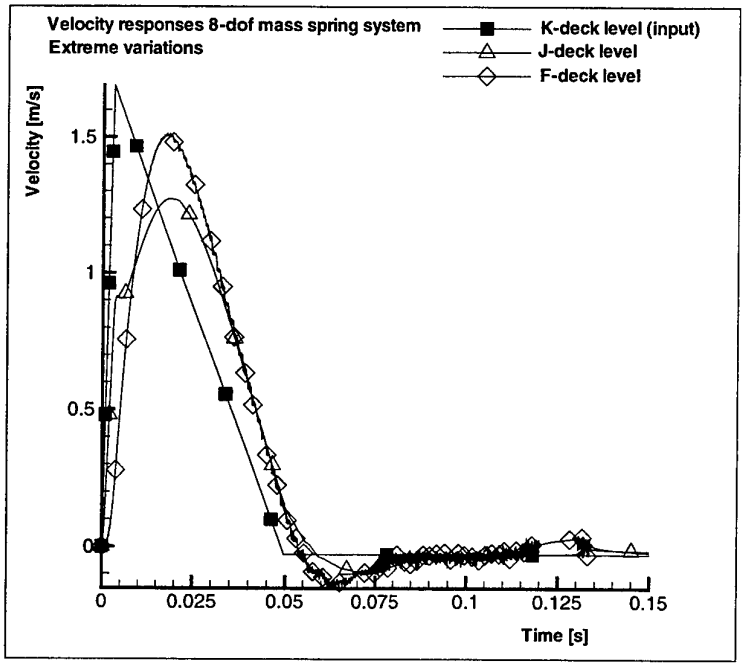

Figure 11.12 c) Velocity responses for 8-dof mass-spring system; Equal masses of 7800 kg; Equal damping of $1.0 \cdot 10^7$ Ns/m; Extreme variation of springs ($2.1 \cdot 10^8$ N/m above K-deck upto $2.1 \cdot 10^{14}$ N/m between B-deck and top of mast level)

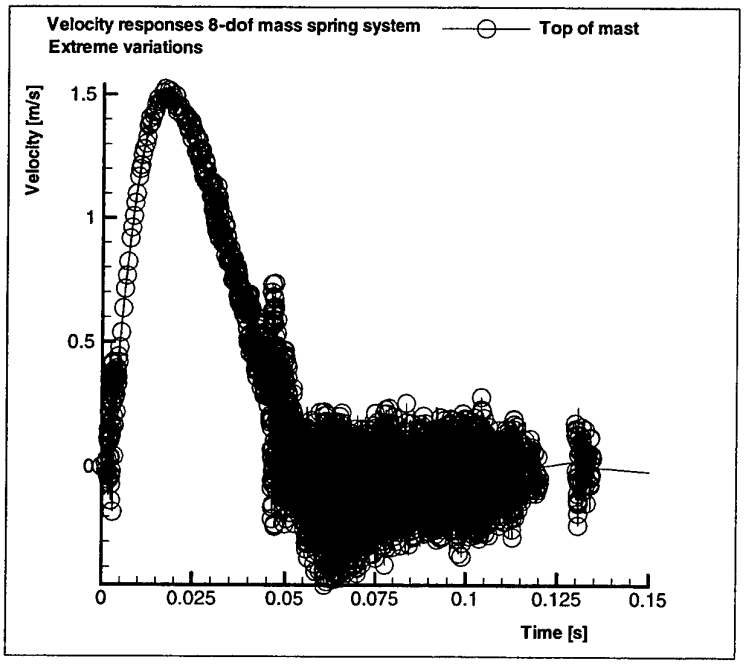

Figure 11.12 d) Velocity responses for 8-dof mass-spring system; Equal masses of 7800 kg; Equal damping of $1.0 \cdot 10^7$ Ns/m; Extreme variation of springs ($2.1 \cdot 10^8$ N/m above K-deck upto $2.1 \cdot 10^{14}$ N/m between B-deck and top of mast level)

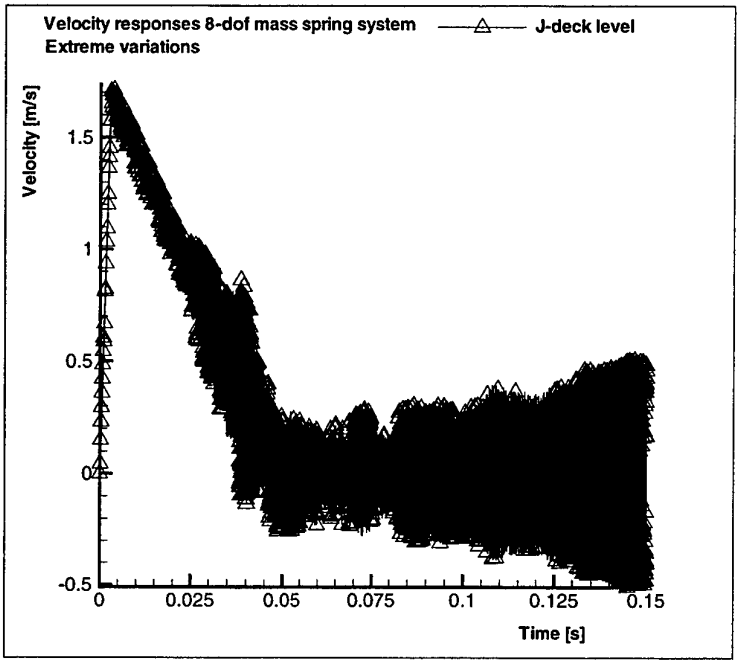

Figure 11.13 a) Velocity responses for 8-dof mass-spring system; Equal masses of 7800 kg; No damping; Extreme variation of spring stiffnesses ($2.1 \cdot 10^{14}$ N/m between K-deck and J-deck upto $2.1 \cdot 10^{8}$ N/m between B-deck and top of mast level)

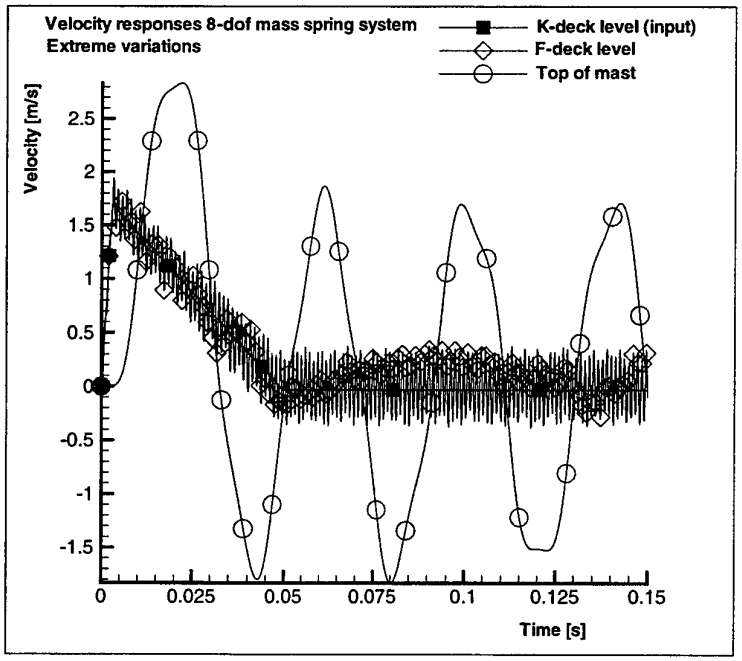

Figure 11.13 b) Velocity responses for 8-dof mass-spring system; Equal masses of 7800 kg; No damping; Extreme variation of spring stiffnesses ($2.1 \cdot 10^{14}$ N/m between K-deck and J-deck upto $2.1 \cdot 10^{8}$ N/m between B-deck and top of mast level)

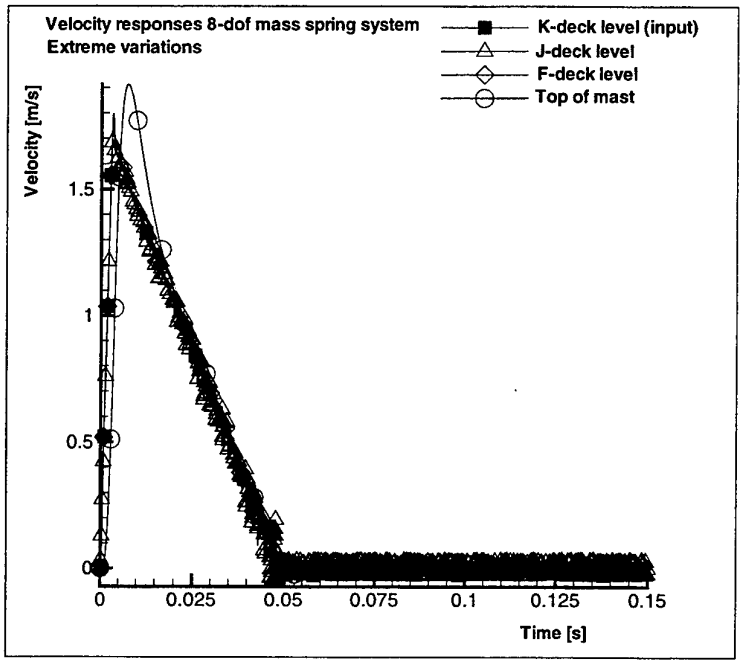

Figure 11.13 c) Velocity responses as calculated using 8-dof mass-spring system; Equal masses of 7800 kg; Equal damping of $1.0 \cdot 10^7$ Ns/m; Extreme variation of spring stiffnesses ($2.1 \cdot 10^{14}$ N/m between K-deck and J-deck upto $2.1 \cdot 10^8$ N/m between B-deck and top of mast level)

REPORT DOCUMENTATION PAGE

1. DEFENCE REPORT NUMBER (MOD-NL) TD 99 - 0.393	2. RECIPIENT'S ACCESSION NUMBER	3. PERFORMING ORGANIZATION REPORT NUMBER 1999-CMC-R 054
4. PROJECT/TASK/WORK UNIT NO. 006.93213/01.01	5. CONTRACT NUMBER A98/KM/118	6. REPORT DATE 13 december 1999
7. NUMBER OF PAGES 115 (excl. RDP & distributionlist)	8. NUMBER OF REFERENCES 9	9. TYPE OF REPORT AND DATES COVERED Final

10. TITLE AND SUBTITLE

Shock transmission analyses of a simplified frigate compartment using LS-DYNA

11. AUTHOR(S)

Ir. W. Trouwborst

12. PERFORMING ORGANIZATION NAME(S) AND ADDRESS(ES)

Centre for Mechanical Engineering
Schoemakerstraat 97
2628 VK DELFT, The Netherlands

13. SPONSORING/MONITORING AGENCY NAME(S) AND ADDRESSES(S)
Sponsor: Netherlands Ministry of Defence
Monitoring agency: TNO Defence Research, Schoemakerstraat 97, 2628 VK DELFT, The Netherlands

14. SUPPLEMENTARY NOTES

The Centre for Mechanical Engineering is part of TNO Building and Construction Research

15. ABSTRACT (MAXIMUM 200 WORDS, 1044 BYTES)

This report gives results as obtained with finite element analyses using the explicit finite element program LS-DYNA for a longitudinal slice of a frigate's compartment loaded with a shock pulse based on the kick-off velocity concept. Effects investigated are nonsymmetry of the bulkhead, Rayleigh damping, plasticity and imperfections. Measurements of a full scale shock trial are shortly discussed. Variations of masses and stiffnesses are investigated to find a better correlation between measurements and analysis results.

16. DESCRIPTORS	IDENTIFIERS
Finite element methods	Underwater shock
Frigates	Shockwave propagation
	Shock analysis

17a SECURITY CLASSIFICATION (OF REPORT) ONGERUBRICEERD	17b. SECURITY CLASSIFICATION (OF PAGE) ONGERUBRICEERD	17c. SECURITY CLASSIFICATION (OF ABSTRACT) ONGERUBRICEERD
18. DISTRIBUTION/AVAILABILITY STATEMENT Unlimited availability, ~~requests shall be referred to sponsor~~		17d. SECURITY CLASSIFICATION (OF TITLES) ONGERUBRICEERD

Distrubutionlist of Report 1999/CMC/R054
Institute: TNO Building and Construction Research, Centre for Mechanical Engineering
Project: A98/KM/118

	Number of copies:
DWOO	1
HWO-Centrale Organisatie	(A)
HWO-KM	1
HWO-KL	(A)
HWO-Klu	(A)
DM&P TNO-DO	1
DMKM, afd. Maritieme Techniek; ir. T.N. Bosman	4
DMKM, afd. Maritieme Techniek, accountcoördinator	(A)
DMKM, afd. Maritieme Techniek; sectie Documentatie	1
TNO – Centrum voor Mechanische Constructies	5
Bibliotheek KMA	3

(A) = Abstract only